IN VIVO IMAGING OF THE *S*-LOCUS RECEPTOR KINASE IN TRANSGENIC SELF-INCOMPATIBLE *ARABIDOPSIS THALIANA*

A Dissertation

Presented to the Faculty of the Graduate School

of Cornell University

in Partial Fulfillment of the Requirements for the Degree of

Doctor of Philosophy

by

Anne C. Rea

May 2012

IN VIVO IMAGING OF THE *S*-LOCUS RECEPTOR KINASE IN TRANSGENIC SELF-INCOMPATIBLE *ARABIDOPSIS THALIANA*

Anne C. Rea, Ph. D.

Cornell University 2012

Self-incompatibility (SI) in the Brassicaceae commences with the haplotype-specific binding and recognition of the pollen coat-localized *S*-locus cysteine rich (SCR) protein by the stigma epidermal cell-localized plasma membrane-spanning *S*-locus receptor kinase (SRK) protein, and culminates in the inhibition of germination of genetically-related pollen at the stigma surface. This self-recognition system allows the cells of the stigma to screen pollen that has landed on its surface for genetic relatedness, which both prevents self-fertilization and increases genetic diversity in the population.

The events downstream of the ligand-receptor interaction are not well understood. However, the transgenic self-incompatible *Arabidopsis thaliana* model system, made possible by the transfer of *SRK* and *SCR* genes from self-incompatible *A. lyrata*, has proven useful in addressing questions related to SI. For example, recent results, including those from this dissertation, challenge the current mechanistic view of SI put forth from studies with *Brassica*. A candidate gene approach that included the use of T-DNA insertional and point mutants, targeted down-regulation, and yeast two-hybrid interaction techniques, was employed for identifying potential downstream signaling components. Candidate genes were selected based on their sequence similarity to genes identified in *Brassica* as being involved in SI, the commonalities between SI and plant immunity, and their high and specific expression in the stigma.

In order to gain clues about the intracellular events that occur prior and subsequent to SKR-SCR recognition, SRK was successfully tagged with fluorescent protein and transformed into *A. thaliana*, where it is expressed and functional in stigma epidermal cells. Confocal microscopy was used to characterize the localization and dynamics of SRK in live cells using several different chimeric genes designed to highlight the localization of the different native protein species produced from the *SRK* gene driven by either its native or a stigma-specific promoter. Results presented in this dissertation provide insight into SRK localization in the context of pollination and floral development, and reveal characteristic architectural features of stigma epidermal cells that will be useful in future studies of this unique cell type.

BIOGRAPHICAL SKETCH

Anne C. Rea was born in Ottawa, Ontario, Canada. As a child, she lived in England for one year. At the age of 7, she moved with her parents to New York State, where she spent her remaining childhood and youth. She graduated third in her class from Tamarac High School in 1999.

Anne is a fourth-generation graduate from The Ohio State University, where she received a Bachelor of Science degree in Biology, with a concentration in Plant Biology, in 2003. She graduated *cum laude*, With Distinction in Biology, and With Honors in the Liberal Arts. Her Senior Honors Research and Thesis work was conducted in the lab of Dr. Fred Sack, and focused on stomatal development in *Arabidopsis thaliana*.

Anne has always been interested in science, and developed her attracttion to the aesthetics of plant anatomy and cells as an undergraduate. This has driven her to pursue a career in plant cell and molecular biology and has sparked her interest in microscopy. Anne came to Cornell University as a graduate student and conducted her dissertation work on self-incompatibility in the Brassicaceae in the lab of Dr. June Nasrallah. While a graduate student, she developed her passion for teaching as a graduate teaching assistant and instructor for several biology courses. Since then, she has been teaching introductory biology lecture and lab courses at the Sage College of Albany.

I dedicate this dissertation to my grandmother, Barbara Rea, who saw the potential for this dissertation well before I did.

ACKNOWLEDGMENTS

First and foremost, I would like to thank June Nasrallah for allowing me to join her lab as a graduate student and for contributing her vast knowledge and immensely helpful discussions to the work described in this dissertation, and without whom this dissertation would not be possible. I would also like to extend my gratitude to the other members of my committee, Jian Hua and Tim Huffaker, for taking part in and supporting me throughout this process. I would specifically like to thank Jian for contributing some of the materials I used in my lab work, such as the yeast two-hybrid library, the *etr1-1*, *ein2-1*, *npr1-1*, *pad4-1*, and *eds1-1* mutant seed, the *35S*pr*::GFP* seed, and the NPR1, PAD4, and EDS1 dCAPS marker primers. I also thank Jian for being willing to sit down and discuss with me, countless times, the details of protocols and results of experiments. I also thank Jeff Dangl and Jane Parker for contributing the *rar1-21* mutant seed and the *sgt1b* mutant seed, respectively. I would also like to thank June and Titima Tantikanjana for making the chimeric constructs containing fluorescent protein tags. I am also grateful to Sandy Lazarowitz and Asako Uchiyama for providing the fluorescent protein marker constructs.

I would also like to thank Mike Nasrallah for his advice pertaining to pollination assays, and for his helpful discussions about my research. I also thank all of the past and present members of the Nasrallah lab whose tenure in the lab overlapped with mine. All contributed to the ambiance and to discussions that helped shape my research. I would especially like to thank Titima for her advice pertaining to cloning experiments, particularly during my rotation in the Nasrallah lab, and for her continued support and discussions regarding both research and life experiences. I thank Chih-Wei Tung for her consistent willingness to help me with any aspect of research at almost any time. I am also appreciative of all the conversations and helpful discussions I had with Chih-Wei, Pei Liu, Sushma Naithani, Sue Sherman-Broyles, Suzy

Strickler, Nathan Boggs, Beth LaLonde, and Hiro Kitashiba. Special thanks to Suzy for her company in the lab. I would also like to extend special thanks to Tiffany Crispell, who helped make some of the materials used in my experiments toward the end of my tenure in the lab.

Ram Dixit, Muthugapatti Kandasamy, and Nate Pumplin helped me in various ways with interpretation of confocal microscopy images, and I am grateful to have had their help. Hélène Javot and Mamta Srivastava, former and current manager of the Plant Cell Imaging Center at the Boyce Thompson Institute, respectively, have provided me with invaluable advice regarding confocal imaging issues, and were very much available to me throughout my entire experience with the confocal microscope.

I would also like to thank André Velásquez for help with Figure 1 of Chapter 3, and for his invaluable edits of the sections relating to plant immunity in Chapter 2 of this dissertation. I am especially thankful for his incalculable help and support in the last couple of years of my dissertation work, both professionally and personally.

And last but not least, I would like to thank my parents, Mary and Mark Rea, for their continued support throughout my entire life. Without them, this dissertation would not have been possible, and words cannot do justice to my gratefulness to them.

This material is based upon work supported in part by the National Science Foundation under Grant No. IOS-0744579. Any opinions, findings, and conclusions or recommendations expressed in this material are those of the author and do not necessarily reflect the views of the National Science Foundation.

TABLE OF CONTENTS

LIST OF FIGURES

Chapter 1

Chapter 2

Chapter 3

LIST OF TABLES

CHAPTER 1

Plant reproduction, self-incompatibility, and a transgenic self-incompatible *Arabidopsis thaliana* model system for SI research[1]

Part I:

Self-incompatibility systems: barriers to self-fertilization in flowering plants

ABSTRACT

Flowering plants (angiosperms) are the most prevalent and evolutionarily advanced group of plants. Success of these plants is owed to several unique evolutionary adaptations that aid in reproduction: the flower, the closed carpel, double fertilization, and the ultimate products of fertilization, seeds enclosed in the fruit. Angiosperms exhibit a vast array of reproductive strategies, including both asexual and sexual, the latter of which includes both self-fertilization and cross-fertilization. Asexual reproduction and self-fertilization are important reproductive strategies in a variety of situations, such as when mates are scarce or the when the environment remains relatively stable. However, reproductive strategies promoting cross-fertilization are critical to angiosperms' success, since they contribute to the creation of genetically diverse populations, which increases the probability that at least one individual in a population will survive given changing environmental conditions. The evolution of several physical and genetic barriers to self-fertilization or fertilization among closely related individuals is thus widespread in angiosperms. A major genetic barrier to self-fertilization is self-incompatibility (SI), which allows female reproductive cells to discriminate between "self" and "non-self" pollen, and

[1] Material in this chapter was published in *Int. J. Dev. Biol.* 52: 627-636 and *Journ. Exp. Bot.* doi: 10.1093/jxb/erp393.

specifically reject self pollen. Evidence for the importance of SI in angiosperm evolution lies in the highly diverse set of mechanisms used by various angiosperm families for recognition of self pollen tube development and preventing self-fertilization.

INTRODUCTION

As for all organisms, reproductive success is critical for survival in plants. All plants have the capacity to reproduce sexually, but given their predominantly sessile lifestyle, it is no wonder that plants have maintained the ability to reproduce without the need for a mate throughout their evolutionary history. Most plant species, but very few animal species, have the capacity to reproduce asexually. Even the most evolutionarily advanced and successful group of plants, the angiosperms (flowering plants), are capable not only of reproducing asexually, but can reproduce sexually via self-fertilization, whereby the egg and sperm from the same plant fuse to produce viable offspring. Hermaphroditism, the condition in which an individual has both male and female reproductive structures, is a pre-requisite for self-fertilization. This condition and the ability to self-fertilize are relatively rare in animals but very common in plants.

While self-fertilization has its advantages under favorable and relatively stable conditions, it can be problematic in more variable and unpredictable environments. Since self-fertilization ultimately results in the production of genetically identical offspring, it can culminate in a population of low genetic diversity, making the perpetuation of populations difficult in the variable environments that plants encounter in nature and often cannot escape. It is therefore not surprising that throughout their history, plants have evolved many different mechanisms for preventing self-fertilization, or at least promoting cross-fertilization, which allow them to avoid the potentially deleterious consequences of inbreeding.

Here, the unique features of fertilization in flowering plants are outlined. Focus is placed on the events that precede egg-sperm fusion, namely the intricate interactions that occur between pollen and pollen tube (which carry the haploid male gametes) on the one hand, and diploid cells of the pistil (the female reproductive structure that harbors the haploid female gametes) on the other hand. These highly orchestrated interactions are critical determinants of reproductive success in flowering plants and as a consequence, they have been primary targets in the evolution of reproductive barriers that promote out-crossing.

SUCCESSFUL FERTILIZATION: CRUCIAL STRUCTURAL FEATURES & EVENTS

Gametophyte development, pollination, and double fertilization

A distinguishing feature of plants (excluding many algae, which some botanists consider to be plants) is alternation of generations, a life cycle in which plants alternate between a multicellular diploid generation (the sporophyte) and a multicellular haploid generation (the gametophyte). The sporophyte undergoes meiosis to produce haploid spores, which in turn undergo mitosis to produce gametophytes. Gametophytes undergo mitosis to produce haploid sperm cells and egg cells, the fusion of which produces a single-celled diploid zygote that undergoes mitosis to produce the new sporophyte. Throughout plant evolutionary history, there has been a trend toward a dominant sporophyte generation, accompanied by a highly reduced gametophyte. In the flowering plants, the female gametophyte (megagametophyte; embryo sac) is completely dependent on the sporophyte for nutrition and protection. The male gametophyte (microgametophyte; pollen grain) is initially dependent on the sporophyte during its development, but is then released from the sporophyte, and is often dispersed, via wind or animal vectors, ideally to other plants of the same species.

A key evolutionary innovation that distinguishes angiosperms from all other major plant groups is the evolution of the flower. Although this simple yet elegant sporophytic reproductive structure can take many forms, it often consists of four distinct floral organ types arranged in four concentric whorls: on the outside are the sepals, which protect the developing flower, followed by the petals, which function as attractive agents for pollinators, and the stamens and carpels, which are, respectively, the specialized male and female floral organs that house the spores and the gametophytes that develop from them (Figure 1). The stamen consists of a stalk-like filament supporting an anther, which houses the pollen grains (the male gametophyte) in two pairs of pollen sacs (Figure 1). A single structure consisting of one carpel, or several fused carpels, is informally called a pistil, and consists of a stigma, style, and ovary (Figure 1). The apical stigma receives pollen, the style serves as an intermediary conduit between the stigma and the ovary, and the ovary houses the ovules, each of which contains an embryo sac (the female gametophyte).

As in other sexually reproducing organisms, plant gametes are produced by meiotic division of diploid progenitor cells, but they are packaged in unique ways. In the anther, each of the haploid products of meiosis develops into a pollen grain having dual gametophytic/sporophytic (haploid/diploid) features: an interior consisting of haploid cells (two or three, depending on the species) derived by mitotic division of the primary meiotic product, and a diploid-encoded exterior coat consisting largely of lipids, carbohydrates, and proteins derived from the diploid nurse cells of the tapetum, a specialized secretory cell layer that lines the pollen sac. At maturity, pollen grains, released by dehiscence of the anthers, are in effect free-living gametophytes, which contain not only the sperm cells that participate in fertilization, but also a vegetative cell that supports the germination and growth of the pollen tube as it

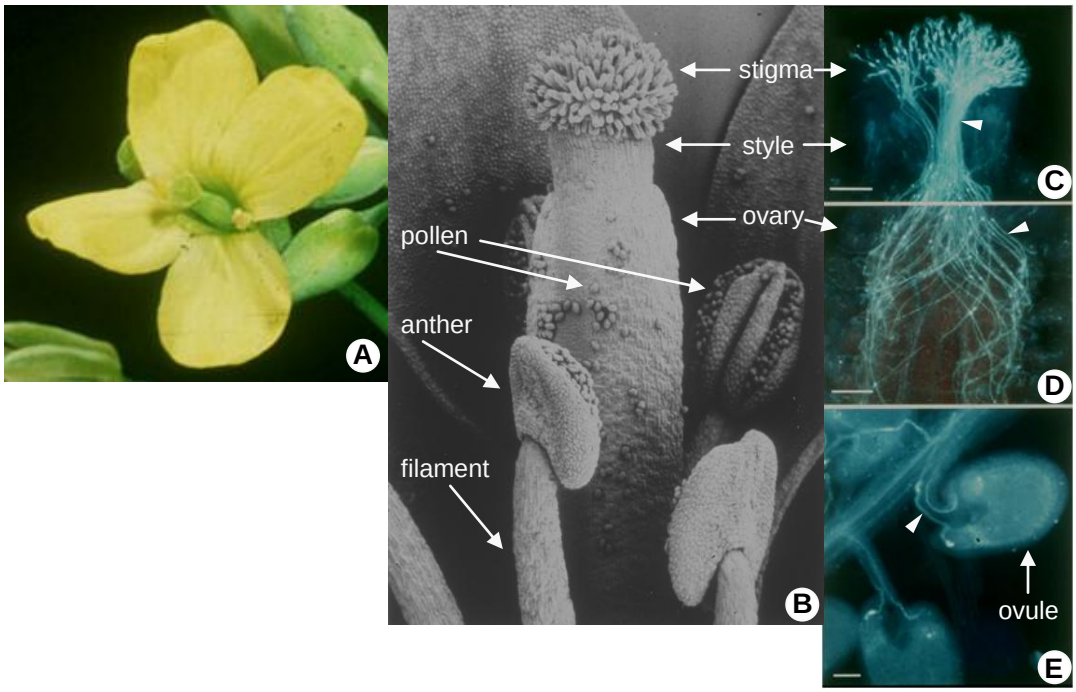

Figure 1. Hermaphroditic flowers of the Brassicaceae family.
(A) A flower of the *Brassica* genus, which includes the cole crops such as broccoli, cabbage, brussel sprouts, and oilseed rape (canola). The yellow petals, displayed in the cruciform pattern that gives the family its "crucifer" common name, surround the centrally-located female (pistil) and male (stamens) reproductive organs. **(B)** A scanning electron micrograph of an *Arabidopsis thaliana* flower, focusing in on the pistil and stamens. The pistil is subdivided into the apical stigma, which receives and screens pollen, the style, through which pollen tubes grow, and the ovary, which houses the ovules. The stamen consists of an apical anther, which houses the pollen, supported by a stalk-like filament. Several mature pollen grains have shed from the anthers. **(C, D, E)** The path of pollen tube growth in an *A. thaliana* pistil. In these epifluorescence images, the fluorescence of pollen tubes (arrowheads) is due to binding of the aniline blue stain to polysaccharides in the tube wall. Pollen grains land on the stigma epidermal cells and if determined compatible by the stigma, they form sperm-cell–containing pollen tubes that grow between sub-epidermal cells of the stigma and are guided down the style (C) and ovary (D). In the ovary, a pollen tube is guided by unknown cues towards an ovule (E), into which it discharges its two sperm cells, which subsequently fuse with embryo sac cells within the ovule in the process of double fertilization (see text). Scale bars, 100µm (C, D); 20µm (E).

journeys within the pistil towards the ovary (for a review of pollen development, see McCormick 2004). In the pistil, meiosis occurs within ovules buried deep inside the ovary and produces, after several mitotic divisions, a haploid embryo sac consisting of seven cells, among which a uninucleate egg cell and a binucleate central cell participate in fertilization. The embryo sac is protected by diploid tissues of the ovule, which form a discontinuous layer surrounding the embryo sac with an opening near the egg cell for pollen tube entry (see Reiser & Fischer 1993 and Yadegari &Drews 2004 for reviews of embryo sac development).

Once a pollen tube enters the embryo sac, it releases its cargo of two sperm cells which effect double fertilization, an evolutionary adaptation unique to angiosperms: one sperm cell fuses with the egg cell to create a diploid zygote that divides by mitosis to become an embryo, while the second sperm cell fuses with the binucleate central cell to create a triploid endosperm that nourishes the developing embryo. At the culmination of embryo development, the ovule has become a seed, with its surrounding diploid tissues having become the seed coat. At maturity, the ovary develops into the fruit, yet another reproductive feature unique to angiosperms, which serves to protect the seed(s) and often functions in seed dispersal. Angiosperms are so-named according to this adaptive advantage of a protected seed: the word "angiosperm" comes from the Greek words *angeion* ("vessel") and *sperma* ("seed") (Raven *et al.* 2005).

Double fertilization is only the last of many steps that are critical for reproductive success in flowering plants. The development of male and female gametes in physically separate structures, even in hermaphroditic flowers, and the fact that female gametes are enclosed deep within the ovary mean that, for fertilization to occur, the single-celled pollen tube must grow across the many layers of diploid cells in the pistil, often traversing long distances at high speed. For example, the maize pollen tube elongates at the astounding speed of 4-10 mm/h (Booy *et al.*

1992) through the long silk of the maize pistil. The pollen tube is not filled with cytoplasm along its length; rather, the cytoplasm is confined to the growing tube tip as a result of β-1,3 glucan (callose) "plugs" akin to fungal septa, which are deposited at regular intervals and separate the cytoplasm from the spent pollen grain and older part of the tube.

The successful journey of the pollen tube towards its ovule targets is dependent on its intricate and highly regulated interactions with diploid cells of the female reproductive apparatus. These interactions occur at all stages of pollen tube development, starting with adhesion and hydration of the pollen grain and germination of the pollen tube at the stigma epidermal surface, continuing with intercellular growth through specialized tissue (called the transmitting tract) in the stigma, style, and ovary, and ending with pollen tube entry into the ovule. In view of these interactions, the pistil acts not only as a passive conduit for pollen tubes, but also as a pre-fertilization selective sieve for screening the many pollen grains from various sources that bombard it, allowing the germination and growth of appropriate grains and preventing the development of inappropriate grains. In this capacity, the pistil is central to preventing non-productive and energetically wasteful inter-specific egg-sperm fusions. Additionally, the pistil can function as an intra-specific pre-zygotic barrier to fertilization, as occurs in plants that exhibit genetic self-incompatibility.

PRE-ZYGOTIC GENETIC BARRIERS TO SELF-FERTILIZATION

Genetic diversity is vital to the long-term success of populations, as it increases the probability that at least one individual in a population will survive in the face of drastic environmental fluctuations. Angiosperms have evolved many methods of avoiding self-fertilization and thus inbreeding, thereby promoting out-crossing and increasing genetic

diversity. Some angiosperms exhibit unisexual male and female flowers that may be located on separate plants (as in holly), which precludes self-fertilization, or on the same individual (as in maize), which reduces but does not prevent self-fertilization. The majority of angiosperms, however, have hermaphroditic flowers in which male and female organs develop coordinately in close proximity to each other. In some of these plants (e.g., sugar maple), differential timing of anther and stigma maturation promotes out-crossing by drastically reducing opportunities for self-fertilization. In others, self-fertilization is prevented and out-crossing is ensured by self-incompatibility systems that discriminate between genetically-related (self) and genetically unrelated (non-self) pollen grains.

Self-incompatibility

Of the ~250,000 species of angiosperms, more than half have evolved self-incompatibility (SI) (de Nettancourt 2001). It should be noted from the outset that the term "self-incompatibility" refers to a variety of molecularly diverse and evolutionarily unrelated mechanisms for preventing self-fertilization. In some self-incompatible species, differences in floral morphology act to reinforce the ability of the pistil to discriminate between self and non-self pollen. For example, primrose (*Primula*) exhibits two floral forms (morphs) that differ in morphology, primarily in the relative placement of stigmas and anthers, and pollinations succeed only between different morphs (de Nettancourt 2001). It is this visually dramatic floral heteromorphism and its association with the ability to cross-pollinate that allowed Darwin and other early botanists to appreciate the existence of self-incompatibility in plants (Darwin 1876; de Nettancourt 2001). However, in most plant groups, SI is not accompanied by differing floral morphology and the outcome of pollination can only be predicted by reciprocal pollination tests

between individual plants. Even among these so-called homomorphic SI systems, there are major differences among families in the number of self-recognition loci that control SI specificity, the genetic control of pollen SI phenotype (i.e., whether it is determined by its own haploid genome or the diploid genome of its parent plant), as well as where along the path of pollen tube growth (stigma, style, or ovary) self-pollination is inhibited and the molecular mechanism that underlies arrest of self pollen. These differences among SI systems suggest that SI has evolved multiple times throughout angiosperm history.

Despite these differences, however, all SI systems analyzed to date, irrespective of their underlying molecular mechanisms, share several features in common. In many systems, including those described below, SI specificity is determined by haplotypes of a single self-recognition locus, traditionally termed the *S* (Sterility) locus. In this context, "self" and "non-self" refer, respectively, to genetic identity and non-identity at the *S* locus. In all SI systems characterized to date, the *S* haplotype consists of two genes, which individually determine SI specificity in pistil or pollen. These genes are highly polymorphic due to strong balancing selection, and a self-incompatible species can exhibit a large number of SI recognition specificities, and therefore of *S* haplotypes: e.g., ~100 different SI specificities are estimated to occur in *Brassica rapa* (Watanabe *et al.* 2000). The SI recognition genes are maintained in tight genetic linkage by reduced recombination, resulting from close physical proximity of the genes and from the extensive structural heteromorphism (rearrangements and haplotype-specific sequences) that distinguish different *S*-locus haplotypes (Nasrallah 2000). In all systems, recognition of self pollen is based on allele-specific interactions (direct or indirect) of the pistil- and pollen-expressed products of *S*-locus genes, which in turn trigger activation of a cellular response in pistil or pollen (depending on the SI system), which culminates in inhibition of

pollen tube development. Thus, unlike other recognition phenomena, which are typically based on recognition and rejection of non-self, SI systems are based on recognition and rejection of self.

A variety of molecular mechanisms for inhibition of self-pollination

To date, the outlines of three molecular mechanisms of self-pollen recognition and inhibition have been elucidated by molecular analysis of only a handful of plant families: the crucifer family (Brassicaceae, including cabbage, broccoli, oilseed rape/canola), the night-shade family (Solanaceae, including tobacco, tomato, potato, petunia), the rose family (Rosaceae, including fruit trees), the snapdragon family (Plantaginaceae), and the poppy family (Papaveraceae). These systems differ from one another with respect to both the recognition and response phases of SI. In particular, the manner in which self pollen is arrested and whether this arrest involves cell death or not is dictated by the site of pollen inhibition, i.e., whether it occurs early or late during the pollen tube's journey through the pistil, which in turn is determined by characteristics of the stigma surface. Thus, in crucifers, the SI response is manifested at the surface of the "dry" (i.e., non-secretory) stigma by failure of pollen germination and tube growth; as a consequence, incompatible pollen tubes rarely grow into the pistil and it stands to reason that their inhibition would not be accompanied by death of the pollen grain or tube. In contrast, pollen tube death is clearly the only way to inhibit incompatible pollen tubes that have already penetrated into the pistil, as occurs in families having a "wet" (i.e., highly secretory) stigma on which pollen grains automatically hydrate and germinate. It may be argued that SI mechanisms operating at the stigma surface are more efficient, energetically and reproductively, than those operating in the transmitting tract of the stigma, style, and ovary, if only because they

preclude the formation of incompatible pollen tubes, which can clog the transmitting tract and interfere with the subsequent growth of compatible pollen tubes.

Early arrest of self pollen: recognition by receptor-ligand interactions at the stigma surface in the crucifer family

The SI system of crucifers operates at the level of interaction between a pollen grain and a stigma epidermal cell. The SI response is very rapid and is typically observed within minutes of pollen-stigma contact. It is also highly localized and involves only the zone of contact between a pollen grain and a stigma epidermal cell. As a result, a single papillar cell can discriminate between genetically different pollen grains, inhibiting a self pollen grain while allowing the development of a non-self pollen grain (Dickinson 1995). Furthermore, incompatible pollen grains that have not formed pollen tubes are still viable for a time after landing on an incompatible stigma, and can form pollen tubes when transferred to a compatible stigma (Geitmann 1999). Thus, inhibition of self pollen in this family does not involve cell death of either pollen or stigma cells.

Consistent with these features, recognition of self-related pollen in crucifers is based on the action of cell surface-localized receptors and ligands encoded by two *S*-locus genes: the *S*-locus receptor kinase (*SRK*) gene, which encodes a single-pass transmembrane serine/threonine kinase localized in the plasma membrane of the stigma epidermal cell (Stein *et al.* 1991, 1996; Takasaki *et al.* 2000), and the *S*-locus cysteine-rich protein (*SCR*) gene (Schopfer *et al.* 1999; also designated *SP11* (*S*-locus protein 11; Suzuki *et al.* 1999)), which encodes a small peptide that is located in the pollen coat and functions as the ligand for the SRK receptor. Contact between a pollen grain and a stigma epidermal cell causes transfer of the SCR peptide, along with other components of the pollen coat, to the stigma surface, allowing SRK-SCR interactions

to take place. *SRK* and *SCR* are highly polymorphic: overall amino acid sequence among alleles can diverge by as much as 35% for SRK and by over 70% for SCR variants. And it is the specific and direct interactions between SRK and SCR variants encoded by the same *S* haplotype that underlie the specific recognition of self pollen (Kachroo *et al.* 2001; Takayama *et al.* 2001; Shimosato *et al.* 2007). The conclusion that SRK and SCR are necessary and sufficient for specific recognition of self pollen has been demonstrated repeatedly by analysis of loss-of-function mutants and by gain-of-function transgenic experiments in which transfer of a particular allele of *SRK* or *SCR* resulted in acquisition of the corresponding SI specificity in stigma or pollen, respectively (Nasrallah 2005; Takayama & Isogai 2005). One of the most dramatic transgenic experiments was the successful inter-specific transfer of the SI trait by transformation of the self-fertile model plant *Arabidopsis thaliana* with an *SRK-SCR* gene pair from the self-incompatible *A. lyrata* (Nasrallah *et al.* 2002, 2004).

The current view of SI in crucifers is based on the ligand-activated receptor paradigm established in animal systems, whereby the binding of SCR to the extracellular domain of SRK activates the receptor's kinase, initiating a signaling cascade within the stigma epidermal cell that culminates in pollen rejection (Figure 2). In this view, all biochemical activity triggered by the SRK-SCR interaction is thought to occur within the stigma, with the pollen grain contributing only the activating ligand. However, and although supported by the fact that pollen grains remain viable after contacting an incompatible stigma, this notion has not been rigorously tested.

The molecules that regulate or orchestrate the SI response downstream of stigma-pollen recognition are poorly understood. Efforts at elucidating the SI signaling pathway have involved yeast 2-hybrid screens for proteins that interact with the kinase domain of SRK (Bower *et al.* 1996; Gu *et al.* 1998; Vanoosthuyse *et al.* 2003) and with one of these SRK-interacting proteins

Figure 2. Receptor-mediated recognition of self and stigmatic inhibition of pollen tube development in self-incompatible crucifers.
The diagram shows an S_1S_2 stigma epidermal cell interacting with a pollen grain derived from an S_1S_2 plant (self pollen) and a pollen grain derived from an S_3S_4 plant (non-self pollen). The SI self-recognition molecules, the stigma SRK receptor and the pollen coat-localized SCR ligand, are color-coded to depict variants with different SI specificities. Pollen grains are shown to display two SCR variants because self-incompatible plants are typically heterozygous at the *S* locus and SCR is produced by tapetal cells, which are derived from diploid cells of the anther; thus, assuming co-dominance of *S* haplotypes, the haploid pollen grains produced by an S_1S_2 plant will be phenotypically S_1S_2 even though genotypically they are S_1 or S_2. SRK is shown as forming ligand-independent homodimers (i.e., in the absence of self pollen), which are maintained in an inactive state by binding to the thioredoxin *h* proteins THL1 and THL2. Allele-specific binding of the SRK extracellular domain to its cognate SCR ligand would activate the receptor by dislodging the inhibitory THL proteins and possibly causing a conformational change in the receptor. This activation would then trigger a localized response within the stigma epidermal cell that culminates in the inhibition of a self pollen grain but does not affect the germination of a non-self pollen grain, whose SCR does not bind and activate SRK. Arrows drawn in the cytoplasm of the stigma epidermal cell depict a largely speculative (question marks) signaling pathway that includes only two effectors: the membrane-bound kinase MLPK and the cytoplasmic E3 ligase ARC1, the latter of which is proposed to ubiquitinate Exo70A1, which both inhibits SI and is required for pollen tube growth, to cause either its degradation or sub-cellular redistribution. Not shown is AtPUB8, another positive effector of SI with predicted E3 ligase activity, which is thought to function largely by regulating the steady-state levels of *SRK* transcripts.

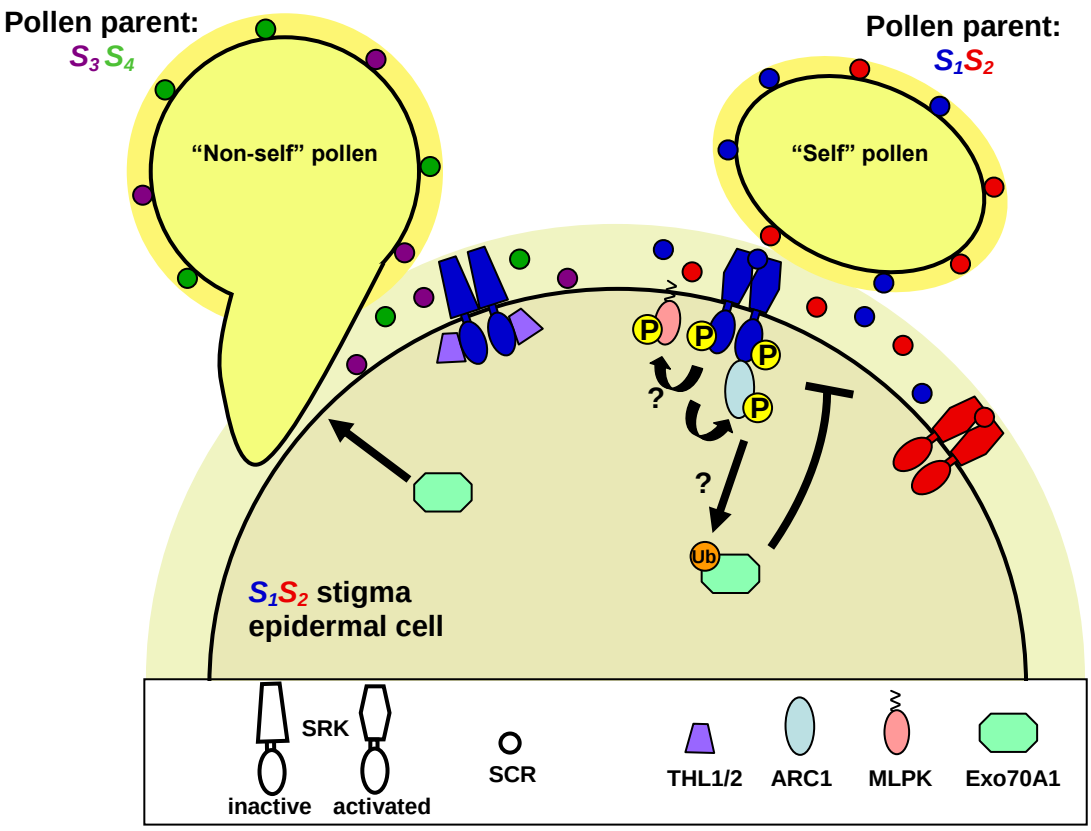
Pollen parent:
S3 S4
"Non-self" pollen
Pollen parent:
S1S2
"Self" pollen
P
P
P
P
?
?
Ub
S1S2 stigma
epidermal cell
SRK
inactive
activated
SCR
THL1/2
ARC1
MLPK
Exo70A1

(Samuel *et al.* 2009), and analysis of mutations that cause breakdown of SI, not only in naturally self-incompatible *Brassica* species (Murase *et al.* 2004), but also in the *A. thaliana* transgenic self-incompatible model (Liu *et al.* 2007). These approaches have identified a few potential candidate effector proteins, only some of which have been shown to function in SI. Two thioredoxin *h*-like proteins, identified in yeast (Bower *et al.* 1996), are thought to function as negative regulators of SI by maintaining SRK in an inactive form in resting stigmas, i.e., in the absence of SCR ligand. Antisense suppression of these proteins causes low-level constitutive rejection of both self and non-self pollen (Haffani *et al.* 2004). Furthermore, a constitutively active variant of SRK is inhibited by thioredoxin, and this inhibition is reversed by addition of self pollen coat proteins (Cabrillac *et al.* 2001). Interestingly, in the stigma, SRK forms dimers in the absence of SCR (Giranton *et al.* 2000) via ligand-independent association domains located in its extracellular region (Naithani *et al.* 2007), suggesting that thioredoxin *h*-like proteins might function to maintain these ligand-independent dimers in an inactive form and that this inhibition would be relieved by interaction of SRK with its cognate SCR (Cabrillac *et al.* 2001). Whether activation of SRK is also accompanied by the formation of higher order receptor complexes or changes in the conformation of the receptor, as described for animal receptors, is not known.

Three molecules have been proposed to function as positive effectors of the SI response in crucifers. MLPK (*M*-locus protein kinase) was identified by map-based cloning and is thought to correspond to a mutation that causes complete loss of SI in the *B. rapa* variety Yellow Sarson (Murase *et al.* 2004). MLPK is a cytosolic serine/threonine protein kinase that occurs as two isoforms, each having a putative N-terminal myristoylation signal that apparently anchors it to the stigma plasma membrane. Because the two MLPK isoforms interact with SRK, they are thought to function in SRK-mediated signaling (Kakita *et al.* 2007).

Another positive effector is *Brassica* ARC1 (Armadillo repeat-containing protein 1; Gu *et al.* 1998), a member of the sub-family of U-box proteins that exhibits E3 ubiquitin ligase activity and contains the Armadillo (Arm) repeat protein interaction domain (Azevedo *et al.* 2001; Stone *et al.* 2003). ARC1 has been implicated in SI because its antisense down-regulation in transgenic *B. napus* was associated with partial breakdown of SI (Stone *et al.* 1999). ARC1 is expressed specifically in stigmas, it interacts in yeast with phosphorylated forms (but not unphosphorylated forms) of the SRK kinase domain (Gu *et al.* 1998), and it localizes with the proteasome and COP9 signalosome only in the presence of a functional SRK (Stone *et al.* 2003). Exo70A1 was recently identified as an interacting protein and potential target of ARC1 ubiquitination and degradation, is involved in both inhibiting SI and promoting pollen tube formation, and is thought to contribute to the exocyst complex involved in exocytosis (Samuel *et al.* 2009). Finally, *AtPUB8* (*Arabidopsis thaliana* plant U-box protein 8) was identified using the *A. thaliana* transgenic SI model as a gene required for expression of SI at late stages of stigma development, apparently by regulating the levels of *SRK* transcripts (Liu *et al.* 2007). Like ARC1, AtPUB8 is predicted to have both a U-box domain and an Arm repeat region (Azevedo *et al.* 2001) and to have E3 ligase activity, but it lacks several domains found in ARC1, indicating that it is not the functional ortholog of *Brassica* ARC1.

The nature of MLPK, ARC1, and Exo70A1 is consistent with a role for both phosphorylation (as expected) and ubiquitination in the regulation or orchestration of the SI response, and has led to the following model of SI signaling (Figure 2). One scenario involves on the one hand, a phosphorylation cascade with MLPK as a possible intermediate and on the other hand, ubiquitination causing degradation or subcellular redistribution of proteins such as Exo70A1, which are thought to function as inhibitors of SI and/or promoters of pollen tube

growth. As yet, no clues have emerged regarding how these two biochemical activities intersect to cause arrest of self pollen tube development at the stigma surface. Furthermore, recent studies using transgenic *A. thaliana* self-incompatible plants have raised questions about the general applicability of this model in crucifer SI (see Part II).

SI by pollen tube cell death: Two distinct mechanisms

In contrast to the early-acting SI system of crucifers, late-acting SI systems, in which incompatible pollen grains germinate and produce pollen tubes that grow into the pistil, typically result in pollen tube death. This phenomenon has been described in two molecularly distinct SI systems: one involving programmed cell death and the other involving degradation of pollen tube RNA.

Programmed cell death of self pollen tubes in poppy

The SI response of poppy (*Papaver rhoeas*) is manifested during or shortly after pollen tube germination at the stigma surface and results in death of pollen tubes after penetration into the stigma (Geitmann 1999). The female determinant of SI specificity is the stigma-localized S protein (recently renamed PrsS (*Papaver rhoeas* stigma S determinant; Wheeler *et al.* 2009)), a small secreted glycoprotein that does not exhibit sequence similarity to proteins of known function. An understanding of the biochemical events that occur within self pollen tubes to cause their arrest is much more advanced in this system than in any other SI system. This progress has largely been due to the development of a robust *in vitro* bioassay for pollen tube growth, in which addition of purified preparations of the PrsS protein faithfully recapitulates the SI response, triggering dramatic cellular responses and ultimate cell death specifically in self pollen

tubes (McClure & Franklin-Tong 2006). Among the observed effects of self PrsS protein (Figure 3) is a rapid influx of calcium just behind the tube tip, which alters the normal cytosolic tip-focused calcium gradients that maintain growth at the pollen tube tip (Franklin-Tong *et al.* 2002). This calcium influx apparently triggers several downstream events that cause initial inhibition of pollen tube growth, among the earliest of which are actin depolymerization and disruption of the actin cytoskeleton (Snowman *et al.* 2002; Thomas *et al.* 2006). These events are followed by calcium/calmodulin-dependent phosphorylation and inactivation of p26, a 26 kDa cytosolic pollen protein with homology to soluble inorganic pyrophosphatases known to drive biosynthesis reactions (Rudd *et al.* 1996; de Graaf *et al.* 2006). Subsequent events include phosphorylation and activation of a putative MAPK (mitogen-activated protein kinase; Rudd *et al.* 2003) and several known hallmarks of programmed cell death, such as leakage of cytochrome *c* from mitochondria into the cytosol, activation of caspases (Thomas & Franklin-Tong 2004), and DNA fragmentation (Jordan *et al.* 2000).

Recently, the PrpS (pollen-localized *Papaver rhoeas* pollen S) protein, which does not exhibit sequence similarity to any known proteins, was identified as the male determinant of SI (Wheeler *et al.* 2009). It is predicted to have between 3 and 5 transmembrane helices, and was found to associate with the plasma membrane of the pollen tube (Figure 3). A 15-amino-acid peptide, part of the predicted extracellular loop of PrpS, interacts with PrsS and rescues the inhibition of pollen tube growth in the *in vitro* bioassays in an S-specific manner, an effect that is also seen with antisense oligodeoxynucleotides against *PrpS* (Wheeler *et al.* 2009). The PrpS protein may function primarily as part of a calcium channel itself, or as a regulator of calcium channel activity, possibly in conjunction with an accessory receptor, the S-protein (PrsS) binding protein SBP (Hearn *et al.* 1996). SBP is an integral membrane proteoglycan that is expressed

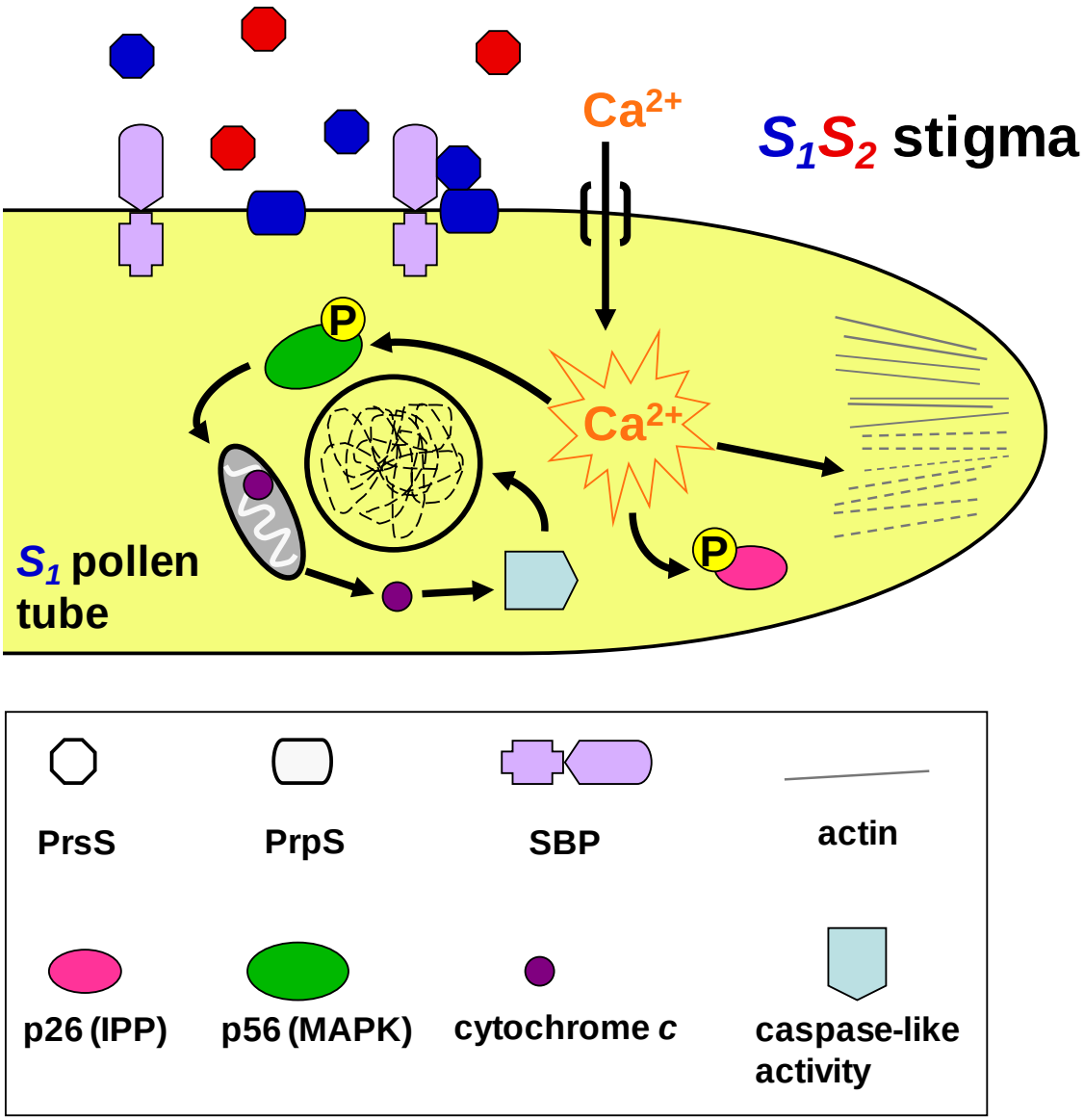

Figure 3. Programmed cell death of self pollen tubes in the poppy stigma.
The diagram shows an S_1 (self) pollen tube growing in an S_1S_2 stigma. The diploid cells of the stigma secrete two PrsS variants (represented by different colors) that accumulate in the extracellular matrix through which the pollen tubes grow. The model postulates that PrsS interacts in an allele-specific manner with pollen tube membrane-localized PrpS, both proteins of which are encoded by the *S* locus. Because the SI phenotype of a pollen tube is determined by its own haploid genotype, each pollen tube is shown as expressing one PrpS receptor variant. The interaction between PrsS and its cognate PrpS receptor, which may recruit the accessory pollen tube membrane protein SBP, somehow initiates opening of calcium channels, of which PrpS is a possible constituent, in the membrane of self pollen tubes and triggers a series of cellular responses that cause death of self pollen tubes. As described in the text, these responses, which have been demonstrated experimentally using an *in vitro* pollen tube growth assay, include a rapid influx of calcium causing actin depolymerization, disruption of tube metabolism, activation of a MAPK, and culminating in various events characteristic of programmed cell death.

specifically in pollen tubes, binds stigmatic PrsS (albeit not in an allele-specific manner), and apparently enhances the ability of PrsS to inhibit self pollen tubes *in vitro* (Jordan *et al.* 1999). It remains to be seen whether or not PrpS also interacts directly or indirectly with SBP via PrsS to initiate programmed cell death in self pollen tubes.

SI by cytotoxic S-RNases and degradation of pollen tube RNA

In the nightshade, rose, and snapdragon families, the SI response is typically manifested within the upper third of the style where incompatible pollen tubes exhibit reduced rates of elongation, loss of membrane integrity, disrupted organelles, and wall thickening, all of which can lead to swelling and bursting of the tube tip (Ebert *et al.* 1989; Lush & Clarke 1997; de Nettancourt 2001). This dramatic cessation of pollen tube elongation is effected by the S-RNase (*S*-locus ribonuclease), an abundant and highly polymorphic pistil-specific glycoprotein encoded by the *S* locus and secreted into the extracellular matrix that lines the path of pollen tube growth (McClure *et al.* 1989; Lee *et al.* 1994; Murfett *et al.* 1994). The S-RNase has a non-specific RNA degrading activity (McClure *et al.* 1990), but similar to *S*-locus products in other SI systems, its activity is directed specifically at self pollen tubes: when self pollen tubes grow alongside non-self pollen tubes in a pistil, only self tubes are arrested while non-self tubes continue their growth towards the ovules.

How S-RNases effect this *S* allele-specific inhibition of self pollen tubes is a major unanswered question. This specificity cannot be ascribed to selective uptake of S-RNase by self pollen tubes because S-RNases are non-specifically taken up by self and non-self pollen tubes alike (Luu *et al.* 2000). Therefore, specificity must result from events that take place within the pollen tube subsequent to S-RNase uptake. A clue derives from the predicted biochemical

activity of the pollen *S* locus-encoded partner of the S-RNase, SLF (*S*-locus F-box; Lai *et al.* 2002; Sijacic *et al.* 2004) [designated SFB (*S*-haplotype-specific F-box) in the rose family (Ushijima *et al.* 2003)]. SLF is a predicted cytoplasmic protein that belongs to the F-box protein family, whose members are known to function as part of an E3 ubiquitin ligase complex. Thus, SLF is thought to function in ubiquitin-mediated proteolysis, with its primary (if not only) target being self S-RNase (i.e., the S-RNase encoded by the same *S* haplotype). Indeed, SLF binds to E3 ligase complex components (Qiao *et al.* 2004; Hua & Kao 2006), and proteasomal inhibitor treatment causes inhibition of compatible, but not incompatible, pollen tubes (Qiao *et al.* 2004). Furthermore, S-RNase and SLF interact. However, while Qiao *et al.* (2004) concluded that their interaction is not allele-specific, i.e., SLF binds to both self and non-self S-RNase, Kubo *et al.* (2010) concluded that each SLF protein does not bind to its cognate S-RNase and instead interacts with a subset of non-self S-RNase proteins. Due to this and other discrepant results, there is still much debate about how these *S*-locus proteins mediate specific RNA degradation and arrest of self pollen tubes.

One scenario is that SLF interacts with any S-RNase that is taken up by the pollen tube, but that only non-self S-RNase molecules are ubiquitinated and degraded, while self S-RNase is protected and remains competent for RNA degradation, either by an additional *S* haplotype-specific interaction with its cognate SLF or by interaction with a putative unknown molecule. However, deletion of the *SLF* gene does not cause the constitutive rejection of self and non-self pollen predicted by this scenario (Sonneveld *et al.* 2005). To accommodate this result, one model of S-RNase-based SI (Figure 4, Model 1) involves non-self recognition. Each *S* haplotype consists of one *S-RNase* and several types of *SLF* genes. Transformation and co-immunoprecipitation experiments revealed that multiple SLF proteins function together as the

Figure 4. RNase-based inhibition of self pollen tubes in the style of the nightshade, rose, and snapdragon families.
The diagram shows S_1 (self) pollen tubes growing intercellularly through the style of an S_1S_2 plant. The diploid style secretes two S-RNase variants (represented by different colors) into the extracellular matrix of the transmitting tract. The S-RNases are taken up non-specifically by pollen tubes, where they interact with their cognate SLF. Each pollen tube expresses SLF derived from one haplotype encoded its own haploid genotype. Two current models of self pollen tube inhibition are shown, both of which attempt to explain how the cytotoxic action of S-RNases is averted in non-self pollen tubes and how the interaction of SLF with S-RNases within the pollen tube results in degradation of cellular RNA in self pollen tubes. Model 1 postulates that several different SLF proteins from one *S* haplotype are each capable of recognizing and inactivating several non-self S-RNases, but not self S-RNase from the same haplotype, thereby maintaining self S-RNase in an active form that is competent for RNA degradation. Model 2 is more complex and invokes dynamic changes in the subcellular localization of S-RNases, effected largely by HT-B, a protein that is secreted by the style and is required for SI. As described in the text, the major postulates of this model are: (1) S-RNases are sequestered within vesicular compartments in pollen tubes; (2) in non-self pollen tubes, S-RNases remain sequestered and any that might escape these compartments are eliminated by a general surveillance system; (3) in self pollen tubes, allele-specific S-RNase−SLF interaction would protect the S-RNase from degradation, cause stabilization of HT-B, which in turn would cause disintegration of S-RNase compartments, release of the S-RNases, and RNA degradation.

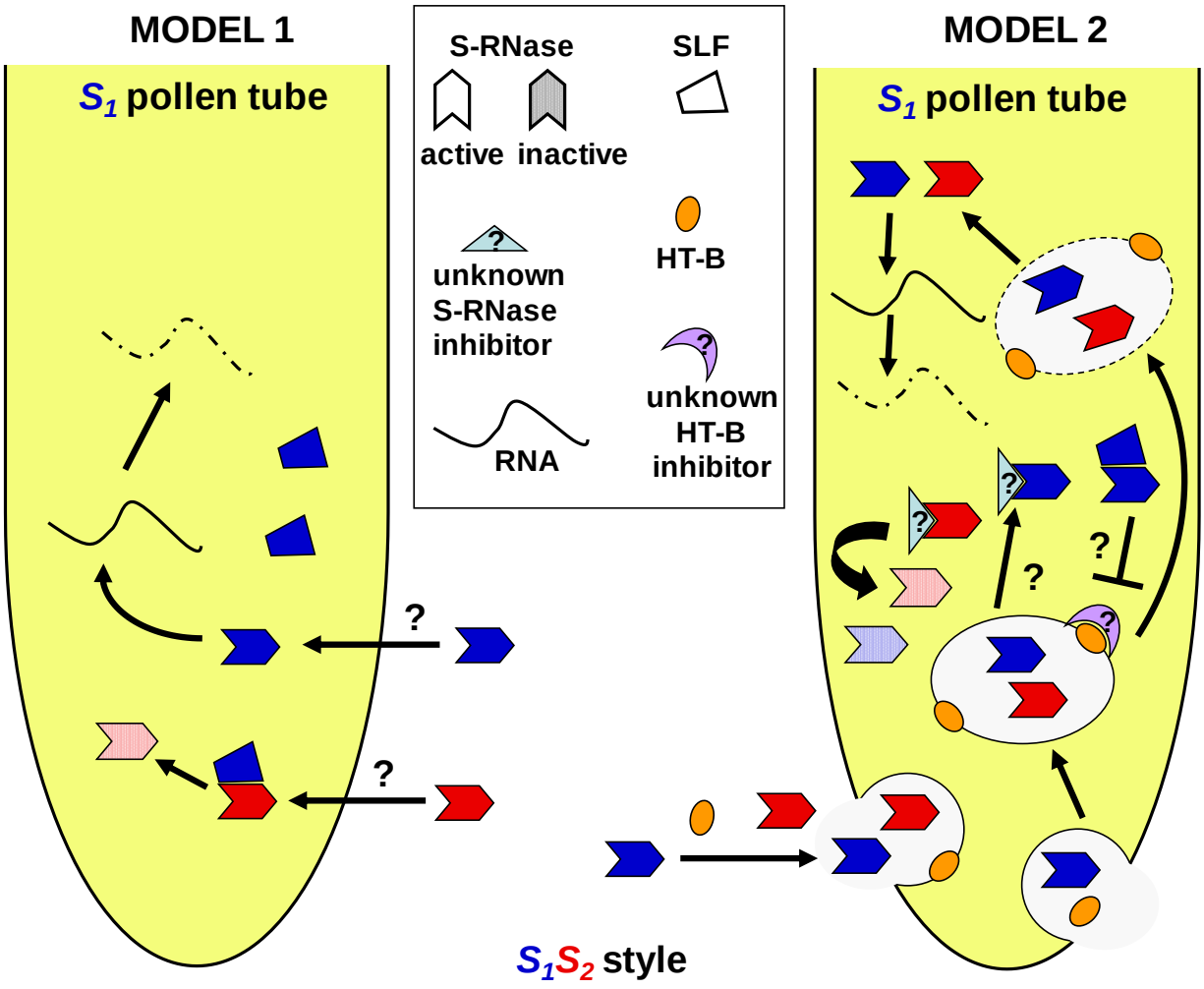
MODEL 1
S1 pollen tube
S-RNase
SLF
active
inactive
unknown
S-RNase
inhibitor
HT-B
unknown
HT-B
inhibitor
RNA
MODEL 2
S1 pollen tube
?
?
?
?
?
?
?
S1S2 style

male determinant, and each recognizes a subset of non-self S-RNases, resulting in their inactivation (Kubo *et al.* 2010). Non-self inhibition would therefore be prevented by loss of one SLF protein if at least one of the other SLF proteins would still be able to inactivate the non-self S-RNases. It follows that self pollen tube growth would be inhibited, on the other hand, because none of the SLF proteins would recognize self S-RNase, leaving it activated to degrade the pollen tube RNA. Support for this model also comes from the finding that self-incompatible pollen had higher S-RNase levels than compatible pollen (Qiao *et al.* 2004).

A weakness of this model is that it fails to accommodate a role for three stylar proteins known to be required for self pollen tube inhibition: the small, asparagine-rich HT-B protein; the 120K glycoprotein, which like S-RNases is taken up non-specifically into the pollen tube; and factor 4936 (Lind *et al.* 1996; McClure *et al.* 1999, 2000; O'Brien *et al.* 2002; Hancock *et al.* 2005). It also does not account for the recently observed dynamic subcellular distribution of S-RNases in pollen tubes. In contrast to the results obtained by Qiao *et al.* (2004), it was found that S-RNases are not degraded after uptake into the pollen tube; rather, they are sequestered along with 120K glycoprotein within endomembrane vesicles in both self and non-self pollen tubes (Goldraij *et al.* 2006). As pollen tube growth progresses, these S-RNase-containing compartments break down in self pollen tubes, presumably releasing S-RNases into the cytoplasm, but they remain intact in non-self tubes. Loss of HT-B, factor 4936, or 120K (e.g., by mutation or down-regulation mediated by antisense or RNAi constructs; McClure *et al.* 1999, 2000; O'Brien *et al.* 2002; Hancock *et al.* 2005), which overcomes SI, also prevents disintegration of S-RNase compartments (Goldraij *et al.* 2006). Furthermore, HT-B accumulates to much lower levels in non-self compared to self tubes, suggesting that destabilization of HT-B is associated with successful pollen tube growth (Goldraij *et al.* 2006).

On the basis of these observations, a different model of S-RNase-based SI (Figure 4, Model 2) ascribes a major role for HT-B in the breakdown of S-RNase-containing compartments and release of sequestered S-RNases into the tube cytoplasm (Goldraij *et al.* 2006; McClure & Franklin-Tong 2006). This model proposes that HT-B enters the pollen tube along with the S-RNase (as well as 120K and factor 4936), and both molecules are sequestered via endocytosis into membrane-bound endosomes that fuse with vacuolar compartments. Since interaction between S-RNases and SLF presumably occurs in the cytoplasm, a small fraction of the S-RNases might exit the endomembrane system, possibly by retrograde transport into the endoplasmic reticulum and subsequent release. In non-self pollen tubes, the released S-RNases would be recognized and degraded by interaction with an unknown general S-RNase inhibitor, possibly a component of a cytoplasmic surveillance system that eliminates cytotoxic molecules. However, in self pollen tubes, allele-specific binding to cognate SLF would protect the released S-RNases from degradation and would lead to stabilization of HT-B, perhaps by SLF-mediated ubiquitination and subsequent degradation of an HT-B inhibitor. HT-B stabilization would somehow lead to endomembrane compartment breakdown, followed by en masse release of sequestered S-RNases that would be too abundant for effective general inhibitor surveillance, leaving the S-RNases active for RNA degradation. In non-self pollinations, the S-RNase–SLF interaction does not take place, HT-B is degraded and endomembrane integrity is maintained, thus keeping the majority of S-RNases sequestered and allowing pollen tube growth to proceed.

FUTURE PROSPECTS

A major insight obtained from the molecular analysis of a handful of SI systems was the realization that SI evolved multiple times during flowering plant evolution and that different

plant families use distinct molecules for recognition of self and different biochemical pathways to arrest self pollen tube development. Despite the substantial progress made in recent years, there are still glaring gaps in the collective understanding of SI mechanisms. While working models have been generated for each of the three SI systems discussed, it is still not possible, in any system, to explain exactly how recognition of self pollen by cells of the pistil translates into inhibition of pollen tube growth and ultimately, of self-fertilization.

New data generated by ongoing studies will no doubt require refinement of some models and may even cause major elements of other models to be discarded. Current research efforts are aimed at filling major gaps in each of the three SI systems, i.e., unraveling the events that are triggered subsequent to recognition in receptor-mediated crucifer and S-RNase-based SI, and identifying the mechanism by which self and non-self is distinguished in the S-RNase system. These are not the only remaining unresolved issues, however. In all three systems, very little is known about the basis of SI specificity in pistil and pollen determinants. Identifying the amino acid residues that determine specificity has proven difficult because of the extreme polymorphisms of *S*-locus proteins, not all of which are critical for specificity. To date, specificity-determining residues have been identified and experimentally validated for only two SCR variants in *Brassica* (Chookajorn *et al.* 2004; Sato *et al.* 2004), one *A. lyrata* and one *Capsella grandiflora* SRK variant (Boggs *et al.* 2009*a*), one S-RNase in *Solanum* (Matton *et al.* 1997), and no stigmatic S proteins in poppy. Compounding the difficulty of these studies is the finding that different amino-acid residues appear to determine the specificity of different variants, at least in the case of SCR (Chookajorn *et al.* 2004). Conversely, the specificity determinants of the two SRK variants tested appear to be localized to two overlapping regions (Boggs *et al.* 2009*a*). Irrespective of these discrepancies, however, progress on this front is

critical. Only then might it be possible to address the challenging question of how pistil and pollen SI determinants co-evolve to maintain their interaction and their competence for self or non-self recognition, and to solve the puzzle of how the large repertoire of SI specificities that exist in self-incompatible species is generated.

Part II:

A transgenic self-incompatible* Arabidopsis thaliana *model for evolutionary and mechanistic studies of crucifer self-incompatibility

ABSTRACT

Molecular genetic studies of self-incompatibility (SI) can be difficult to perform in non-model self-incompatible species. Recently, an *Arabidopsis thaliana* transgenic model was developed for analysis of the SI system that operates in the Brassicaceae by inter-species transfer of genes encoding the *S*-locus receptor kinase (SRK) and its ligand, the *S*-locus cysteine-rich (SCR) protein, which are the determinants of SI specificity in stigma and pollen, respectively. The many advantages of *A. thaliana* and the extensive tools and resources available in this model species have allowed the use of transgenic self-incompatible *SRK-SCR* plants to address long-standing issues related to the mechanism and evolution of SI in the Brassicaceae. A candidate gene approach can also be utilized for determining if genes related to genes previously reported to be involved in the SI response of *Brassica* are required for SI in *A. thaliana.* These various studies have provided novel insight into the basis of specificity in the SRK-SCR interaction, the nature of the signaling cascade that culminates in inhibition of "self" pollen, and the

physiological and morphological changes that are associated with transitions between the outbreeding and inbreeding modes of mating in the Brassicaceae.

INTRODUCTION

The large arsenal of genetic and molecular resources available in *Arabidopsis thaliana* have made this species the model of choice for analysis of a large variety of physiological, developmental, and evolutionary processes. However, there are limits to the usefulness of *A. thaliana*, because some biological phenomena do not occur in this model species. One phenomenon for which the *A. thaliana* model seems at first glance inappropriate is self-incompatibility (SI). Although operative in several species of the genus *Arabidopsis*, SI has not been reported in *A. thaliana*, and all of the hundreds of its accessions collected from various geographical locations are highly self-fertile. Indeed, all *A. thaliana* accessions analyzed to date contain non-functional versions of one or both of the two *S*-locus-encoded proteins whose allele-specific interaction determines SI specificity in the Brassicaceae (crucifers): the *S*-locus receptor kinase (SRK), which is displayed at the stigma surface, and the *S*-locus cysteine-rich (SCR) protein (also designated SP11; Takayama *et al.* 2001), which is located in the pollen coat and is the ligand of the SRK receptor (reviewed in Rea & Nasrallah 2008). However, transgenic inter-specific and inter-generic complementation experiments demonstrated the transfer of the SI trait into *A. thaliana* by transformation with *SRK-SCR* gene pairs isolated from the self-incompatible crucifers *A. lyrata* or *Capsella grandiflora* (Figure 5) (Nasrallah *et al.* 2002, 2004; Boggs *et al.* 2009*b*, *c*). This transgenic self-incompatible *A. thaliana* model, which has taken several years to develop, is now beginning to fulfill its promise and yield important results related to the evolution and mechanism of the self-incompatibility response of the Brassicaceae.

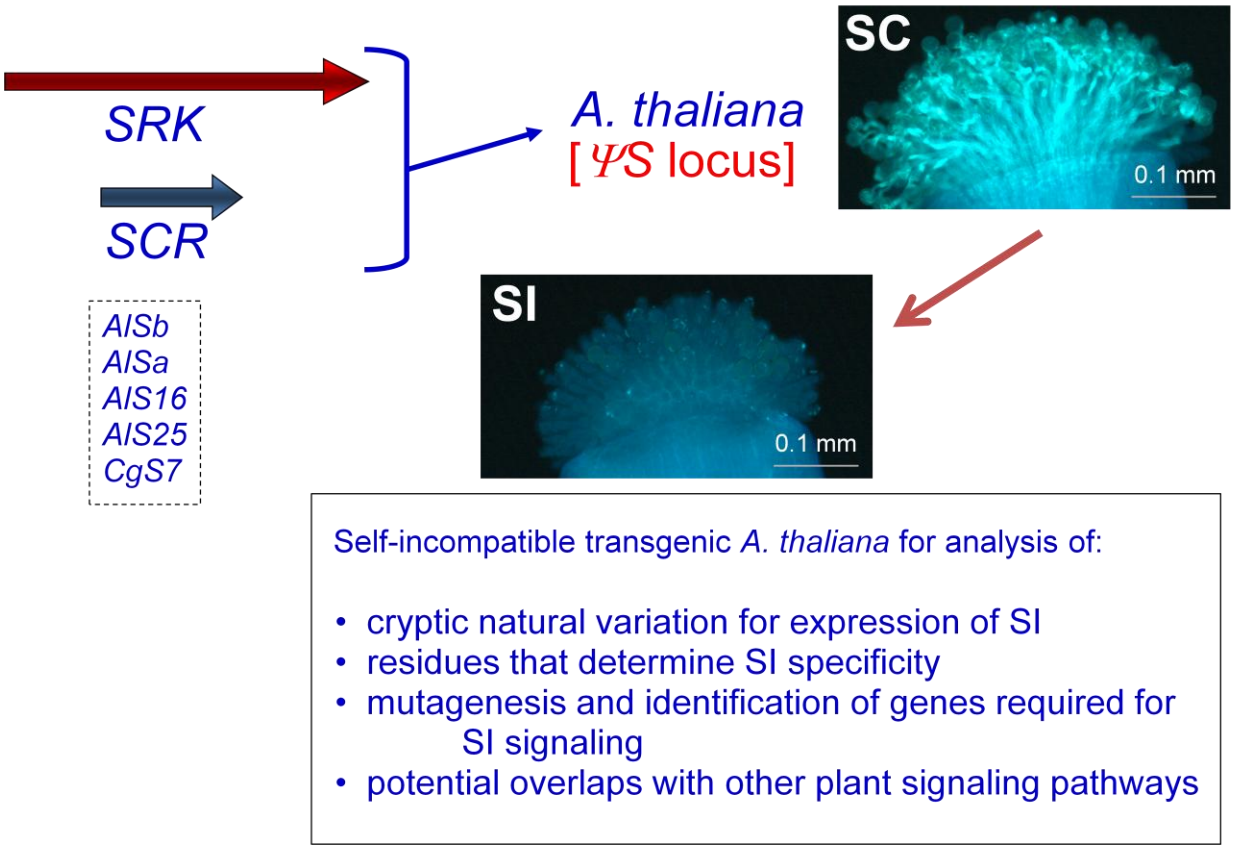

Figure 5. Transfer of the SI trait into *A. thaliana*.
The diagram shows that transfer of *SRK-SCR* gene pairs isolated from several *S* haplotypes of *Arabidopsis lyrata* (*AlSb*, *AlSa*, *AlS16*, and *AlS25*) or *Capsella grandiflora* (*CgS7*) converts the self-compatible (SC) *A. thaliana* plant, which typically produces numerous pollen tubes upon self-pollination (SC panel), into a self-incompatible (SI) plant, the stigmas of which inhibit the development of pollen tubes upon self-pollination (SI panel). The various questions that are being addressed using *A. thaliana SRK-SCR* transgenic plants are listed. Scale bars on micrographs = 100 µm.

INVESTIGATING EVOLUTIONARY SWITCHES TO SELF-FERTILITY AND DIVERSIFICATION OF THE SI RECOGNITION REPERTOIRE

The switch to self-fertility in *A. thaliana*

One set of studies used the self-incompatible transgenic *SRK-SCR A. thaliana* model in conjunction with the large numbers of *A. thaliana* geographical accessions available through stock centers to investigate issues related to mating system evolution in the Brassicaceae. Transformation of several of these accessions with *A. lyrata SRK-SCR* genes uncovered substantial cryptic natural variation in expression of SI (Figure 5) (Nasrallah *et al.* 2002, 2004; Boggs *et al.* 2009*c*). *SRK-SCR* transformants of some accessions expressed a robust and developmentally-stable SI phenotype similar to that observed in naturally self-incompatible species, and these accessions are inferred to have become self-fertile as a direct result of inactivation of the *S* locus. In contrast, *SRK-SCR* transformants of other accessions expressed transient SI (i.e., stigmas of young floral buds expressed strong SI, which broke down in older flowers) similar to many naturally-occurring pseudo-self-compatible plants, and still other accessions expressed only weak SI or no SI (Figure 6). The latter accessions are inferred to carry inactive alleles of SI modifier genes (i.e., genes that are required for SI but are located outside the *S* locus proper) in addition to having a non-functional *S*-locus, and it is impossible at present to determine if the initial loss of SI in these accessions was caused by a mutation at the *S* locus or at a modifier locus. In any case, the observation that *A. thaliana* harbors polymorphisms at the *S* locus and at SI modifier loci (Sherman-Broyles *et al.* 2007; Tang *et al.* 2007; Boggs *et al.* 2009*c*) strongly suggests that the species transitioned to self-fertility multiple times, and that loss of SI was caused by independent mutations in different geographical accessions.

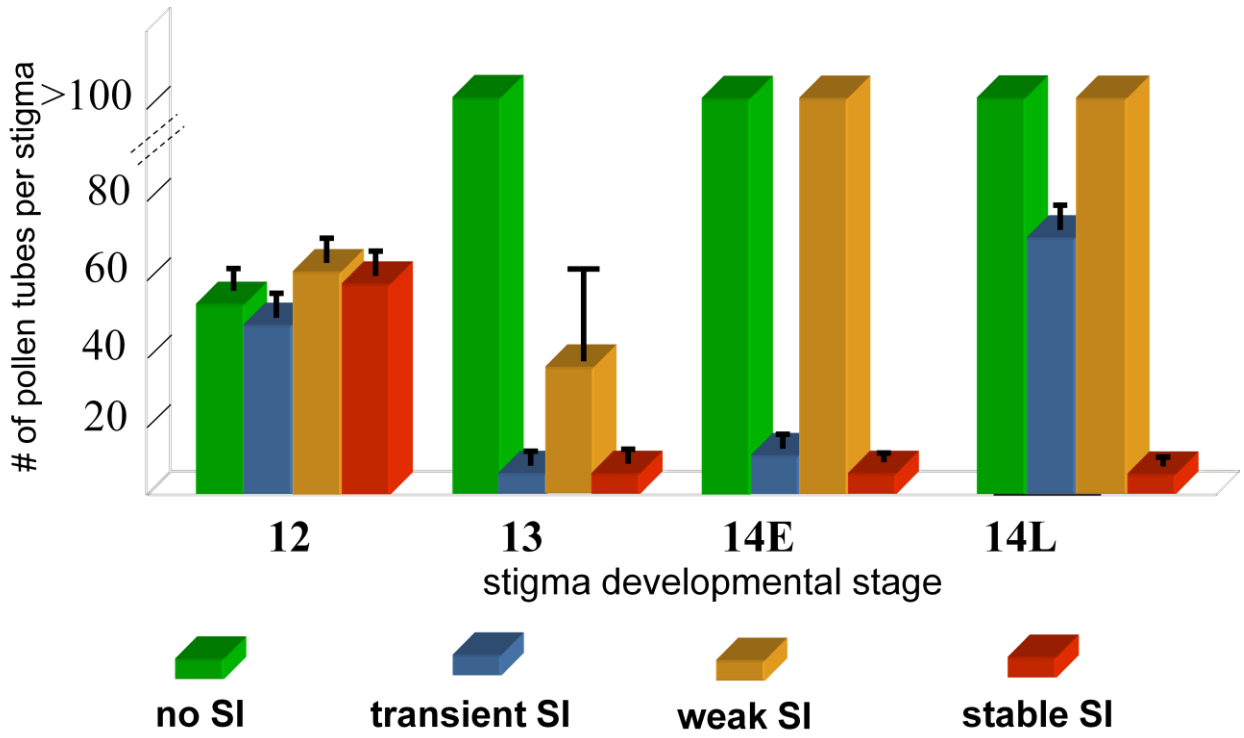

Figure 6. Cryptic natural variation for expression of SI in *SRK-SCR* transformants of various *A. thaliana* accessions.
The histogram shows that *SRK-SCR* transformants of various *A. thaliana* accessions vary for the strength or stability of SI expression as described in Nasrallah *et al.* 2004 and Boggs *et al.* 2009*c*. X-axis: stigmas from floral buds at different stages of development numbered according to Smyth *et al.* 1990 and Nasrallah *et al.* 2002. Y-axis: number of pollen tubes produced upon self-pollination at each stage of stigma development. Note that some accessions express a robust and developmentally-stable SI response identical to that observed in naturally self-incompatible plants (i.e., numerous pollen tubes in immature stigmas but very few pollen tubes in mature stigmas upon self-pollination). In contrast, other accessions exhibit only weak SI (manifested by the escape of a substantial number of pollen tubes upon self-pollination at all stages of stigma development) or transient SI (manifested by robust SI in stage-13 and early stage-14 (14E) stigmas, followed by breakdown of SI in older stigmas).

Crosses between accessions that differed in expression of SI demonstrated the segregation of recessive "self-fertility" alleles at several loci (Liu *et al.* 2007; Boggs *et al.* 2009*c*). Analysis of an inter-accession cross between C24, which expresses developmentally-stable SI, and RLD, which expresses transient SI, showed that transient SI is caused by a hypomorphic allele of *PUB8*, a gene located at one boundary of the *S* locus that encodes a previously uncharacterized Arm-repeat- and U-box-containing protein that regulates *SRK* transcript levels (Liu *et al.* 2007). This result underscores the conclusion that disruption or down-regulation of the *S*-locus recognition genes, particularly of *SRK*, was a major mechanism for the switch to self-fertility in *A. thaliana*.

Identification of amino-acid residues that determine SRK specificity

Another series of experiments that used the *A. thaliana SRK-SCR* model investigated the basis of SRK specificity and diversification of the SI recognition repertoire. It had been known for several years that specificity in the SI response was based on allele-specific interactions between the highly polymorphic SRK and SCR proteins (Kachroo *et al.* 2001; Takayama *et al.* 2001), whereby an SCR protein can bind and activate the SRK protein encoded in the same *S*-locus haplotype, but not SRK proteins encoded in other *S* haplotypes. A major unanswered question in SI research is how the large numbers of extant SRK and SCR variants have co-evolved to maintain their highly specific interaction and more generally, how new SI specificities were generated. To gain insight into this question, it is important to identify the amino-acid residues that determine specificity in the SRK-SCR interaction. This issue was partially addressed for SCR by analysis in *Brassica*, which identified the few residues that are responsible for specificity in some SCR variants (Chookajorn *et al.* 2004; Sato *et al.* 2004). In the case of

SRK, hypervariable regions (Figure 7) and amino-acid residues bearing signals of positive selection had been identified within the extracellular ligand-binding domain and inferred to function as specificity determinants (Miege *et al.* 2001; Schierup *et al.* 2001; Charlesworth *et al.* 2003; Sainudiin *et al.* 2005). However, no studies had demonstrated empirically how many and which of these residues are responsible for SI specificity, largely due to technical difficulties in implementing the necessary experiments. Identification of specificity-determining residues requires *in planta* analysis of large numbers of receptor variants generated by domain swapping or site-directed mutagenesis of individual residues that differ between pairs of SRK variants. Such analyses are impractical to perform in naturally self-incompatible species such as *Brassica* species and *A. lyrata*, due to the laborious or inefficient transformation methods available for these species. In contrast, *A. thaliana* is easily and efficiently transformed by the *Agrobacterium*-mediated floral dip method, and is ideally suited for these studies.

A pre-requisite for identifying residues important for SRK specificity in the *A. thaliana* self-incompatible model requires expression of different SI specificities in this species. Accordingly, several *SRK-SCR* gene pairs derived from *A. lyrata* or *C. grandiflora* were isolated and tested for functionality in transgenic *A. thaliana* (Boggs *et al.* 2009*a*). Out of five different functional *SRK-SCR* gene pairs (Figure 5), two pairs were subjected to detailed site-directed mutagenesis of polymorphic residues within the SRK extracellular domain. *In planta* analysis of these SRK sequence variants showed that the majority of SRK residues previously reported to show signals of positive selection are not essential for specificity in the SRK-SCR interaction (Boggs *et al.* 2009*a*). Indeed, out of the approximately 100 polymorphic amino-acid residues that differed between the extracellular domains of the two pairs of SRK variants analyzed, only 6 or 7 residues were found to be required for ligand-specific activation of the SI response (Boggs *et al.*

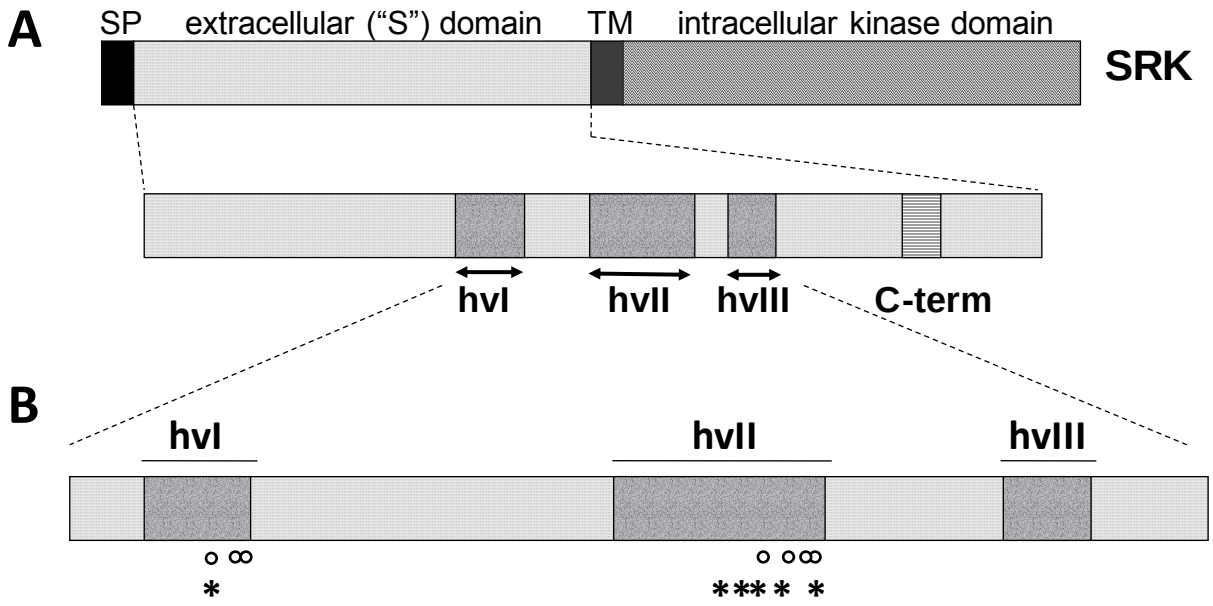

Figure 7. Structure of SRK and amino-acid residues required for SI in the SRK extracellular domain.
(A) Structure of the SRK protein (top), consisting of the N-terminal signal peptide (SP), the extracellular ("S") domain (detailed on bottom), the transmembrane domain (TM), and the intracellular kinase domain. The location within the S domain of the hypervariable regions (hvI, hvII, hvIII, and the C-terminal variable region) that are enriched for variable amino-acid residues is shown. **(B)** Amino-acid residues required for SI specificity. Residues essential for SI were identified by *in planta* analysis of site-directed SRK mutants (see Boggs *et al.* 2009*a* for details). Circles and asterisks correspond to the approximate locations of residues essential for SRK7 and SRK25 function, respectively. Note that these residues are located in overlapping segments of the hvI and hvII regions in the two SRK variants analyzed. Diagrams are not drawn to scale.

2009*a*). As shown in Figure 7, these residues are clustered within two non-contiguous regions located at equivalent positions in the two variants tested, and these sites were also found to be highly polymorphic in other SRK proteins. These results suggest that for the majority, if not all, of SRK variants, specificity is determined primarily by short stretches of amino-acid residues located in these non-contiguous regions. High-resolution structural analysis of the SRK protein in its ligand-bound and unbound forms is required to determine if these regions are surface-exposed and are brought into close proximity in the three-dimensional SRK structure to form part of an SCR-binding pocket.

MUTATIONAL ANALYSIS OF SI

A. thaliana SRK-SCR transformants, specifically those expressing transient SI such as the Col accession, are particularly useful for mutational analysis of SI in search of genes required for full expression of this trait. Because Col *SRK-SCR* plants set abundant seed, they may be subjected to chemical mutagenesis using the standard protocols typically used in *A. thaliana.* Ethyl methane sulfonate mutagenesis of these plants did, indeed, produce mutations that affect the SI response, some of which caused loss of SI in young floral bud stigmas, while others caused enhancement of SI in older flower stigmas. Positional cloning of an enhancer mutation identified the RNA-dependent RNA polymerase RDR6, which functions in *trans*-acting siRNA (ta-siRNA) production, as a negative regulator of SI (Tantikanjana *et al.* 2009). Interestingly, this recessive enhancer mutation has pleiotropic effects: it simultaneously enhances SI and causes stigma exsertion, without associated increases in *SRK* transcript levels. Although *rdr6* mutants had been shown previously to exhibit stochastic stigma exsertion (Peragine *et al.* 2004), analysis of the *SRK-SCR rdr6* plants demonstrated that SRK further enhances pistil elongation and stigma

exsertion in this mutant background. Interestingly, this enhancement requires SRK catalytic activity and its extent is positively correlated with *SRK* transcript levels (Tantikanjana *et al.* 2009). Thus, the *rdr6* mutation revealed that, in addition to functioning in SI, SRK plays a previously-unsuspected role in pistil development. It has been observed that changes in floral architecture, including stigma exsertion, often accompany transitions between the out-crossing and selfing modes of mating (Barrett 2002; Goodwillie *et al.* 2010). The dual role of SRK in SI and pistil development revealed by the *rdr6* mutation provides a molecular explanation for this poorly-understood coordinate evolution of physiological and morphological traits. The data further suggest that positive regulators or effectors of SI and pistil development are regulated by ta-siRNA(s). Identifying the targets of these ta-siRNAs is expected to illuminate the mechanism of SI and the molecular overlaps between signaling at the stigma surface and the pistil developmental pathway.

EXPLORING SRK-MEDIATED SIGNALING USING A CANDIDATE GENE APPROACH

Analysis of SI signaling components: the case of ARC1, Exo70A1, and MLPK

As discussed in Part I, ARC1, Exo70A1, and MLPK have been proposed to function as components of SRK-mediated signaling. The availability of transgenic self-incompatible *A. thaliana* plants allowed a test of the involvement of these genes in SI.

A. thaliana genes that exhibit the highest degree of sequence similarity to *Brassica ARC1* and *MLPK*, *AtPUB17* (At1g29340) and *APK1b* (At2g28930), respectively, were tested for their requirement for SI in *A. thaliana* by acquiring separate T-DNA insertion lines that inactivate these genes and crossing them to *A. thaliana* plants containing *SRK* and *SCR* driven by their native promoters (Rea *et al.* 2010; Kitashiba *et al.* 2011). The robust SI response of *SRKb-SCRb*

plants homozygous for the T-DNA insertions was identical to that of *SRKb-SCRb* plants lacking the T-DNA insertions (Rea *et al.* 2010; Kitashiba *et al.* 2011). A gene related to *APK1b*, *APK1a*, was also tested for its involvement in SI by crossing *A. thaliana* transformed with an artificial miRNA transgene that caused reduced *APK1a* transcripts to *A. thaliana* plants containing *SRKb-SCRb* (Kitashiba *et al.* 2011). The presence of the artificial miRNA transgene had no effect on the strength of the SI response in *SRKb-SCRb* plants (Kitashiba *et al.* 2011). This result indicates either that these *A. thaliana* genes are not required for SI or that their role in SI is masked by the redundant activities of other genes. It was determined, however, that *APK1b* resides in a chromosomal region that exhibits synteny between *Brassica* and *A. thaliana*, indicating that it is the likely *A. thaliana* ortholog of *MLPK* (Kitashiba *et al.* 2011). In addition, comparative genomic analysis among *Brassica*, *A. lyrata*, and *A. thaliana* determined that the likely *A. thaliana* ortholog of *ARC1* is a pseudogene. Finally, the likely *A. thaliana* ortholog of *Brassica Exo70A1*, *AtExo70A1*, was identified based on synteny and extent of sequence similarity, and its overexpression in transgenic self-incompatible *A. thaliana* had no weakening effect on SI (Kitashiba *et al.* 2011), in contrast to what was found in *Brassica* (Samuel *et al.* 2009). Therefore, genes identified in *Brassica* to be involved in SI do not seem to be involved in SI in *A. thaliana*.

Interestingly, even within the *Brassica* genus, some results do not support the involvement of previously-identified genes in SI. For example, *B. rapa* plants homozygous for a hypomorphic *ARC1* allele were found to exhibit a 10-fold reduction in *ARC1* transcripts as compared to *B. rapa* plants homozygous for a different allele (Rea *et al.* 2010). However, both genotypes exhibited an equally robust SI response (Rea *et al.* 2010). Because the level of reduction in *ARC1* transcripts is equivalent to that seen in *ARC1* antisense lines of *B. napus*,

which exhibit a weakening of the SI response, these results suggest either that *ARC1* is not involved in SI in the *B. rapa* species, or more likely, that the *B. napus* antisense lines are reducing expression of a gene other than *ARC1* involved in the SI response (Rea *et al.* 2010).

Taken together, these results suggest that neither *ARC1* nor *MLPK* are likely to be involved in the common SI mechanism of the Brassicaceae.

CONCLUSIONS AND PERSPECTIVES

The transgenic self-incompatible *A. thaliana SRK-SCR* model is beginning to fulfill its promise as an excellent platform for investigating SI in the Brassicaceae. The transfer of several different SI specificities into *A. thaliana*, combined with the ability to generate large numbers of transformants and to perform efficient map-based cloning of induced and spontaneous mutations in this model species, has permitted the ability to address longstanding issues in SI research. Analysis of *SRK-SCR* transformants has elucidated aspects of the evolution of self-fertility in *A. thaliana*, and more generally, the physiological and morphological changes that are associated with transitions between the out-crossing and inbreeding modes of mating in the Brassicaceae. *In planta* functional assays of site-directed SRK variants has pinpointed domains and amino acids responsible for SRK specificity. Chemical mutagenesis of *SRK-SCR* plants and analysis of the cryptic natural variation for expression of SI that differentiates various accessions have identified novel genes required for SI. Additionally, the wealth of insertional mutations available in *A. thaliana* has allowed the use of a candidate gene approach to assess the role in SI of the *A. thaliana* genes most closely related to genes previously reported to function in the SI response of *Brassica*. None of the genes tested by this approach were found to be required for SI, a result that was unexpectedly corroborated in the case of *ARC1* in *B. rapa.* Additional studies involving

gene-silencing approaches, which are easily performed in the *A. thaliana* model, are required to exclude the possibility of genetic redundancy and provide definitive evidence for or against the involvement of specific genes in SI. There is every expectation that future molecular genetic studies of the *A. thaliana SRK-SCR* transgenic plants will continue to provide important insight into the mechanism and evolution of SI.

Part III:

Aims of dissertation

This dissertation describes experiments aimed at investigating several outstanding questions in self-incompatibility (SI) research using the transgenic self-incompatible *A. thaliana* system.

In Chapter 2, the use of a candidate gene approach was employed to assess the role in SI of the putative *A. thaliana* orthologs of *Brassica* genes previously identified as being involved in SI signaling, by generating knock-down mutations by antisense down-regulation or by analyzing T-DNA insertional mutants. In addition, parallels between SI and plant immunity (PI) prompted the use of null point mutations in genes known to be components of the various PI pathways in order to potentially identify SI pathway genes. Due to their seemingly dual roles in both SI and PI, candidate AtPUB proteins were tested for their ability to interact with the SRKb kinase domain in a heterologous yeast system. Furthermore, the *AtPUB8* gene, identified as a regulator of *SRK* transcript levels in transgenic self-incompatible *A. thaliana*, was used to screen a cDNA library for potential protein interaction partners in yeast. Finally, a stigma-specific, highly-

expressed gene was analyzed for a potential role in SI or compatible pollination by analysis of a T-DNA insertion strain.

In Chapter 3, confocal microscopic studies were employed to visualize the distribution and localization patterns of fluorescent-protein-tagged SRKb protein in stigma epidermal cells. Co-localization of SRKb with various organelle-specific markers and plasmolysis experiments were performed, and protein dynamics were examined in both unpollinated and self- and cross-pollinated stigmas. Confocal imaging parameters were established that were vital to the interpretation of subcellular localization patterns of organelles and proteins in stigma epidermal cells. Moreover, comparisons between stigma and leaf epidermal cells were made in order to aid in the interpretation of protein localization results.

The results presented in this dissertation should aid in the future understanding of the SI mechanism utilized in the Brassicaceae family.

REFERENCES

Azevedo C, Santos-Rosa MJ, Shirasu K. 2001. The U-box protein family in plants. *Trends in Plant Science* **6**, 354-358.

Barrett SCH. 2002. The evolution of plant sexual diversity. *Nature Reviews Genetics* **3**, 274-284.

Boggs NA, Dwyer KG, Nasrallah ME, Nasrallah JB. 2009*a*. In vivo detection of residues required for ligand-selective activation of the S-locus receptor in *Arabidopsis*. *Current Biology* **19**, 786-791.

Boggs NA, Dwyer KG, Shah P, McCulloch AA, Bechsgaard J, Schierup MH, Nasrallah ME, Nasrallah JB. 2009*b*. Expression of distinct self-incompatibility specificities in *Arabidopsis thaliana. Genetics* **182**, 1313-1321.

Boggs NA, Nasrallah JB, Nasrallah ME. 2009*c*. Independent *S*-locus Mutations Caused Self-Fertility in *Arabidopsis thaliana*. *PLoS Genetics* **5**, e1000426.

Booy G, Krens FA, Bino RJ. 1992. Analysis of pollen-tube growth in cultured maize silks. *Sexual Plant Reproduction* **5**, 227-231.

Bower MS, Matias DD, Fernandes-Carvalho E, Mazzurco M, Gu T, Rothstein SJ, Goring DR. 1996. Two Members of the Thioredoxin-h Family Interact with the Kinase Domain of a *Brassica S* Locus Receptor Kinase. *The Plant Cell* **8**, 1641-1650.

Cabrillac D, Cock JM, Dumas C, Gaude T. 2001. The *S*-locus receptor kinase is inhibited by thioredoxins and activated by pollen coat proteins. *Nature* **410**, 220-223.

Charlesworth D, Bartolomé C, Schierup MH, Mable BK. 2003. Haplotype Structure of the Stigmatic Self-Incompatibility Gene in Natural Populations of *Arabidopsis lyrata*. *Molecular Biology and Evolution* **20**, 1741–1753.

Chookajorn T, Kachroo A, Ripoll DR, Clark AG, Nasrallah JB. 2004. Specificity determinants and diversification of the *Brassica* self-incompatibility pollen ligand. *Proceedings of the National Academy of Sciences of the United States of America* **101**, 911-917.

Darwin C. 1876. The effects of cross and self fertilisation in the vegetable kingdom. J. Murray, London.

Dickinson H. 1995. Dry stigmas, water and self-incompatibility in *Brassica*. *Sexual Plant Reproduction* **8**, 1-10.

Ebert PR, Anderson MA, Bernatzky R, Altschuler M, Clarke AE. 1989. Genetic Polymorphism of Self-Incompatibility in Flowering Plants. *Cell* **56**, 255-262.

Franklin-Tong VE, Holdaway-Clarke TL, Straatman KR, Kunkel JG, Hepler PK. 2002. Involvement of extracellular calcium influx in the self-incompatibility response of *Papaver rhoeas*. *The Plant Journal* **29**, 333-345.

Geitmann A. 1999. Cell Death of Self-Incompatible Pollen Tubes: Necrosis or Apoptosis? *In* Fertilization in Higher Plants: Molecular and Cytological Aspects. Cresti M., Cai G, Moscatelli A. [eds.], Springer-Verlag, Berlin, Heidelberg, New York. 113-137.

Giranton J-L, Dumas C, Cock JM, Gaude T. 2000. The integral membrane *S*-locus receptor kinase of *Brassica* has serine/threonine kinase activity in a membranous environment and spontaneously forms oligomers *in planta*. *Proceedings of the National Academy of Sciences of the United States of America* **97**, 3759-3764.

Goldraij A, Kondo K, Lee CB, Hancock CN, Sivaguru M, Vazquez Santana S, Kim S, Phillips TE, Cruz-Garcia F, McClure B. 2006. Compartmentalization of S-RNase and HT-B degradation in self-incompatible *Nicotiana*. *Nature* **439**, 805-810.

Goodwillie C, Sargent RD, Eckert CG, Elle E, Geber MA, Johnston MO, Kalisz S, Moeller DA, Ree, RH, Vallejo-Marin M, Winn AA. 2010. Correlated evolution of mating system and floral display traits in flowering plants and its implications for the distribution of mating system variation. *New Phytologist* **185**, 311-321.

de Graaf BHJ, Rudd JJ, Wheeler MJ, Perry RM, Bell EM, Osman K, Franklin FCH, Franklin-Tong VE. 2006. Self-incompatibility in *Papaver* targets soluble inorganic pyrophosphatases in pollen. *Nature* **444**, 490-493.

Gu T, Mazzurco M, Sulaman W, Matias, DD, Goring DR. 1998. Binding of an arm repeat protein to the kinase domain of the *S*-locus receptor kinase. *Proceedings of the National Academy of Sciences of the United States of America* **95**, 382-387.

Haffani YZ, Gaude T, Cock JM, Goring DR. 2004. Antisense suppression of thioredoxin *h* mRNA in *Brassica napus cv.* Westar pistils causes a low level constitutive pollen rejection response. *Plant Molecular Biology* **55**, 619-630.

Hancock CN, Kent L, McClure BA. 2005. The stylar 120 kDa glycoprotein is required for *S*-specific pollen rejection in *Nicotiana*. *The Plant Journal* **43**, 716-723.

Hearn MJ, Franklin FCH, Ride JP. 1996. Identification of a membrane glycoprotein in pollen of *Papaver rhoeas* which binds stigmatic self-incompatibility (S-) proteins. *The Plant Journal* **9**, 467-475.

Hua Z, Kao T-H. 2006. Identification and Characterization of Components of a Putative *Petunia S*-Locus F-Box-Containing E3 Ligase Complex Involved in S-RNase-Based Self-Incompatibility. *The Plant Cell* **18**, 2531-2553.

Jordan ND, Franklin FCH, Franklin-Tong VE. 2000. Evidence for DNA fragmentation triggered in the self-incompatibility response in pollen of *Papaver rhoeas*. *The Plant Journal* **23**, 471-479.

Jordan ND, Kakeda K, Conner A, Ride JP, Franklin-Tong VE, Franklin FCH. 1999. S-protein mutants indicate a functional role for SBP in the self-incompatibility reaction of *Papaver rhoeas*. *The Plant Journal* **20**, 119-125.

Kachroo A, Schopfer CR, Nasrallah ME, Nasrallah, JB. 2001. Allele-specific receptor-ligand interactions in *Brassica* self-incompatibility. *Science* **293**, 1824-1826.

Kakita M, Murase K, Iwano M, Matsumoto T, Watanabe M, Shiba H, Isogai A, Takayama S. 2007. Two Distinct Forms of *M*-Locus Protein Kinase Localize to the Plasma Membrane and Interact Directly with *S*-Locus Receptor Kinase to Transduce Self-Incompatibility Signaling in *Brassica rapa*. *The Plant Cell* **19**, 3961-3973.

Kitashiba H, Liu P, Nishio T, Nasrallah JB, Nasrallah ME. 2011. Functional test of *Brassica* self-incompatibility modifiers in *Arabidopsis thaliana*. *Proceedings of the National Academy of Sciences of the United States of America* **44**, 18173-18178.

Kubo K, Entani T, Takara A, Wang N, Fields AM, Hua Z, Toyoda M, Kawashima S, Ando T, Isogai A, Kao T, Takayama S. 2010. Collaborative Non-Self Recognition System in S-RNase−Based Self-Incompatibility. *Science* **330**, 796-799.

Lai Z, Ma W, Han B, Liang L, Zhang Y, Hong G, Xue Y. 2002. An F-box gene linked to the self-incompatibility (*S*) locus of *Antirrhinum* is expressed specifically in pollen and tapetum. *Plant Molecular Biology* **50**, 29-42.

Lee H-S, Huang S, Kao T-H. 1994. S proteins control rejection of incompatible pollen in *Petunia inflata*. *Nature* **367**, 560-563.

Lind JL, Bönig I, Clarke AE, Anderson MA. 1996. A style-specific 120 kDa glycoprotein enters pollen tubes of *Nicotiana alata* in vivo. *Sexual Plant Reproduction* **9**, 75-86.

Liu P, Sherman-Broyles S, Nasrallah ME, Nasrallah JB. 2007. A cryptic modifier causing transient self-incompatibility in *Arabidopsis thaliana*. *Current Biology* **17**, 734-740.

Lush WM, Clarke AE. 1997. Observations of pollen tube growth in *Nicotiana alata* and their implications for the mechanism of self-incompatibility. *Sexual Plant Reproduction* **10**, 27-35.

Luu D-T, Qin X, Morse D, Cappadocia M. 2000. S-RNase uptake by compatible pollen tubes in gametophytic self-incompatibility. *Nature* 407: 649-651.

Matton DP, Maes O, Laublin G, Xike Q, Bertrand C, Morse D, Cappadocia M. 1997. Hypervariable Domains of Self-Incompatibility RNases Mediate Allele-Specific Pollen Recognition. *The Plant Cell* **9**, 1757-1766.

McClure B, Mou B, Canevascini S, Bernatzky R. 1999. A small asparagine-rich protein required for S-allele-specific pollen rejection in *Nicotiana*. *Proceedings of the National Academy of Sciences of the United States of America* **96**, 13548-13553.

McClure BA, Franklin-Tong, V. 2006. Gametophytic self-incompatibility: understanding the cellular mechanisms involved in "self" pollen tube inhibition. *Planta* **224**, 233-245.

McClure BA, Cruz-Garcia F, Beecher B, Sulaman W. 2000. Factors Affecting Inter- and Intra-specific Pollen Rejection in *Nicotiana*. *Annals of Botany* **85** (Supplement A), 113-123.

McClure BA, Gray JE, Anderson MA, Clarke AE. 1990. Self-incompatibility in *Nicotiana alata* involves degradation of pollen rRNA. *Nature* **347**, 757-760.

McClure BA, Haring V, Ebert PR, Anderson MA, Simpson RJ, Sakiyama F, Clarke AE. 1989. Style self-incompatibility gene products of *Nicotiana alata* are ribonucleases. *Nature* **342**, 955-957.

McCormick S. 2004. Control of Male Gametophyte Development. *The Plant Cell* **16** Supplement, S142-S153.

Miege C, Ruffio-Châble V, Schierup MH, Cabrillac D, Dumas C, Gaude T, Cock JM. 2001. Intrahaplotype polymorphism at the Brassica *S* locus. *Genetics* **159**, 811–822.

Murase K, Shiba H, Iwano M, Che F-S, Watanabe M, Isogai A, Takayama S. 2004. A membrane-anchored protein kinase involved in *Brassica* self-incompatibility signaling. *Science* **303**, 1516-1519.

Murfett J, Atherton TL, Mou B, Gasser CS, McClure BA. 1994. *S*-RNase expressed in transgenic *Nicotiana* causes *S*-allele-specific pollen rejection. *Nature* **367**, 563-566.

Naithani S, Chookajorn T, Ripoll DR, Nasrallah JB. 2007. Structural modules for receptor dimerization in the *S*-locus receptor kinase extracellular domain. *Proceedings of the National Academy of Sciences of the United States of America* **104**, 12211-12216.

Nasrallah JB. 2005. Recognition and rejection of self in plant self-incompatibility: comparisons to animal histocompatibility. *TRENDS in Immunology* **26**, 412-418.

Nasrallah ME, Liu P, Nasrallah JB. 2002. Generation of self-incompatible *Arabidopsis thaliana* by transfer of two *S* locus genes from *A. lyrata*. *Science* **297**, 247-249.

Nasrallah ME, Liu P, Sherman-Broyles S, Boggs N, Nasrallah JB. 2004. Natural variation in expression of self-incompatibility in *Arabidopsis thaliana*: Implications for the evolution of selfing. *Proceedings of the National Academy of Sciences of the United States of America* **101**, 16070-16074.

Nasrallah JB. 2000. Cell-cell signaling in the self-incompatibility response. *Current Opinion in Plant Biology* **3**, 368-373.

de Nettancourt D. 2001. Incompatibility and Incongruity in Wild and Cultivated Plants, 2nd ed. Springer-Verlag, Berlin, Heidelberg, New York.

O'Brien M, Kapfer C, Major G, Laurin M, Bertrand C, Kondo K, Kowyama Y, Matton, DP. 2002. Molecular analysis of the stylar-expressed *Solanum chacoense* small asparagine-rich protein family related to the HT modifier of gametophytic self-incompatibility in *Nicotiana*. *The Plant Journal* **32**, 985-996.

Peragine A, Yoshikawa M, Wu G, Albrecht HL, Poethig RS. 2004. *SGS3* and *SGS2/SDE1/RDR6* are required for juvenile development and the production of *trans*-acting siRNAs in *Arabidopsis*. *Genes & Development* **18**, 2368–2379.

Qiao H, Wang H, Zhao L, Zhou J, Huang J, Zhang Y, Xue Y. 2004. The F-box Protein AhSLF-S_2 Physically Interacts with S-RNases That May Be Inhibited by the Ubiquitin/26S Proteasome Pathway of Protein Degradation During Compatible Pollination in Antirrhinum. *The Plant Cell* **16**, 582-595.

Raven PH, Evert RF, Eichhorn SE. 2005. Biology of Plants, 7th ed. W.H. Freeman and Company, New York, NY.

Rea AC, Liu P, Nasrallah JB. 2010. A transgenic self-incompatible *Arabidopsis thaliana* model for evolutionary and mechanistic studies of crucifer self-incompatibility. *Journal of Experimental Botany* doi:10.1093/jxb/erp393.

Rea AC, Nasrallah JB. 2008. Self-incompatibility systems: barriers to self-fertilization in flowering plants. *The International Journal of Developmental Biology* **52**, 627-636.

Reiser L, Fischer RL. 1993. The Ovule and the Embryo Sac. *The Plant Cell* **5**, 1291-1301.

Rudd JJ, Franklin FCH, Lord JM, Franklin-Tong VE. 1996. Increased Phosphorylation of a 26-kD Pollen Protein Is Induced by the Self-Incompatibility Response in *Papaver rhoeas*. *The Plant Cell* **8**, 713-724.

Rudd JJ, Osman K, Franklin FCH, Franklin-Tong, VE. 2003. Activation of a putative MAP kinase in pollen is stimulated by the self-incompatibility (SI) response. *FEBS Letters* **547**, 223-227.

Sainudiin R, Wong WSW, Yogeeswaran K, Nasrallah JB, Yang Z, Nielsen R. 2005. Detecting Site-Specific Physicochemical Selective Pressures: Applications to the Class I HLA of the Human Major Histocompatibility Complex and the SRK of the Plant Sporophytic Self-Incompatibility System. *Journal of Molecular Evolution* **60**, 315–326.

Samuel MA, Chong YT, Haasen KE, Aldea-Brydges MG, Stone SL, Goring DR. 2009. Cellular Pathways Regulating Responses to Compatible and Self-Incompatible Pollen in *Brassica* and *Arabidopsis* Stigmas Intersect at Exo70A1, a Putative Component of the Exocyst Complex. *The Plant Cell* **21**, 2655-2671.

Sato Y, Okamoto S, Nishio T. 2004. Diversification and Alteration of Recognition Specificity of the Pollen Ligand SP11/SCR in Self-Incompatibility of Brassica and Raphanus. *The Plant Cell* **16**, 3230-3241.

Schierup MH, Mable BK, Awadalla P, Charlesworth D. 2001. Identification and Characterization of a Polymorphic Receptor Kinase Gene Linked to the Self-Incompatibility Locus of *Arabidopsis lyrata*. *Genetics* **158**, 387–399.

Schopfer CR, Nasrallah ME, Nasrallah JB. 1999. The Male Determinant of Self-Incompatibility in *Brassica*. *Science* **286**, 1697-1700.

Sherman-Broyles S, Boggs N, Farkas A, Liu P, Vrebalov J, Nasrallah ME, Nasrallah JB. 2007. *S* Locus Genes and the Evolution of Self-Fertility in *Arabidopsis thaliana*. *The Plant Cell* **19**, 94-106.

Shimosato H, Yokota N, Shiba H, Iwano M, Entani T, Che F-S, Watanabe,M, Isogai A, Takayama S. 2007. Characterization of the SP11/SCR High-Affinity Binding Site Involved in Self/Nonself Recognition in *Brassica* Self-Incompatibility. *The Plant Cell* **19**, 107-117.

Sijacic P, Wang X, Skirpan AL, Wang Y, Dowd PE, Mccubbin AG, Huang S, Kao T-H. 2004. Identification of the pollen determinant of S-RNase-mediated self-incompatibility. *Nature* **429**, 302-305.

Smyth DR, Bowman JL, Meyerowitz EM. 1990. Early Flower Development in *Arabidopsis*. *The Plant Cell* **2**, 755-767.

Snowman BN, Kovar DR, Shevchenko G, Franklin-Tong VE, Staiger CJ. 2002. Signal-Mediated Depolymerization of Actin in Pollen during the Self-Incompatibility Response. *The Plant Cell* **14**, 2613-2626.

Sonneveld T, Tobutt KR, Vaughan SP, Robbins TP. 2005. Loss of Pollen-*S* Function in Two Self-Compatible Selections of *Prunus avium* Is Associated with Deletion/Mutation of an *S* Haplotype-Specific F-Box Gene. *The Plant Cell* **17**, 37-51.

Stein JC, Howlett B, Boyes DC, Nasrallah ME, Nasrallah JB. 1991. Molecular cloning of a putative receptor protein kinase gene encoded at the self-incompatibility locus of *Brassica oleracea*. *Proceedings of the National Academy of Sciences of the United States of America* **88**, 8816-8820.

Stein JC, Dixit R, Nasrallah ME, Nasrallah JB. 1996. SRK, the Stigma-Specific S Locus Receptor Kinase of Brassica, Is Targeted to the Plasma Membrane in Transgenic Tobacco. *The Plant Cell* **8**, 429-445.

Stone SL, Anderson EM, Mullen RT, Goring DR. 2003. ARC1 Is an E3 Ubiquitin Ligase and Promotes the Ubiquitination of Proteins during the Rejection of Self-Incompatible *Brassica* Pollen. *The Plant Cell* **15**, 885-898.

Stone SL, Arnoldo M, Goring DR. 1999. A Breakdown of *Brassica* Self-Incompatibility in ARC1 Antisense Transgenic Plants. *Science* **286,** 1729-1731.

Suzuki G, Kai N, Hirose T, Fukui K, Nishio T, Takayama S, Isogai A, Watanabe M, Hinata K. 1999. Genomic Organization of the *S* Locus: Identification and Characterization of Genes in *SLG/SRK* Region of S^9 Haplotype of *Brassica campestris* (syn. *rapa*). *Genetics* **153**, 391-400.

Takasaki T, Hatakeyama K, Suzuki G, Watanabe M, Isogai A, Hinata K. 2000. The *S* receptor kinase determines self-incompatibility in *Brassica* stigma. *Nature* **403**, 913-916.

Takayama S, Shimosato H, Shiba H, Funato M, Che F-S, Watanabe M, Iwano M, Isogai A. 2001. Direct ligand-receptor complex interaction controls *Brassica* self-incompatibility. *Nature* **413**, 534-538.

Takayama S, Isogai A. 2005. Self-Incompatibility in Plants. *Annual Review of Plant Biology* **56**, 467-489.

Tang C, Toomajian C, Sherman-Broyles S, Plagnol V, Guo Y-L, Hu TT, Clark RM, Nasrallah JB, Weigel D, Nordborg M. 2007. The Evolution of Selfing in *Arabidopsis thaliana. Science* **317**, 1070-1072.

Tantikanjana T, Rizvi N, Nasrallah ME, Nasrallah JB. 2009. A Dual Role for the *S*-Locus Receptor Kinase in Self-Incompatibility and Pistil Development Revealed by an *Arabidopsis rdr6* Mutation. *The Plant Cell* **21**, 2642-2654.

Thomas SG, Franklin-Tong VE. 2004. Self-incompatibility triggers programmed cell death in *Papaver* pollen. *Nature* **429**, 305-309.

Thomas SG, Huang S, Li S, Staiger CJ, Franklin-Tong VE. 2006. Actin depolymerization is sufficient to induce programmed cell death in self-incompatible pollen. *The Journal of Cell Biology* **174**, 221-229.

Ushijima K, Sassa H, Dandekar AM, Gradziel TM, Tao R, Hirano H. 2003. Structural and Transcriptional Analysis of the Self-Incompatibility Locus of Almond: Identification of a Pollen-Expressed F-Box Gene with Haplotype-Specific Polymorphism. *The Plant Cell* **15**, 771-781.

Vanoosthuyse V, Tichtinsky G, Dumas C, Gaude T, Cock JM. 2003. Interaction of Calmodulin, a Sorting Nexin and Kinase-Associated Protein Phosphatase with *Brassica oleracea S* Locus Receptor Kinase. *Plant Physiology* **133**, 919-929.

Watanabe M, Ito A, Takada Y, Ninomiya C, Kakizaki T, Takahata Y, Hatakeyama K, Hinata K, Suzuki G, Takasaki T, Satta Y, Shiba H, Takayama S, Isogai A. 2000. Highly divergent sequences of the pollen self-incompatibility (*S*) gene in class-I *S* haplotypes of *Brassica campestris* (syn. *rapa*) L. *FEBS Letters* **473**, 139-144.

Wheeler MJ, de Graaf BHJ, Hadjiosif N, Perry RM, Poulter NS, Osman K, Vatovec S, Harper A, Franklin CH, Franklin-Tong VE. 2009. Identification of the pollen self-incompatibility determinant in *Papaver rhoeas*. *Nature Letters* **459**, 992-995.

Yadegari R, Drews GN. 2004. Female Gametophyte Development. *The Plant Cell* **16** Supplement, S133-S141.

CHAPTER 2

Candidate genes for self-incompatibility in transgenic self-incompatible *Arabidopsis thaliana*[2]

INTRODUCTION

Genes previously identified in *Brassica* as SI signaling components

In the Brassicaceae family, the self-incompatibility (SI) response is initiated with the recognition of the pollen-coat-localized *S*-locus cysteine-rich protein (SCR) by the stigma-epidermis membrane-spanning *S*-locus receptor kinase (SRK) (Stein *et al.* 1991, 1996; Schopfer *et al.* 1999; Suzuki *et al.* 1999; Takasaki *et al.* 2000). These male and female determinants of SI specificity, respectively, are encoded by tightly-linked genes in the highly-polymorphic *S* (*Sterility*) locus. The receptor-ligand interaction between SRK and SCR proteins of the same haplotype initiates a poorly-understood signaling cascade leading to the rejection of genetically-related ("self") pollen, thereby preventing self-fertilization.

Arabidopsis thaliana, a normally self-compatible member of the Brassicaceae family, was successfully made self-incompatible by transgenic introduction of functional *SRKb* and *SCRb* genes from self-incompatible *Arabidopsis lyrata*. Due to *A. thaliana*'s short generation time, small genome, and the vast resources and genetic tools available for this species, it serves as a great model to study SI in the Brassicaceae family, and has proven to be useful in studies focused on identifying the signaling components downstream of SRK-SCR recognition, identifying important amino-acid residues responsible for determining SI specificity, and

[2] Material in this chapter was published in *Journ. Exp. Bot.* doi: 10.1093/jxb/erp393.

investigating genetic variation among *S* haplotypes to gain clues as to how these specificity determinants have arisen and been maintained throughout evolution.

Studies in *Brassica* have led to a proposed model for SI signaling whereby the negative regulators of SI, thioredoxin *h*-like proteins THL1 and THL2, interact with the SRK kinase domain in the absence of SCR ligand to keep SRK in an inactive state (Bower *et al.* 1996; Cabrillac *et al.* 2001; Haffani *et al.* 2004). Upon ligand binding, THL1 and THL2 dissociate from the SRK kinase domain, allowing activation of positive regulators of SI, the *mod*-locus protein kinase (MLPK) and the Arm repeat-containing 1 protein (ARC1), the latter of which ubiquitinates Exo70A1, a negative regulator of SI and a positive regulator of pollen tube formation, causing its degradation (Stone *et al.* 2003; Murase *et al.* 2004; Samuel *et al.* 2009).

Challenges to this proposed SI signaling model have been put forth recently. For example, ARC1 does not seem to be required for SI in all *Brassica* species. *B. rapa* plants homozygous for a hypomorphic *ARC1* allele were identified which have a 10-fold reduction in *ARC1* transcripts (Rea *et al.* 2010), similar to *B. napus* plants containing an antisense transgene targeting *ARC1* (Stone *et al.* 1999). However, while the latter plants exhibited a breakdown in the SI response (Stone *et al.* 1999), the former plants had just as robust an SI response as those without a 10-fold reduction in *ARC1* transcripts (Rea *et al.* 2010). Additionally, studies with transgenic self-incompatible *A. thaliana* have shown that *Arabidopsis thaliana* plant U-box protein 17 (*AtPUB17*) and *Arabidopsis* protein kinase 1b (*APK1b*), the *A. thaliana* genes with the most sequence similarity to *Brassica ARC1* and *MLPK*, respectively, are not required for SI (Rea *et al.* 2010; Kitashiba *et al.* 2011). Furthermore, comparative genome analyses among *Brassica*, *A. lyrata*, and *A. thaliana* have shown that the likely ortholog of *Brassica MLPK* in *A. thaliana* is indeed *APK1b*, and that of *ARC1* is a pseudogene, supporting the conclusion that *ARC1* and

MLPK orthologs are dispensable for SI in the *A. thaliana* SI model (Kitashiba *et al.* 2011). Lastly, overexpression of *AtExo70A1*, the likely ortholog of *Brassica Exo70A1*, based on comparative genome analysis and sequence similarity, did not weaken the SI response (Kitashiba *et al.* 2011). These results suggest that a reevaluation of the previous model of SI in the Brassicaceae is needed.

Links between SI and plant immunity

The parallels that exist between SI and plant immunity (PI) have often been noted (for extensive reviews, see Hodgkin *et al.* 1988; Nasrallah 2005; Sanabria *et al.* 2008). PI involves at least two different, but coordinated molecular processes, the earlier-acting pathogen-associated molecular pattern (PAMP)-triggered immunity (PTI) and the later-acting effector-triggered immunity (ETI) (for a review of PI, PTI, and ETI, see Jones & Dangl 2006). PTI results when plasma-membrane-spanning pattern recognition receptors (PRRs) recognize PAMPs (or microbe-associated molecular patterns, MAMPs), molecules (e.g., flagellin and chitin) that are conserved among several groups of microorganisms (Jones & Dangl 2006). In order to suppress PTI and become established within a plant, successful pathogens secrete effectors and toxins that collectively contribute to their virulence (Jones & Dangl 2006). ETI results when these pathogen effectors are recognized by plant R (Resistance) proteins, which usually triggers the hypersensitive response (HR), a type of programmed cell death (Jones & Dangl 2006). Although SI and PI exhibit several distinct differences, both PTI and ETI exhibit commonalities with SI. While SI involves recognition and rejection of genetically-similar ("self") pollen grains, PI involves recognition and rejection of "non-self" pathogens. However, the similarities between PTI and SI in the Brassicaceae are particularly striking. Both processes occur at the epidermal

cell surface where certain molecules, including small peptide ligands, contributed by pathogens in PI and by "self" pollen grains in SI, are perceived by plasma-membrane-spanning receptor kinases. For example, both the SRK receptor and the Flagellin sensing 2 (FLS2) receptor, a PRR which functions in PTI against bacterial pathogens by detecting flagellin, are single-pass transmembrane serine/threonine kinases (Stein *et al.* 1991; Gómez-Gómez and Boller 2000). Activation of both SRK and PRRs triggers signaling cascades that culminate in inhibited growth and penetration into subepidermal tissues of pollen tubes in SI and of fungal hyphae or bacteria in PI. Furthermore, SI and PI can have similar cytological manifestations, such as calcium fluxes and callose deposition at the site of contact between the interacting cells (Hodgkin *et al.* 1988; Elleman & Dickinson 1999), and changes to the organization of the actin cytoskeleton and distribution of secretory vesicles (Iwano *et al.* 2007).

Additionally, both SI and ETI are based on highly-specific molecular interactions. Just as recognition specificity in SI is achieved via the activity of highly polymorphic *S*-locus genes, recognition specificity in ETI is achieved via highly polymorphic *R* genes. Polymorphism among different *S* alleles confers a multitude of haplotype-specific interactions between cognate SRK and SCR proteins. Similarly, polymorphism among different *R* alleles confers, in many cases, different functional specificities (Tiffin & Moeller 2006). However, unlike the activation of SRK by SCR, some R proteins may not be activated via direct interaction with pathogen effectors (Jones & Dangl 2006).

Nevertheless, molecular linkages have been made between PI and SI, strengthening the hypothesis that the PI genetic network was co-opted for recognition of "self" pollen in SI. Thus, programmed cell death, which is often triggered in PI, also occurs in the inhibition of "self" pollen tubes in *Papaver* (Thomas & Franklin-Tong 2004). In addition, similar molecules have

been implicated in PI and the SI response of some plant families. A tobacco RNase belonging to the same family as the RNase that determines specificity in S-RNase-based SI systems was found to inhibit hyphal elongation of plant pathogens (Hugot *et al.* 2002). Another example is provided by the Cf-9–mediated gene-for-gene resistance (i.e., ETI) of tomato, in which Cf-9, a receptor-like type I transmembrane R protein, and the Avr9 avirulence peptide effector from the fungal pathogen *Cladosporium fulvum*, elicit the HR and confers resistance against the pathogen. In Cf-9–Avr9 resistance, a thioredoxin was found to be a negative regulator of Cf-9–mediated signaling (Rivas *et al.* 2004), similar to the situation in *Brassica*, where a thioredoxin negatively regulates SRK in the absence of SCR ligand (Cabrillac *et al.* 2001). Interestingly, similarity in tertiary structure, but not primary sequence, exists between SCR proteins of the Brassicaceae SI system and plant (and animal) defensins, which function in immunity as broad-spectrum antimicrobial molecules (Segura *et al.* 1998; Schopfer *et al.* 1999; Lay *et al.* 2003; Chookajorn *et al.* 2004). Furthermore, although the roles of *ARC1* and *MLPK* in SI are questionable, and *AtPUB17* does not seem to be required for SI, ACRE276/AtPUB17 and ACIK1, two proteins that share extensive sequence similarity with *Brassica* ARC1 and MLPK, respectively, are required for full disease resistance in the Cf-9–Avr9 interaction (Rowland *et al.* 2005; Yang *et al.* 2006). These findings provide additional evidence for the use of similar signaling pathways in SI and ETI, if it is assumed that *ARC1*-like and *MLPK*-like genes, rather than the *ARC1* and *MLPK* genes themselves, do function in SI. Also involved in the Cf-9–Avr9 interaction is CMPG1, an E3 ubiquitin ligase that functions as a positive regulator of ETI, and in *A. thaliana*, exhibits the highest sequence similarity with AtPUB20 and AtPUB21 (González-Lamothe *et al.* 2006). Other *AtPUB* genes seem to play negative regulatory roles in PAMP-triggered immunity, as has been shown for the negative regulators *AtPUB22*, *AtPUB23*, and *AtPUB24* (Trujillo *et al.*

2008), and *AtPUB12* and *AtPUB13* (Lu *et al.* 2011). Interestingly, *AtPUB8* was found to regulate *SRK* transcripts in transgenic self-incompatible *A. thaliana* (Liu *et al.* 2007). These results indicate that *AtPUB* genes are used for regulating both SI and PI.

Additional, albeit more indirect, links between PI and SI in the Brassicaceae are suggested by the observation that two members of the *A. thaliana SRK*-like (*SRKL*) gene family, *ARK1* and *ARK3*, as well as several *Brassica SRKL* genes, are induced upon wounding and bacterial infection (Pastuglia *et al.* 2002). Based on microarray experiments, *ARK1* and *ARK3* were also identified as putative primary targets of a key regulator of systemic acquired resistance (SAR; a phenomenon of PI that confers broad-spectrum resistance against pathogens and that is distinct from both PTI and ETI), *NPR1*, and other *S*-domain *RLK* genes were rapidly elicited by treatment with a peptide derived from bacterial flagellin (Navarro *et al.* 2004; Zipfel *et al.* 2004; Wang *et al.* 2005).

Experimental approach

Prior to realizing the recent results suggesting that the likely orthologs of *MLPK* and *ARC1* are not required for SI in transgenic self-incompatible *A. thaliana*, antisense constructs were made, and T-DNA lines were obtained, for potentially reducing the expression of some of the putative *A. thaliana* orthologs of the *Brassica* genes identified as participating in SI signaling. These lines were then crossed to transgenic self-incompatible *A. thaliana* plants to determine if these candidate genes are involved in SI. The potential overlap between PI and SI signaling pathways can also be tested in transgenic self-incompatible *A. thaliana*, as many null mutations in single genes of the known PI pathways exist in *A. thaliana*. Mutants were crossed to transgenic self-incompatible *A. thaliana* to determine if any of the tested PI genes also function

in SI. In light of the involvement of *AtPUB* genes in PI, experiments with candidate *AtPUB* genes could simultaneously identify a potential *ARC1* ortholog and establish a direct connection between PI and SI. Given the role of *AtPUB8* in SI, a yeast two-hybrid screen was performed to identify potential targets of AtPUB8 ubiquitination. Other genes, such as those expressed specifically in the stigma, also serve as good candidates for SI signaling. T-DNA insertions were obtained in one such gene, *AtS1*, to determine if it may function directly in SI signaling or in reproductive development. This chapter presents the results of these experiments.

MATERIALS & METHODS

Antisense construct design, cloning, and bacterial transformation

In order to create the antisense constructs for targeting mRNA, primers designed to span most of the mRNA sequence from either the *TRX-H-3* (At5g42980) gene or the *AtPUB17* (At1g29340) gene were generated. KpnI sites were added to the 5' ends of the primers for eventual cloning of the fragments into the pCAMBIA1300 binary vector directly downstream of the *AtS1* promoter, which was cut out of a previously cloned pBLUESCRIPT vector using SacI at the 5' end and KpnI at the 3' end and cloned into pCAMBIA1300. The primer sequences used were 5'(GGTACC)CTATAAGAACCGACACAGAGACG3' and 5'(GGTACC)ACAATAGAATCCCCAAAGAGTAAA3' for *TRX-H-3*, and5'(GGTACC)TCCGGCGTCGCACTTGTT3' and 5'(GGTACC)CCACCGTCTCTATTCCCATTTGTA3' for *AtPUB17*. The appropriate *TRX-H-3* DNA fragment was amplified from an *A. thaliana* cDNA library because the *TRX-H-3* gene contains introns, while the *AtPUB17* DNA fragment was amplified from genomic DNA, which is more easily obtainable than cDNA, because the *AtPUB17* lacks introns. All cloning was

performed in the DH5α strain of *Escherichia coli*. The DNA fragments were first cloned into the pGEM-T Easy vector, digested with KpnI, then cloned into the KpnI-digested pCAMBIA1300 vector treated with shrimp alkaline phosphatase. Clones containing the insert were identified by KpnI digestion. Antisense-oriented clones were identified and selected by digesting separately with XhoI and EcoRI, and then sequencing with a primer (5'GGTGACGTTATCGACTAATGACAG3') designed to specifically anneal to a stretch of sequence near the 3' end of the *AtS1* promoter and to extend into the sequence immediately downstream of the promoter. Sequencing was performed at the sequencing facility of the Cornell University Life Sciences Core Laboratories Center. Vectors were subsequently introduced into the *Agrobacterium tumefaciens* GV3101 strain by electroporation, and *Agrobacterium* transformants were grown at 28-30 ºC on LB medium supplemented with Kanamycin (50 µg/mL), Gentamycin (50 µg/mL), and Rifampicin (100 µg/mL).

DNA extraction

Genomic DNA was extracted from plants using a CTAB method (modified from Doyle & Doyle 1990) for the antisense transgene experiments, a β-mercaptoethanol method (modified from Dellaporta *et al.* 1983) for the T-DNA insertion experiments, and a sucrose method (Berendzen *et al.* 2005) for the plant immunity mutant experiment.

RT-PCR

RNA was extracted from stigmas with TRIZOL® reagent, using the included protocol (Invitrogen™). Reverse transcriptase polymerase chain reaction (RT-PCR) was performed using the SuperScript™ III One-Step RT-PCR System with Platinum® *Taq* DNA Polymerase

(Invitrogen™). Sample results were normalized using *ACTIN 2* (At3g18780) primers and ImageQuant™.

Plant material, transformation, and growth conditions

T-DNA insertion lines were obtained from the Arabidopsis Biological Resource Center at The Ohio State University (Columbus, OH). *etr1-1*, *ein2-1*, *npr1-1*, *pad4-1*, and *eds1-1* mutant seed and the NPR1, PAD4, and EDS1 dCAPS marker primers were provided by Jian Hua, *rar1-21* mutant seed was provided by Jeff Dangl, and *sgt1b* mutant seed was provided by Jane Parker. Nathan Boggs provided the *SRKb*- and *SCRb*-specific primers, and Titima Tantikanjana provided the Kanamycin-specific primers.

Transformation of the antisense construct into wild type C24 plants was performed via the floral dip method (modified from Clough & Bent 1998 and Martinez-Trujillo *et al.* 2004), using *Agrobacterium* cells harboring the plasmid of interest that were grown to an $O.D._{600}$ between 0.8 and 2 and resuspended in infiltration medium consisting of 5% sucrose and 0.02 or 0.005% Silwet L-77 as surfactant.

For growth of wild type, mutant, T-DNA, and transformed *A. thaliana* plants, seeds were sterilized in 20% (v/v) bleach with vigorous shaking for 5-20 minutes, and then washed 4-5 times with sterile Milli-Q® H_2O in a sterile hood. Using sterile toothpicks, sterilized seeds were plated on Murashige and Skoog (MS) agar medium supplemented with 1% (w/v) sucrose (pH 5.7). Wild type (untransformed or non-mutant) and mutant seeds were plated on medium without antibiotics. To select for the transgenes, seeds of plants transformed with the antisense transgenes were plated on medium containing Hygromycin (60 µg/mL), while seeds of plants transformed with the *SRKb-SCRb* transgene were plated on medium with Kanamycin (30

μg/mL). Seeds of plants with the T-DNA insertions were grown on medium either with or without Kanamycin. Plated seeds were stratified at 4 ºC in the dark for 3-5 days and subsequently placed in growth chambers (20-25 ºC) to allow germination and seedling growth. Seedlings were transplanted to Metro-Mix® 200 (Sun Gro®) soil and returned to the same chambers. Seeds, seedlings, and mature plants were grown in either growth rooms or chambers equipped with fluorescent bulbs alone, high-pressure sodium and metal halide bulbs, or metal halide bulbs alone, and were subjected to constant light in growth rooms, or 16 hr. light / 8 hr. dark cycles in chambers. Plants were oftentimes watered with water supplemented with Nitrogen-Phosphorus-Potassium fertilizer.

Pollination assays

Pollination assays were performed to assess the presence, absence, or strength of the SI response. These assays used the most mature floral buds on an inflorescence, at the −1-stage of development, which is just prior to, or at the commencement of, anthesis (or flower opening). These buds were used for two reasons: (1) their stigmas express an intense SI response, and (2) the −1 developmental stage precedes anther dehiscence, and as a result the stigmas of −1-stage floral buds are free of pollen. For each pollination assay, floral buds were removed at their pedicels from the inflorescence stems and placed pedicel-down in 0.4% agarose to maintain hydration of the bud tissues. Fine-tipped forceps and a stereoscope were used to pollinate the stigma of each bud using mature pollen from open flowers. After 2-4 hours, which is sufficient time to allow growth of pollen tubes in compatible pollinations, the buds were fixed in 3 parts ethanol : 1 part acetic acid at 4 ºC overnight. Fixative was then removed and buds were washed twice with H_2O. The buds were then treated with 1M NaOH and incubated at 60-65 ºC for 15-30

minutes to soften the tissue. The NaOH solution was then removed, and buds were washed twice with H_2O. The buds were subsequently treated with decolorized aniline blue solution to stain callose. The pistils of treated buds were excised and mounted on microscope slides in order to visualize pollen tubes under UV light using anOlympus Vanox-T (model AHBT) epifluorescence microscope. Pollination images were captured using a Polaroid MP-4 camera and DMC 2 (version 2.0.1) software.

Yeast two-hybrid interaction assays

For pair-wise yeast two-hybrid (Y2H) assays, the pGAD-C1 and pGBD-C1 vectors (James *et al.* 1996) were used for cloning or for use as controls. The *AtPUB* full-length or C-terminal gene sequences, and the *SRKb* kinase domain sequence, were cloned in-frame with either the activation domain sequence of the pGAD vector or the DNA binding domain sequence of the pGBD vector. All cloning was performed in the DH5α strain of *E. coli*. Plasmid DNA from each pair of test clones was co-transformed into the PJ69-4a/α strain of yeast *Saccharomyces cerevisiae* (using a method modified from Dr. Fields' lab, Howard Hughes Medical Institute, Department of Genome Sciences & Medicine, University of Washington, Seattle, WA).

Y2H screens were performed using a non-directional *A. thaliana* MATCHMAKER cDNA library from 3-week-old green vegetative tissue (CLONTECH). Plasmid DNA from positive-interacting clones was extracted using a Zymolyase (Zymo Research) and miniprep method (http://130.15.90.245/zymolase_plasmid_recovery_from_yeast.htm; website of Dr. Chin-Sang's lab, Department of Biology, Queen's University, Kingston, ON, Canada). cDNA sequences from positive clones were identified by performing PCR on the extracted plasmid

DNA using forward and reverse primers flanking the cloning site. Sequencing was performed at the sequencing facility of the Cornell University Life Sciences Core Laboratories Center.

RESULTS & DISCUSSION

TRX-H-3: the likely ortholog of the *Brassica THL1* gene

Brassica THL1 and *THL2* were implicated as negative regulators of SI (Bower *et al.* 1996; Haffani *et al.* 2004). The *A. thaliana* genes with the highest sequence similarities to *THL1* and *THL2* are *TRX-H-3* (At5g42980) and *TRX-H-4*, respectively. Interestingly, both the TRX-H-3 protein and the TRX-H-4 protein were found to interact with the *Brassica* SRK-910 kinase domain, whereas TRX-H-1 and TRX-H-2 were not (Mazzurco *et al.* 2001). Therefore, *TRX-H-3* and *TRX-H-4* may be functional orthologs of *THL1* and *THL2*, respectively.

An antisense construct targeting the *TRX-H-3* gene was designed to express antisense RNA only in stigmatic tissue under the control of the stigma-specific *AtS1* promoter. It was reasoned that the *TRX-H-3* gene may have functions elsewhere in the plants that are unrelated to SI and if down-regulated, may cause unforeseen developmental defects that could potentially preclude interpretation of an SI-related phenotype. It is also possible that the antisense transgene may down-regulate other thioredoxin genes that share sequence identity with *TRX-H-3*, which could increase the probability of such an outcome.

The *TRX-H-3* antisense construct was transformed into wild type C24 plants and primary transformants were crossed to C24 *SRKb-SCRb* plants (Nasrallah *et al.* 2002). Because the C24 ecotype is known to exhibit stable SI when transformed with *SRKb* and *SCRb* from *A. lyrata* (Nasrallah *et al.* 2004), SI phenotypes can be approximated by observing the extent of seed-set in these plants. All F_1, F_2, and F_3 plants containing both the *SRKb-SCRb* and the *TRX-H-3* antisense

transgenes, as determined by PCR, exhibited a low or slightly intermediate seed-setting phenotype and as expected, all tested plants were found to be self-incompatible via pollination assays with −1-stage buds. Because THL1 is proposed to be a negative regulator of SI, it was hypothesized that THL1/TRX-H-3 functions to keep SRK in an inactive state and therefore, without it, would cause the plants to exhibit constitutive SI. To test this hypothesis, pollination assays were performed on plants containing both the *SRKb-SCRb* and the *TRX-H-3* antisense transgenes to determine whether the stigmas of these plants also inhibit WT pollen lacking SCRb. All plants permitted normal growth of WT pollen tubes. Therefore, in an *SRKb-SCRb* background, the presence of the antisense transgene had no effect on incompatible or compatible pollinations: self-pollinations and reciprocal pollinations with *SRKb-SCRb* stigmas and pollen produced little to no (0-5) pollen tubes, while reciprocal pollinations with WT stigmas and pollen produced many (20-50) pollen tubes.

The negative result obtained could be due to many factors, including that (1) *TRX-H-3* is not involved in SI in *A. thaliana*, (2) it is not the functional homolog of *THL1*, (3) neither the *THL1* gene nor the *TRX-H-3*gene is truly involved in SI, (4) functional redundancy for the *TRX-H-3* gene in *A. thaliana* prevents the revelation of a phenotype, (5) silencing of the transgene(s) *in planta* is occurring, and (6) the antisense transgene is unable to reduce *TRX-H-3* RNA, or to a low enough extent to produce a phenotypic effect. RT-PCR was performed using stigma RNA extracts from three F_1 plants having both the *SRKb-SCRb* and *TRX-H-3* antisense transgenes, and one WT C24 plant, using *ACTIN 2* primers for normalization. The largest difference between the WT sample and one F_1 plant was 1.88×, in which WT RNA levels were higher. However, this result may not be significant, since another F_1 plant sample appeared to have more endogenous

TRX-H-3 mRNA than WT, which is unexpected. These differences could merely be attributed to pipetting error or to random, inherent differences in PCR amplification.

AtPUBs: genes related to *Brassica ARC1*

The ARC1 protein has 3 distinct domains: an ARM-repeat region involved in protein-protein interaction, a U-box domain, characteristic of E3 ubiquitin ligases, and a more recently discovered U-box N-terminal domain (UND; Mudgil *et al.* 2004). In *A. thaliana*, there are 108 predicted ARM-repeat proteins, 42 of which also have a U-box domain (Mudgil *et al.* 2004; TAIR, http://www.arabidopsis.org/browse/genefamily/pub.jsp), making the U-box-containing proteins the largest group of ARM-repeat proteins. Fourteen proteins of this U-box / ARM-repeat group have a UND (Mudgil *et al.* 2004). There are potentially 61 AtPUBs (*Arabidopsis thaliana* Plant U-box proteins); thus, not all U-box proteins have an ARM repeat region. The 42 AtPUBs that do have an ARM repeat region belong to the Class II and Class III sub-classes. There are 7 sub-classes of AtPUBs (TAIR).

Several *AtPUB* genes were considered to be good candidates for being involved in SI signaling. One such gene is *AtPUB17* (At1g29340), which was found to be most similar in sequence to the *Brassica ARC1* gene. *AtPUB17*, like *Brassica ARC1*, has the UND, and although *AtPUB17* does not exhibit stigma-specific expression (Mudgil *et al.* 2004), it is nevertheless expressed in the stigma itself (TAIR, Genevestigator, Affymetrix microarray), with a stigma expression mean value of 708, which is ranked #5 of the U-box / ARM genes in terms of highest expression in the stigma (TAIR, Gene Atlas). It is also up-regulated in response to cycloheximide (TAIR, Genevestigator), which is known to break down the SI response in *Brassica* (Stead *et al.* 1980; Sarker *et al.* 1988; Dixit & Nasrallah, unpublished). Additionally,

AtPUB17 is required for effector-triggered immunity (ETI) (Yang *et al.* 2006), which supports other parallels noted between plant immunity (PI) and SI.

AtPUB8 (At4g21350) has been found to positively regulate SI maintenance in later developmental stages of the stigma in transgenic self-incompatible *A. thaliana* (Liu *et al.* 2007). This gene is linked to the *S* locus (Liu *et al.* 2007), and is expressed in the stigma (TAIR, Genevestigator, Affymetrix microarray), with a stigma expression mean value of 481 (TAIR, Gene Atlas).

Another *AtPUB* gene that is a good candidate for a role in SI is *AtPUB2* (At5g67340), which is expressed most highly in the stigma as compared to all other organs and tissue types tested (TAIR, Genevestigator, Affymetrix microarray), with a stigma mean expression value of 6,107, which is ranked #1 of all the *AtPUB* genes in terms of highest expression in the stigma (TAIR, Gene Atlas), implicating it as a potential stigma-specific gene. It should be noted, however, that the expression value is nowhere near that of the only stigma-specific *A. thaliana* gene identified to date, *AtS1*, whose stigma mean expression value is 41,638. Other evidence suggesting *AtPUB2* is stigma-specific is that one replicate of a microarray experiment that compared wild-type stigmas with stigmas in which stigma epidermal cells were genetically ablated by expression of diphtheria toxin subunit A showed transcripts derived from this gene were reduced by more than 1.5-fold (Tung *et al.* 2005, unpublished results), suggesting that it is expressed in stigma epidermal cells. *AtPUB2* also has the UND (Mudgil *et al.* 2004), and is up-regulated in response to cycloheximide (TAIR, Genevestigator).

Another candidate gene, *AtPUB22* (At3g52450), is expressed in the stigma (TAIR, Genevestigator, Affymetrix microarray), with a stigma mean expression value of 26 (TAIR, Gene Atlas), and like *AtPUB2*, it was found to exhibit more than 1.5-fold reduced transcript

levels in ablated sigmas relative to wild type (Tung *et al.* 2005, unpublished results). Interestingly, the expression of this gene was also induced by SCRb (Tung & Nasrallah, unpublished), and it is up-regulated in response to cycloheximide (TAIR, Genevestigator). It is also a negative regulator of PAMP-triggered immunity (PTI) (Trujillo *et al.* 2008), which supports other parallels noted between PI and SI.

AtPUB17 *antisense line*

In agreement with the T-DNA knock-out results in the Col-0 ecotype, *AtPUB17* was not found to have an effect on SI when an antisense construct expressed specifically in the stigma and targeting the *AtPUB17* gene was introgressed into C24 plants having the *SRKb-SCRb* transgene. Plants containing both transgenes exhibited low seed set, and pollinations indicated that there is no breakdown of SI: pollination phenotypes were similar to plants containing only the *SRKb-SCRb* transgene.

AtPUB22 *T-DNA line*

An *A. thaliana* line with a T-DNA insertion in *AtPUB22* was obtained and crossed to transgenic SI *A. thaliana*, and F_2 and F_3 progeny were generated; these plants were analyzed for pollination phenotypes to determine if *AtPUB22* may play a role in SI. In the F_2 progeny, there did not appear to be any obvious correlation between pollination phenotype and genotype, namely, zygosity of the T-DNA insertion in combination with the presence of the *SRKb-SCRb* transgene. However, there may be a correlation between pollination phenotype and zygosity of the *SRKb-SCRb* transgene in combination with homozygosity of the T-DNA insertion; if this is the case, it would imply that knocking out the *AtPUB22* gene influences SI, but only in the

context of *SRKb* and/or *SCRb* expression levels. In order to test this hypothesis, a plant that is hemizygous for the *SRKb-SCRb* transgene and homozygous for the T-DNA insertion can be identified, its pollinations phenotypes determined, and its progeny, which would be segregating for the *SRKb-SCRb* transgene, analyzed for genotype and phenotype. In order to identify which plants are hemizygous and which are homozygous for the *SRKb-SCRb* transgene, the next-generation plants have to be screened by PCR for segregation and no segregation of the *SRKb-SCRb* transgene, respectively, as only presence and absence of the *SRKb-SCRb* transgene can be determined by PCR analysis.

An F_2 plant that displayed slight breakdown of SI in self-pollinations was found to be hemizygous for the *SRKb-SCRb* transgene and homozygous for the T-DNA insertion by PCR analysis of the F_2 plant and the derived F_3 plants. The F_3 plants displayed three phenotypic categories based on a subjective assessment of SI phenotype: SI, partial SI, and SC. It has yet to be determined whether these phenotypes correlate with the respective plants' hemizygosity or homozygosity for the *SRKb-SCRb* transgene. Seed from each of the tested F_3 plants were harvested and grown, and leaf tissue was collected from the resulting F_4 plants for genomic DNA extraction. PCR analysis on these F_4 plants from each F_3 plant will be performed to determine if there is, or is not, segregation of the *SRKb-SCRb* transgene in the F_4 population, suggesting that the parent F_3 plant was hemizygous, or homozygous, respectively, for the transgene. It will then be determined if the three phenotypic categories correlate with the three potential transgene zygosity genotypes.

Yeast two-hybrid pairwise assays

All four candidate AtPUB proteins (C-terminal and/or full-length versions), AtPUB17, AtPUB8, AtPUB2, and AtPUB22, were tested for their potential interaction with the SRKb kinase domain using pairwise yeast two-hybrid (Y2H) assays. The C-terminal fragment consisted of the entire ARM-repeat region of each protein, and is equivalent to the ARC1 C-terminal fragment initially identified in the yeast two-hybrid screen as mediating its interaction with the kinase domain of SRK (Gu *et al.* 1998). None of the tested AtPUB proteins were found to interact with the SRKb kinase domain (Table 1). Interestingly, AtPUB8 was found to interact with itself, which does not appear to necessarily be a common feature of all AtPUB proteins, as AtPUB17 did not exhibit self interaction (Table 1, Figure 1). Additionally, AtPUB8 does not appear to interact with other AtPUB proteins: e.g., no interaction was detected between AtPUB8 and AtPUB17 (Table 1, Figure 1). The fact that at least one positive interaction was found in the pairwise Y2H assays suggests that negative interactions did not result from faulty experimental set-up and execution. However, a positive interaction does not necessarily equate to biological significance, especially *in planta*. Statistically, since 23 different interactions were tested, a positive interaction might be found by chance alone. On the other hand, the fact that no interaction was found between any of the four candidate AtPUB proteins and the SRKb kinase domain does not exclude the possibility that any one of the AtPUB proteins may interact with SRKb *in planta*.

Yeast two-hybrid screens with AtPUB8

Due to the finding that AtPUB8 is involved in SI (Liu *et al.* 2007), two Y2H screens, one using full-length AtPUB8 as bait, and the other using the C-terminal AtPUB8 fragment as bait,

Table 1. Yeast two-hybrid pairwise assay results.
All possible combinations of yeast two-hybrid pairwise assays are depicted. Different colors represent different proteins. Light shades of color represent the full-length protein and darker shades of the same color represent the C-terminal protein fragment. AD = GAL4 activation domain; BD = GAL4 binding domain; PUB = *Arabidopsis thaliana* Plant U-box protein; SRKbKD = SRKb kinase domain. Example: AD-PUB8C, the GAL4 activation domain fused in-frame with the AtPUB8 C-terminal fragment. −, negative interaction between the two proteins tested (no growth of yeast); +, positive interaction between the two proteins tested (growth of yeast). Blank boxes indicate those combinations not tested.

	AD-SRKbKD	AD-PUB2	AD-PUB2C	AD-PUB8	AD-PUB8C	AD-PUB17	AD-PUB17C	AD-PUB22	AD-PUB22C	AD
BD-SRKbKD	−		−	−	−		−			−
BD-PUB2										
BD-PUB2C	−									
BD-PUB8	−			+		−				−
BD-PUB8C	−									−
BD-PUB17				−		−				
BD-PUB17C	−									−
BD-PUB22										
BD-PUB22C	−									−
BD	−			−	−		−			

Figure 1. Depiction of a positive yeast two-hybrid pairwise assay interaction between the full-length AtPUB8 fragment and itself, and a negative interaction between the full-length AtPUB8 fragment and the full-length AtPUB17 fragment. The left-hand side of the plates show the growth of 12 separate yeast clones co-transformed with the plasmid containing the GAL4 activation domain fused in-frame with the full-length AtPUB8 fragment (AD-PUB8 f-l) and the plasmid containing the GAL4 binding domain fused in-frame with the full-length AtPUB8 fragment (BD-PUB8 f-l). The right-hand side of the plates show the lack of growth of 12 separate yeast clones co-transformed with the plasmid containing the GAL4 activation domain fused in-frame with the full-length AtPUB17 fragment (AD-PUB17 f-l) and BD-PUB8 f-l. The co-transformed yeast clones were streaked on agar plates of drop-out synthetic complete medium without adenine (DO-Ade; **(A)**) and agar plates of drop-out medium without histidine, supplemented with 40 mM 3-aminotriazole (DO-His + 40 mM 3-AT; **(B)**). The 3-AT amount was used and optimized to prevent the autoactivation of BD-AtPUB8 observed on DO-His medium. Growth of the yeast on DO-Ade and DO-His is reflective of a positive interaction between the two proteins tested, since the promoters, *GAL2* and *GAL1*, driving the expression of two of the reporter genes, *ADE2* and *HIS3*, respectively, are being activated upon the reconstitution of the DNA binding domain and activation domain of the GAL4 transcription factor due to the interaction between the two proteins of interest. The PJ69-4a yeast strain cannot grow on DO-Ade and/or DO-His if it is either untransformed, or transformed with non-interacting proteins, due to mutations in the *ADE2* and *HIS3* genes.

(A)

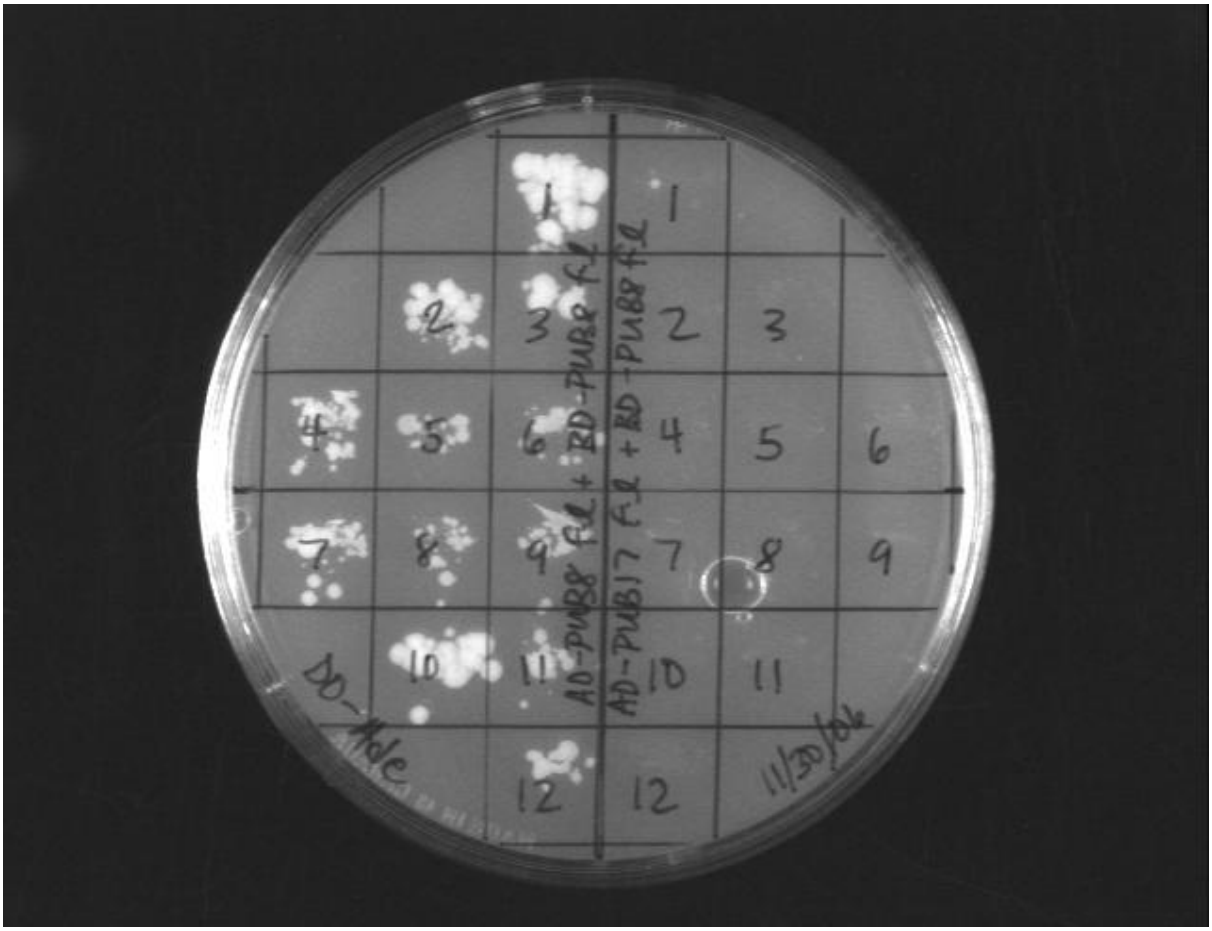

(B)

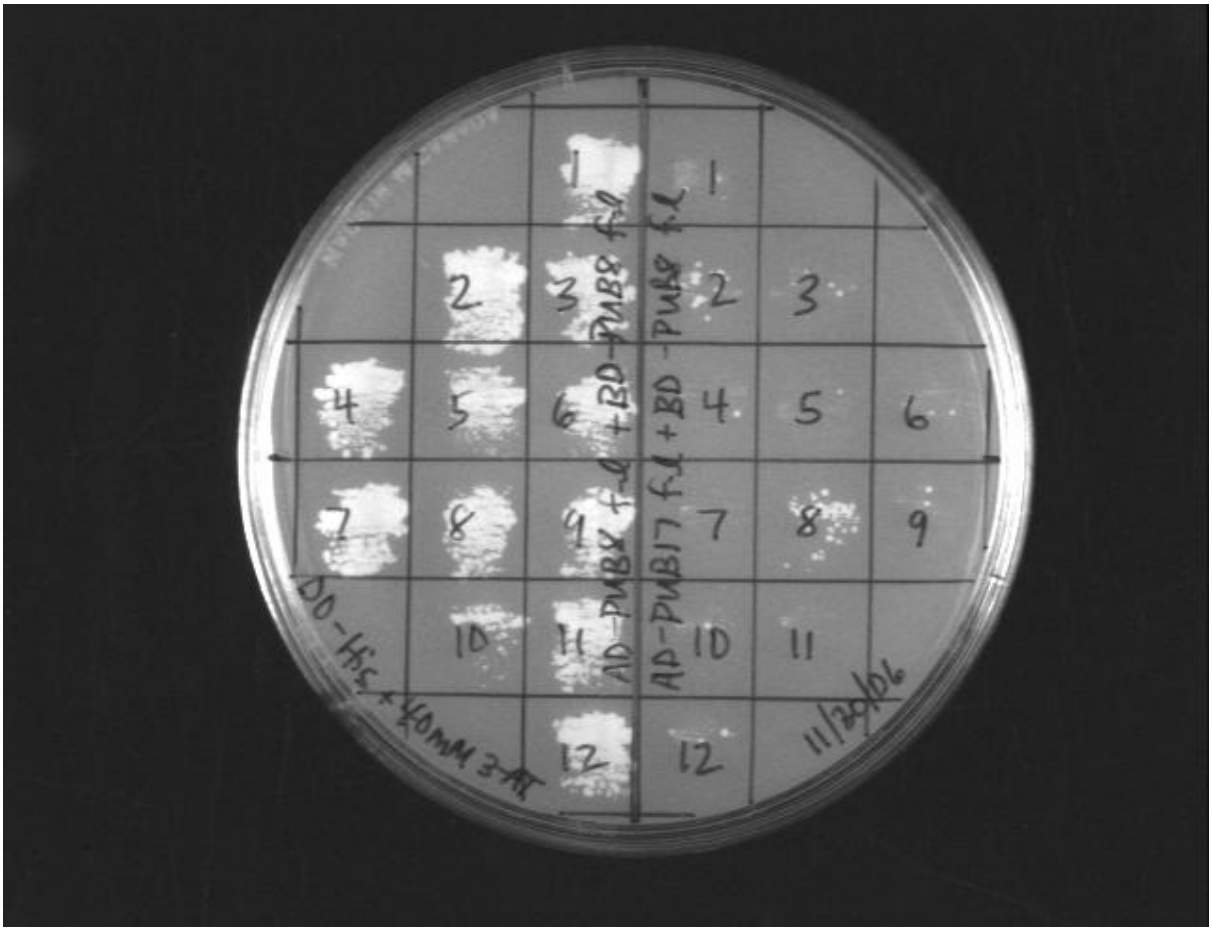
AD-PUB8 f.l
AD-PUB8 f.l + BD
AD-PUB17 f.l + BD
AD-PUB8 f.l + BD-PUB8
SD-His + 40mM 3-AT
11/20/06

were performed using an *A. thaliana* cDNA library made from 3-week-old vegetative tissue (CLONTECH), in order to determine if any interacting partners or potential targets of AtPUB8 could be identified. Approximately one thousand clones from the screens were picked, the genes represented by the cDNAs of approximately one hundred clones were sequenced and identified, and the interesting clones found to be in frame with the activation domain were selected for further study. Some of these selected sequences did not prove to be true interactors based upon subsequent interaction trials with the AtPUB8 bait in yeast. Several sequences that were identified using the full-length AtPUB8 bait proved to be true interactors. However, these sequences encoded RING / Zn finger-containing proteins that may function as other ubiquitin ligases. As such, they did not provide any new information about SI.

AtS1: A stigma-specific gene

AtS1 is a highly-expressed, stigma-specific gene in *A. thaliana*, and is homologous to the *SLR1* (*S*-locus related protein 1) gene of *Brassica* (Dwyer *et al.* 1992, 1994). Due to their very high and specific expression in the stigma, *AtS1* and *SLR1* may function in stigma development, pollination, fertility, SI, or any combination of these processes. Previous work has suggested that SLR1 functions in the adhesion of pollen to the stigma surface in *Brassica* (Luu *et al.* 1999).

Two separate T-DNA lines with insertions in *AtS1* (At3g12000) were obtained, and homozygous lines were generated. The T-DNA insertions were also introduced separately into transgenic self-incompatible *A. thaliana SRKb-SCRb* plants via crossing. Plants that were homozygous for each of the T-DNA insertions and containing the *SRK-SCRb* transgene were generated. These plants and plants homozygous for the T-DNA insertion but lacking *SRKb-SCRb* were analyzed for potential effects on (1) the self-incompatibility phenotype via pollination

assays, (2) pollen-stigma interactions (e.g., delayed pollen tube formation, stigma receptivity to pollen, and pollen viability), (3) stigma morphology (e.g., papillar cell length) via light microscopy, and (4) seed-setting phenotypes. No consistent or quantifiable effects that could be conclusively attributed to the T-DNA insertion were observed. Although these results may suggest that *AtS1* is not involved in these processes, it is possible that no effects were observed because the T-DNA insertions were unable to knock out the *AtS1* gene. RT-PCR on the *AtS1* gene would be required to determine if this is the case.

Plant immunity genes

The possibility that the same signaling components are used in the SI and PI signaling pathways is readily testable in *A. thaliana* because a large number of PI mutants are available in this species. In order to identify signaling components that might be shared by the two pathways, transgenic self-incompatible *A. thaliana SRKb-SCRb* plants were crossed to plants carrying single-gene mutations at various loci known to function in PI. Progeny plants that carried the *SRKb-SCRb* transgene and were homozygous for the mutation of interest were then assayed for SI. A gene would be inferred to function in SI if these plants failed to exhibit the SI phenotype.

The following PI pathway mutations were tested: *etr1-1* (Bleecker *et al.* 1988), *ein2-1* (Guzmán & Ecker 1990), *npr1-1* (Cao *et al.* 1994), *pad4-1* (Glazebrook *et al.* 1996), *rar1-21* (Tornero *et al.* 2002), *sgt1b* (Tör *et al.* 2002), and *eds1-1* (Parker *et al.* 1996). These mutations disrupt genes that function in different types of PI pathways in *A. thaliana*, including PTI, ETI, and SAR (Glazebrook 2001; Boutrot *et al.* 2010). All of these mutations were generated in the Col-0 accession, with the exception of *eds1-1*, which is in the Wassilewskija (Ws) accession. Initial crosses of these PI mutants were made to C24 plants carrying the *A. lyrata SRKb-SCRb*

genes (Nasrallah *et al.* 2004), which exhibit stable SI. However, it was observed that the F_1 generation plants resulting from the cross between self-incompatible C24 *SRKb-SCRb* plants and the Col-0 PI mutant plants were very late-flowering when compared to either parent, even when grown under the long-day conditions known to hasten flowering in *A. thaliana*, a facultative long-day plant (Napp-Zinn 1985). The very late-flowering phenotype of F_1 plants of the C24 x Col-0 cross, as well as the highly divergent flowering time phenotypes of their F_2 progenies, was previously reported to be caused by the combination of one copy of the late-flowering *FRI* allele from C24 and one copy of the late-flowering *FLC* allele from Col (Sanda & Amasino 1995).

In order to avoid these and other potential secondary genetic effects that might affect interpretation of pollination phenotypes in inter-accession crosses, Col-0 *SRKb-SCRb* plants were used in crosses to PI pathway mutants, since all but one of these mutants were generated in the Col-0 background. The exception, *eds1-1,* is in the Ws accession, which, like Col-0, expresses transient SI when transformed with both *SRKb* and *SCRb* genes (Nasrallah *et al.* 2004). Therefore, crosses between Ws and Col-0 were expected to cause very little, if any, genetic variation in F_2 progenies with respect to expression of SI.

Each PI mutant was used as the female parent in crosses to Col-0 *SRKb-SCRb* to ensure that any antibiotic (kanamycin, in this case)-resistant progeny would have resulted from successful crosses to the *SRKb-SCRb* parent rather than from spontaneous selfing of the *SRKb-SCRb* parent. Kanamycin-resistant F_1 and F_2 progeny plants were confirmed to carry the *SRKb-SCRb* transgene by amplification of genomic DNA using *SRKb*- and *SCRb*-specific primers as well as kanamycin-specific primers (Table 2). The presence or absence of the PI mutant alleles was also assessed by amplification of the same genomic DNA using dCAPS marker primers

Table 2. Primers used in analysis of *SRK-SCR* plants carrying PI pathway mutations.

Primer Target	Primer 1 (5'→3')	Primer 2 (5'→3')	Primer Type	dCAPS Enzyme
ETR1	CAGTTTGGTGCTTTTATCGTTCTTA	TAGTCATCACAAGCGCCACGGTT	dCAPS	DdeI
EIN2	GACGGATCAAGAAATCCGTTCG	CATCAGAGTCTTCCTTAAGACTACTAACTC	dCAPS	XhoI
NPR1	AATGTGAAGACCGCAACAGAT	CTTCCGCATCGCAGCATCAT	dCAPS	BspHI
PAD4	TCGCATAAGACTAGGTAAGTCTT	GCGTAAATCCATTTCTTTCCTA	dCAPS	DdeI
RAR1	GGAATGAAAGAGTGGAGCTGCTGCACG	CAGAGGAATTATTATGAGGGGGTAC	dCAPS	MaeII
EDS1	AAATGTCAACTTCCAGATGAGTT	GGTAGTTTGCAATATCAAGAAGCT	dCAPS	HindIII
SGT1b	AACGATTTTGGGTATTTGTCTGC	GCTTCCGTTGCTAGTGGTGTT	gene-specific	N/A
SRKb	TTACTTCCACAGATGAAAATGGGTTGGGATGTC	GCACAAAAACCCATC	gene-specific	N/A
SCRb	GTCGGATCCCAGAAGAACAAGTGCATG	GATGAATTCGCAAAATCTACAGTC	gene-specific	N/A
Kan^R	GGGCGCCCGGTTCTTTTTG	ACACCCAGCCGGCCACAGTCG	gene-specific	N/A

(Table 2) designed using dCAPS Finder 2.0 (http://helix.wustl.edu/dcaps/dcaps.html; Neff *et al.* 2002), or in the case of *sgt1b*, gene-specific primers.

To evaluate the effect of PI mutations on SI, self-pollination assays were performed on stigmas of −1-stage floral buds, in which strong SI is expressed in *SRKb-SCRb* transformants of both Col-0 and Ws. In the case of the dominant *etr1-1* mutation, phenotypic analysis was performed on F_1 plants. In the case of the remaining mutant alleles, all of which are recessive, self-pollination phenotypes were assessed in F_2 plants homozygous for these mutant alleles and having at least one copy of the *SRKb-SCRb* transgene. For several plants, phenotypes were confirmed in the subsequent generation (F_2 generation plants for *etr1-1* and F_3 generation plants for the other mutant alleles). A pollination was considered compatible if numerous pollen tubes (equivalent to the numbers obtained upon self-pollinations of wild-type and mutant non-transgenic plants) were observed in the transmitting tract of a pollinated pistil, or incompatible if 10 or fewer pollen tubes (equivalent to numbers obtained upon self-pollination of wild-type *SRKb-SCRb* transformants), were observed (Figure 2). For each pollination assay, wild-type untransformed Col-0 and wild-type transgenic Col-0 *SRKb-SCRb* plants were used as controls.

Table 3 summarizes the self-pollination results from *SRKb-SCRb* plants homozygous for the recessive *ein2-1*, *npr1-1*, *pad4-1*, *rar1-21*, *sgt1b*, or *eds1-1* alleles or *SRKb-SCRb* plants carrying at least one copy of the dominant *etr1-1* allele; all of these plants were found to exhibit an SI response that was as robust and stable as that of the *SRKb-SCRb* parent plant (Table 3, Figure 2). The observation that the SI response was not even weakened by the PI mutations strongly suggests that the *ETR1*, *EIN2*, *NPR1*, *PAD4*, *RAR1*, *SGT1b*, and *EDS1* genes are not required for SI. It should be noted, however, that the results do not exclude the possibility that for at least some of these genes, a related paralog might function in SI. Simultaneous down-

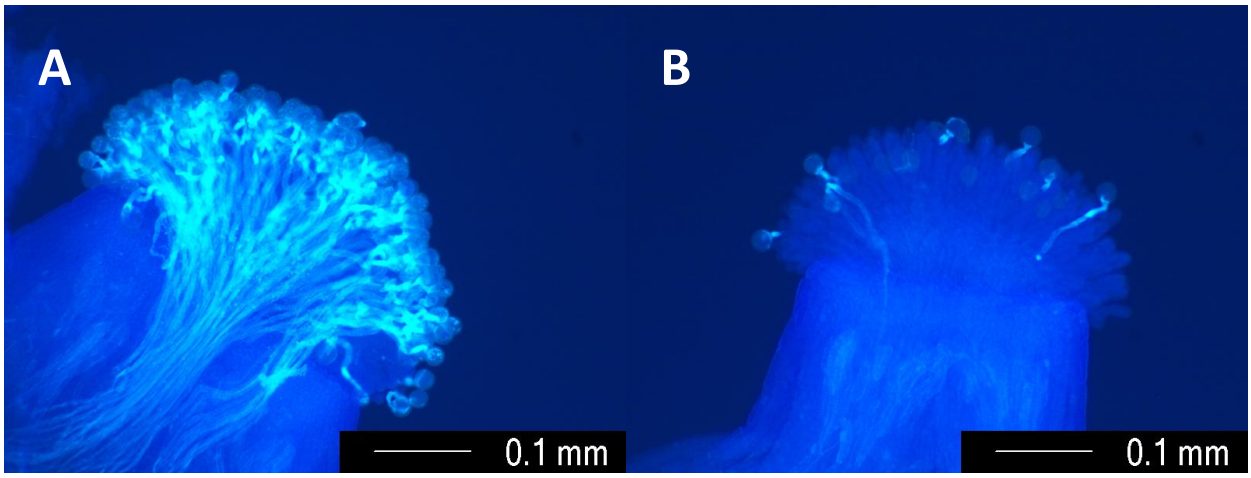

Figure 2. Self-incompatible pollination phenotype of *SRK-SCR* plants carrying mutations in PI pathway genes.
The images contrast the pollination results obtained upon manual self-pollination of stigmas from −1-stage floral buds of two plants: **(A)** a Col-0 untransformed wild-type plant, in which numerous elongated pollen tubes are observed; and **(B)** a Col-0 F_2 *SRKb-SCRb* plant homozygous for the *rar1-21* mutation, in which inhibition of pollen germination and tube growth is observed. Note that all *SRKb-SCRb* plants homozygous for mutations in all tested PI pathway genes were self-incompatible and produced the same pollination results as *SRKb-SCRb rar1-21* homozygotes.

Table 3. Pollination phenotypes of *SRKb-SCRb* plants homozygous for PI pathway mutations.

[a] Pollination phenotype was determined by performing manual self-pollinations on stigmas of −1-stage floral buds, treating the buds with aniline blue to stain callose, and counting pollen tubes visualized with epifluorescence microscopy (see Figure 2). For each plant, the functionality of stigma and pollen was confirmed via pollination assays using wild-type Col-0 pollen and wild-type Col-0 stigmas, respectively.

[b] For the vast majority of plants (47/63; ~75%), two stigmas were tested for pollination phenotype via self-pollination assays. For the remaining plants, one, three, or four stigmas were tested.

[c] For each PI mutation, one or two separate homozygous mutant plants were crossed to Col-0 *SRKb-SCRb* to generate F_1 plants, the latter of which were allowed to self-fertilize and produce F_2 plants. In most cases, F_2 plants were allowed to self-fertilize and produce F_3 plants. A "family" is defined as a group of plants that were generated from a single, initial crossing event, and a "sub-family" is defined as the plants generated from one plant of a single family.

[d] One F_2 *SRKb-SCRb eds1-1* homozygous plant was scored as self-compatible in one pollination assay using two stigmas. However, this result seems to have been due to a failed pollination assay and not to the *eds1-1* mutation, since the F_3 progeny plants derived from this plant were all SI.

PI mutant w/ *SRKb-SCRb*	**pollination phenotype[a]**	**total # plants tested[b]**	**# families (# plants/family)[c]**	**# sub-families (# plants/sub-family)[c]**
etr1-1	SI	7	1 (7)	3 (3, 3, 1)
ein2-1	SI	8	1 (8)	1 (8)
npr1-1	SI	13	2 (7, 6)	1 (7), 1 (6)
pad4-1	SI	10	2 (7, 3)	1 (7), 1 (3)
rar1-21	SI	4	1 (4)	2 (3, 1)
sgt1b	SI	12	2 (8, 4)	1 (8), 1 (4)
eds1-1	SI[d]	9	1 (9)	1 (9)

regulation of more than one member of the same gene family by gene silencing methods such as RNA interference may help address this possibility. It is also possible that some of these PI genes might function in SI, but inactivation of individual genes may not be sufficient for abolishing or even weakening the SI response due to cross-talk among various pathways. Indeed, knocking out one PI pathway is not always sufficient to abolish PI (Zipfel *et al.* 2004). For example, *NPR1*, *PAD4*, and *EDS1* are not universally required for all PI pathways: they are required for salicylic-acid-mediated resistance but, although they are up-regulated upon flagellin induction, they are not required for flagellin-induced PTI. Combining several mutations in *SRK-SCR* plants is required to test these possibilities.

CONCLUSIONS

The transgenic self-incompatible *A. thaliana* model for self-incompatibility (SI) has proven to be useful for several approaches in studying many aspects of SI, including testing the involvement in SI of candidate genes. Despite the fact that transformation into *A. thaliana* of only the *SRKb* and *SCRb* genes from *A. lyrata* are required to impart a robust SI response in *A. thaliana*, there has yet to be a confirmation that any of the genes identified in *Brassica* as being involved in SI translate into the transgenic self-incompatible *A. thaliana* model. The negative results described here raise the question of whether these genes are definitively involved in the SI response of the Brassicaceae.

It appears that there may be dual roles of *AtPUB* genes in both plant immunity (PI) and SI, but direct evidence for this connection is still lacking. Thus far, in *A. thaliana*, of the *AtPUB* genes, only *AtPUB8* has been shown to be involved in SI, but as a regulator of *SRKb* transcript levels and not as a signaling intermediate. Nevertheless, transgenic self-incompatible *A. thaliana*

is likely to be a very helpful tool for exploring potential molecular overlaps between SI and PI pathways.

REFERENCES

Berendzen K, Searle I, Ravenscroft D, Koncz C, Batschauer A, Coupland G, Somssich IE, Ülker B. 2005. A rapid and versatile combined DNA/RNA extraction protocol and its application to the analysis of a novel DNA marker set polymorphic between *Arabidopsis thaliana* ecotypes Col-0 and Landsberg *erecta*. *Plant Methods* **1**, 4.

Bleecker AB, Estelle MA, Somerville C, Kende H. 1988. Insensitivity to ethylene conferred by a dominant mutation in *Arabidopsis thaliana*. *Science* **241**, 1086-1089.

Boutrot F, Segonzac C, Chang KN, Qiao H, Ecker JR, Zipfel C, Rathjen JP. 2010. Direct transcriptional control of the *Arabidopsis* immune receptor FLS2 by the ethylene-dependent transcription factors EIN3 and EIL1. *Proceedings of the National Academy of Sciences of the United States of America* **107**, 14502-14507.

Bower MS, Matias DD, Fernandes-Carvalho E, Mazzurco M, Gu T, Rothstein SJ, Goring DR. 1996. Two Members of the Thioredoxin-h Family Interact with the Kinase Domain of a *Brassica S* Locus Receptor Kinase. *The Plant Cell* **8**, 1641-1650.

Cabrillac D, Cock JM, Dumas C, Gaude T. 2001. The *S*-locus receptor kinase is inhibited by thioredoxins and activated by pollen coat proteins. *Nature* **410**, 220-223.

Cao H, Bowling SA, Gordon AS, Dong X. 1994. Characterization of an *Arabidopsis* Mutant That Is Nonresponsive to Inducers of Systemic Acquired Resistance. *The Plant Cell* **6**, 1583-1592.

Chookajorn T, Kachroo A, Ripoll DR, Clark AG, Nasrallah JB. 2004. Specificity determinants and diversification of the *Brassica* self-incompatibility pollen ligand. *Proceedings of the National Academy of Sciences of the United States of America* **101**, 911-917.

Clough S, Bent AF. 1998. Floral dip: a simplified method for *Agrobacterium*-mediated transformation of *Arabidopsis thaliana*. *The Plant Journal* **16**, 735-743.

Dellaporta SL, Wood J, Hicks JB. 1983. A plant DNA minipreparation: Version II. *Plant Molecular Biology Reporter* **1**, 19-21.

Doyle JJ, Doyle JL. 1990. Isolation of Plant DNA from Fresh Tissue. *Focus* **12**, 13-15.

Dwyer KG, Lalonde BA, Nasrallah JB, Nasrallah ME. 1992. Structure and expression of *AtS1*, an *Arabidopsis thaliana* gene homologous to the *S*-locus related genes of *Brassica*. *Molecular and General Genetics* **231**, 442-448.

Dwyer KG, Kandasamy MK, Mahosky DI, Acciai J, Kudish BI, Miller JE, Nasrallah ME, Nasrallah JB. 1994. A Superfamily of *S* Locus-Related Sequences in Arabidopsis: Diverse Structures and Expression Patterns. *The Plant Cell* **6**, 1829-1843.

Elleman CJ, Dickinson HG. 1999. Commonalities between pollen/stigma and host/pathogen interactions: calcium accumulation during stigmatic penetration by *Brassica oleracea* pollen tubes. *Sexual Plant Reproduction* **12**, 194-202.

Glazebrook J. 2001. Genes controlling expression of defense responses in *Arabidopsis* – 2001 status. *Current Opinion in Plant Biology* **4**, 301-308.

Glazebrook J, Rogers EE, Ausubel FM. 1996. Isolation of Arabidopsis mutants with enhanced disease susceptibility by direct screening. *Genetics* **148**, 973-982.

Gómez-Gómez L, Boller T. 2000. FLS2: An LRR receptor-like kinase involved in the perception of the bacterial elicitor flagellin in *Arabidopsis*. *Molecular Cell* **5**, 1003-1011.

González-Lamothe R, Tsitsigiannis DI, Ludwig AA, Panicot M, Shirasu K, Jones JDG. 2006. The U-Box Protein CMPG1 Is Required for Efficient Activation of Defense Mechanisms Triggered by Multiple Resistance Genes in Tobacco and Tomato. *The Plant Cell* **18**, 1067-1083.

Gu T, Mazzurco M, Sulaman W, Matias, DD, Goring DR. 1998. Binding of an arm repeat protein to the kinase domain of the *S*-locus receptor kinase. *Proceedings of the National Academy of Sciences of the United States of America* **95**, 382-387.

Guzmán P, Ecker JR. 1990. Exploiting the triple response of *Arabidopsis* to identify ethylene-related mutants. *The Plant Cell* **2**, 513-523.

Haffani YZ, Gaude T, Cock JM, Goring DR. 2004. Antisense suppression of thioredoxin *h* mRNA in *Brassica napus cv.* Westar pistils causes a low level constitutive pollen rejection response. *Plant Molecular Biology* **55**, 619-630.

Hodgkin T, Lyon GD, Dickinson HG. 1988. Recognition in flowering plants: A comparison of the *Brassica* self-incompatibility system and plant pathogen interactions. *New Phytologist* **110**, 557-569.

Hugot K, Ponchet M, Marais A, Galiana E. 2002. A tobacco S-like RNase inhibits hyphal elongation of plant pathogens. *Molecular Plant-Microbe Interactions* **15**, 243-250.

Iwano M, Shiba H, Matoba K, Miwa T, Funato M, Entani T, Nakayama P, Shimosato H, Takaoka A, Isogai A, Takayama S. 2007. Actin dynamics in papilla cells of *Brassica rapa* during self- and cross-pollination. *Plant Physiology* **144**, 72-81.

James P, Halladay J, Craig EA. Genomic Libraries and a Host Strain Designed for Highly Efficient Two-Hybrid Selection in Yeast. *Genetics* **144**, 1425-1436.

Jones JDG, Dangl JL. 2006. The plant immune system. *Nature* **444**, 323-329.

Kitashiba H, Liu P, Nishio T, Nasrallah JB, Nasrallah ME. 2011. Functional test of *Brassica* self-incompatibility modifiers in *Arabidopsis thaliana*. *Proceedings of the National Academy of Sciences of the United States of America* **44**, 18173-18178.

Lay FT, Schirra HJ, Scanlon MJ, Anderson MA, Craik DJ. 2003. The three-dimensional solution structure of NaD1, a new floral defensin from *Nicotiana alata* and its application to a homology model of the crop defense protein alfAFP. *Journal of Molecular Biology* **325**, 175-188.

Liu P, Sherman-Broyles S, Nasrallah ME, Nasrallah JB. 2007. A cryptic modifier causing transient self-incompatibility in *Arabidopsis thaliana*. *Current Biology* **17**, 734-740.

Lu D, Lin W, Gao X, Wu S, Cheng C, Avila J, Heese A, Devarenne TP, He P, Shan L. 2011. Direct Ubiquitination of Pattern Recognition Receptor FLS2 Attenuates Plant Innate Immunity. *Science* **332**, 1439-1442.

Luu D-T, Marty-Mazars D, Trick M, Dumas C, Heizmann P. Pollen-Stigma Adhesion in *Brassica* spp Involves SLG and SLR1 Glycoproteins. *The Plant Cell* **11**, 251-262.

Martinez-Trujillo M, Limones-Briones V, Cabrera-Ponce JL, Herrera-Estrella L. 2004. Improving Transformation Efficiency of *Arabidopsis thaliana* by Modifying the Floral Dip Method. *Plant Molecular Biology Reporter* **22**, 63-70.

Mazzurco M, Sulaman W, Elina H, Cock JM, Goring DR. 2001. Further analysis of the interactions between the *Brassica S* receptor kinase and three interacting proteins (ARC1, THL1 and THL2) in the yeast two-hybrid system. *Plant Molecular Biology* **45**, 365-376.

Mudgil Y, Shiu S-H, Stone SL, Salt JN, Goring DR. A Large Complement of the Predicted Arabidopsis ARM Repeat Proteins Are Members of the U-Box E3 Ubiquitin Ligase Family. *Plant Physiology* **134**, 59-66.

Murase K, Shiba H, Iwano M, Che F-S, Watanabe M, Isogai A, Takayama S. 2004. A membrane-anchored protein kinase involved in *Brassica* self-incompatibility signaling. *Science* **303**, 1516-1519.

Napp-Zinn K. 1985. *Arabidopsis thaliana*. In: Halevy HA, ed. *Handbook of Flowering*, Vol. 1. Boca Raton, FL: CRC press, 492-503.

Nasrallah JB. 2005. Recognition and rejection of self in plant self-incompatibility: comparisons to animal histocompatibility. *TRENDS in Immunology* **26**, 412-418.

Nasrallah ME, Liu P, Nasrallah JB. 2002. Generation of self-incompatible *Arabidopsis thaliana* by transfer of two *S* locus genes from *A. lyrata*. *Science* **297**, 247-249.

Nasrallah ME, Liu P, Sherman-Broyles S, Boggs N, Nasrallah JB. 2004. Natural variation in expression of self-incompatibility in *Arabidopsis thaliana*: Implications for the evolution of selfing. *Proceedings of the National Academy of Sciences of the United States of America* **101**, 16070-16074.

Navarro L, Zipfel C, Rowland O, Keller I, Robatzek S, Boller T, Jones JDG. 2004. The transcriptional innate immune response to flg22. Interplay and overlap with Avr gene-dependent defense responses and bacterial pathogenesis. *Plant Physiology* **135**, 1113-1128.

Neff MM, Turk E, Kalishman M. 2002. Web-based primer design for single nucleotide polymorphism analysis. *TRENDS in Genetics* **18**, 613-615.

Parker JE, Holub EB, Frost LN, Falk A, Gunn ND, Daniels MJ. 1996. Characterization of *eds1*, a Mutation in Arabidopsis Suppressing Resistance to *Peronospora parasitica* Specified by Several Different *RPP* Genes. *The Plant Cell* **8**, 2033-2046.

Pastuglia M, Swarup R, Rocher A, Saindrenan P, Roby D, Dumas C, Cock JM. 2002. Comparison of the expression patterns of two small gene families of S gene family receptor kinase genes during the defence response in *Brassica oleracea* and *Arabidopsis thaliana*. *Gene* **282**, 215–225.

Rea AC, Liu P, Nasrallah JB. 2010. A transgenic self-incompatible *Arabidopsis thaliana* model for evolutionary and mechanistic studies of crucifer self-incompatibility. *Journal of Experimental Botany* doi:10.1093/jxb/erp393.

Rivas S, Rougon-Cardoso, A, Smoker M, Schauser L, Yoshioka H, Jones JDG. 2004. CITRX thioredoxin interacts with the tomato Cf-9 resistance protein and negatively regulates defence. *The European Molecular Biology Organization Journal* **23**, 2156–2165.

Rowland O, Ludwig AA, Merrick CJ, Baillieul F, Tracy FE, Durrant WE, Fritz-Laylin L, Nekrasov V, Sjölander K, Yoshioka H, Jones JDG. 2005. Functional Analysis of *Avr9/Cf-9 Rapidly Elicited* Genes Identifies a Protein Kinase, ACIK1, That Is Essential for Full Cf-9–Dependent Disease Resistance in Tomato. *The Plant Cell* **17**, 295-310.

Samuel MA, Chong YT, Haasen KE, Aldea-Brydges MG, Stone SL, Goring DR. 2009. Cellular Pathways Regulating Responses to Compatible and Self-Incompatible Pollen in *Brassica* and *Arabidopsis* Stigmas Intersect at Exo70A1, a Putative Component of the Exocyst Complex. *The Plant Cell* **21**, 2655-2671.

Sanabria N, Goring D, Nürnberger T, Dubery I. 2008. Self/nonself perception and recognition mechanisms in plants: a comparison of self-incompatibility and innate immunity. *New Phytologist* **178**, 503-514.

Sanda SL, Amasino RM. 1995. Genetic and physiological analysis of flowering time in the C24 line of *Arabidopsis thaliana.* Weeds World **2**, 2-8.

Sarker RH, Elleman CJ, Dickinson HG. Control of pollen hydration in *Brassica* requires continued protein synthesis, and glycosylation is necessary for intraspecific incompatibility. *Proceedings of the National Academy of Sciences of the United States of America* **85**, 4340-4344.

Schopfer CR, Nasrallah ME, Nasrallah JB. 1999. The Male Determinant of Self-Incompatibility in *Brassica*. *Science* **286**, 1697-1700.

Segura A, Moreno M, Molina A, García-Olmedo F. 1998. Novel defensin subfamily from spinach (*Spinacia oleracea*). *FEBS Letters* **435**, 159-162.

Stead AD, Roberts IN, Dickinson HG. 1980. Pollen-stigma interaction in *Brassica oleracea*: the role of stigmatic proteins in pollen grain adhesion. *Journal of Cell Science* **42**, 417-423.

Stein JC, Howlett B, Boyes DC, Nasrallah ME, Nasrallah JB. 1991. Molecular cloning of a putative receptor protein kinase gene encoded at the self-incompatibility locus of *Brassica oleracea*. *Proceedings of the National Academy of Sciences of the United States of America* **88**, 8816-8820.

Stein JC, Dixit R, Nasrallah ME, Nasrallah JB. 1996. SRK, the Stigma-Specific S Locus Receptor Kinase of Brassica, Is Targeted to the Plasma Membrane in Transgenic Tobacco. *The Plant Cell* **8**, 429-445.

Stone SL, Anderson EM, Mullen RT, Goring DR. 2003. ARC1 Is an E3 Ubiquitin Ligase and Promotes the Ubiquitination of Proteins during the Rejection of Self-Incompatible *Brassica* Pollen. *The Plant Cell* **15**, 885-898.

Stone SL, Arnoldo M, Goring DR. 1999. A Breakdown of *Brassica* Self-Incompatibility in ARC1 Antisense Transgenic Plants. *Science* **286,** 1729-1731.

Suzuki G, Kai N, Hirose T, Fukui K, Nishio T, Takayama S, Isogai A, Watanabe M, Hinata K. 1999. Genomic Organization of the *S* Locus: Identification and Characterization of Genes in *SLG/SRK* Region of S^9 Haplotype of *Brassica campestris* (syn. *rapa*). *Genetics* **153**, 391-400.

Takasaki T, Hatakeyama K, Suzuki G, Watanabe M, Isogai A, Hinata K. 2000. The *S* receptor kinase determines self-incompatibility in *Brassica* stigma. *Nature* **403**, 913-916.

Thomas SG, Franklin-Tong VE. 2004. Self-incompatibility triggers programmed cell death in *Papaver* pollen. *Nature* **429**, 305-309.

Tiffin P, Moeller DA. 2006. Molecular evolution of plant immune system genes. *TRENDS in Genetics* **22**, 662–670.

Tör M, Gordon P, Cuzick A, Eulgem T, Sinapidou E, Mert-Türk F, Can C, Dangl JL, Holub EB. 2002. Arabidopsis SGT1b Is Required for Defense Signaling Conferred by Several Downy Mildew Resistance Genes. *The Plant Cell* **14**, 993-1003.

Tornero P, Merritt P, Sadanandom A, Shirasu K, Innes RW, Dangl JL. 2002. *RAR1* and *NDR1* Contribute Quantitatively to Disease Resistance in Arabidopsis, and Their Relative Contributions Are Dependent on the *R* Gene Assayed. *The Plant Cell* **14**, 1005-1015.

Trujillo M, Ichimura K, Casais C, Shirasu K. 2008. Negative Regulation of PAMP-Triggered Immunity by an E3 Ubiquitin Ligase Triplet in *Arabidopsis*. *Current Biology* **18**, 1396-1401.

Tung C-W, Dwyer KG, Nasrallah ME, Nasrallah JB. 2005. Genome-Wide Identification of Genes Expressed in Arabidopsis Pistils Specifically along the Path of Pollen Tube Growth. *Plant Physiology* **138**, 977-989.

Wang D, Weaver ND, Kesarwani M, Dong X. 2005. Induction of Protein Secretory Pathway Is Required for Systemic Acquired Resistance. Science **308,** 1036-1040.

Yang C-W, González-Lamothe R, Ewan RA, Rowland O, Yoshioka H, Shenton M, Ye H, O'Donnell E, Jones JDG, Sadanandom A. 2006. The E3 Ubiquitin Ligase Activity of *Arabidopsis* PLANT U-BOX17 and Its Functional Tobacco Homolog ACRE276 Are Required for Cell Death and Defense. *The Plant Cell* **18**, 1084-1098.

Zipfel C, Robatzek S, Navarro L, Oakeley EJ, Jones JDG, Felix G, Boller T. 2004. Bacterial disease resistance in *Arabidopsis* through flagellin perception. *Nature* **428**, 764-767.

CHAPTER 3

Visualization of SRK, the female self-incompatibility specificity determinant, in the stigma of transgenic self-incompatible *Arabidopsis thaliana*, using confocal microscopy

INTRODUCTION

Little is known about the cellular events that are triggered in the self-incompatibility (SI) response after the *S*-locus receptor kinase (SRK) in the plasma membrane of the stigma epidermal (papillar) cells is bound and activated by its cognate *S*-locus cysteine-rich (SCR) ligand in the pollen coat. In particular, the subcellular distribution and dynamics of the SRK receptor before and after pollination with incompatible pollen has not been described, and this lack of information represents a gap in our understanding of SRK-mediated signaling. Understanding SRK dynamics in response to its SCR ligand is particularly important in view of the highly localized nature of the SI response in the Brassicaceae, whereby a single stigma epidermal cell is able to distinguish between self and non-self pollen grains and to inhibit the development of self pollen tubes while allowing the growth of non-self pollen tubes.

A common strategy for visualizing a protein of interest in live cells is to tag it with a fluorescent protein (FP) and monitor its behavior by confocal microscopy. Such an approach has been used for analysis of other plant receptors (e.g., FLS2, BRI1, and CLV1) (Robatzek *et al.* 2006; Geldner *et al.* 2007; Nimchuk *et al.* 2011), but it has not as yet been used successfully for SRK. In one report, an attempt to express a green fluorescent protein (GFP)-tagged SRK (*Brassica oleracea* SRK_3) in transgenic *Arabidopsis lyrata* was unsuccessful (Fobis-Loisy *et al.* 2007). This chapter describes the visualization of functional FP-tagged versions of SRK in a transgenic self-incompatible *A. thaliana* model. Although *A. thaliana* is normally self-

compatible, it can be made to express the SI trait by transformation with *SRK-SCR* gene pairs isolated from self-incompatible *A. lyrata* or *Capsella gandiflora* (Nasrallah *et al.* 2002, 2004; Boggs *et al.* 2009*a*). Indeed, *SRK-SCR* transformants of several *A. thaliana* ecotypes (e.g., C24) express a robust SI response identical to that of naturally self-incompatible *A. lyrata* or *Brassica* species (Nasrallah *et al.* 2004; Boggs *et al.* 2009*a*). This transgenic self-incompatible *A. thaliana* system has been used successfully for structure-function studies of SRK (Boggs *et al.* 2009*b*). It is also an excellent platform for analyzing SRK subcellular localization, not only because of the ease with which *A. thaliana* transformants may be generated and propagated, but most importantly, because *A. thaliana* lacks functional SRK, and any FP-tagged SRK that is visualized via confocal microscopy would represent the entire pool of SRK.

FP-tagged versions of the SRKb variant (Kusaba *et al.* 2001) were expressed in *A. thaliana* using the *SRKb* promoter or a promoter active specifically in stigma epidermal cells. FP-tagged SRKb was visualized by confocal microscopy and its subcellular distribution was assessed by co-localization with markers for various subcellular compartments. In addition to providing a first view of SRK distribution in live cells, the study also provides useful information on the architecture of the stigma epidermal cell in comparison to other commonly studied epidermal cells, such as those from leaves.

MATERIALS & METHODS

Construct design, cloning, and bacterial transformation

The chimeric genes used to express fluorescent protein (FP)-tagged SRKb proteins in stigma epidermal cells are listed in Table 1. One set of chimeric genes was designed to express SRKb with the Citrine yellow fluorescent protein variant (cYFP) tag at its N terminus (tag

Table 1. cYFP-tagged SRKb constructs transformed into *Arabidopsis thaliana*.
Table depicting (1) the various constructs transformed separately into *A. thaliana* plants, (2) which SRKb proteins are presumably produced from these constructs, and (3) whether ("yes") or not ("no") these proteins are predicted to be tagged with cYFP, allowing them to be visualized by fluorescence microscopy. The only cYFP-tagged protein produced from the *SRKb-cYFP* constructs should be the full-length SRKb protein because the *cYFP* gene was cloned at the C terminus of the *SRKb* gene, the end of the protein kinase domain, a domain which is lacking in the eSRKb and tSRKb proteins. The *cYFP-SRKb* constructs should produce all three proteins (full-length SRKb, tSRKb, and eSRKb) with the cYFP tag, as the *cYFP* gene was cloned at the N terminus of the *SRKb* gene, and all three proteins have the same N terminus derived from the *SRKb* gene sequence. The *cYFP-SRKb*(cDNA) constructs should lack the eSRKb protein altogether because these constructs lack the *SRKb* introns, the first of which contains the alternative splice site necessary to produce eSRKb; thus, the cYFP-tagged proteins produced from these constructs are full-length SRKb and tSRKb, only. N/A, not applicable.

Construct	full-length SRKb		tSRKb		eSRKb	
	present	fluorescent	present	fluorescent	present	fluorescent
AtS1 pr::*SRKb:cYFP*	yes	yes	yes	no	yes	no
AtS1 pr::*cYFP:SRKb*	yes	yes	yes	yes	yes	yes
AtS1 pr::*cYFP:SRKb* + *SCRb* pr::*SCRb*	yes	yes	yes	yes	yes	yes
SRKb pr::*cYFP:SRKb* + *SCRb* pr::*SCRb*	yes	yes	yes	yes	yes	yes
AtS1 pr::*cYFP:SRKb* (cDNA) + *SCRb* pr::*SCRb*	yes	yes	yes	yes	no	N/A
SRKb pr::*cYFP:SRKb* (cDNA) + *SCRb* pr::*SCRb*	yes	yes	yes	yes	no	N/A

inserted directly downstream of the signal sequence), while others were designed to express SRKb with a cYFP or the mCherry red fluorescent protein variant (mC) tag at its C terminus (tag inserted directly upstream of the stop codon). In all constructs, the FP tag, along with a linker sequence (to minimize the probability of improper folding) was inserted using recombinant PCR into a pCAMBIA1300 derivative containing the *SRKb* transcriptional unit (including introns) or *SRKb* cDNA. Expression of the FP fusion was driven by either an ≈900-bp fragment corresponding to the *SRKb* promoter (Kusaba *et al.* 2001) or an ≈360-bp fragment (Dwyer *et al.* 1994; Boggs *et al.* 2009*c*) corresponding to the promoter of the *AtS1* (At3g12000) gene, which is highly active in stigma epidermal cells (Dwyer *et al.* 1994). Additionally, the *SCRb* genomic sequence was included in some of the constructs.

Transformation constructs designed to express mC-tagged organelle markers in stigma epidermal cells for co-localization with cYFP-tagged SRKb were generated as follows. Plasmids containing chimeric genes in which the CaMV double *35S* promoter drives expression of mC-tagged markers for the plasma membrane (PM), the endoplasmic reticulum (ER), the vacuolar membrane (tonoplast), Golgi, peroxisomes, and mitochondria (Nelson *et al.* 2007) (obtained from Sandy Lazarowitz) are available at the Arabidopsis Biological Resource Center (ABRC). To ensure adequate expression of these organelle markers in stigma epidermal cells, the double CaMV *35S* promoter, which is not highly active in stigma epidermal cells (Wilkinson *et al.* 1997), was replaced with the *AtS1* promoter by recombinant PCR. Organelle markers carrying the mC tag were selected for co-localization with cYFP-tagged SRKb because the cYFP and mC absorption and emission spectra are sufficiently separated for simultaneous confocal imaging of the two proteins.

All chimeric genes were assembled in *Escherichia coli* DH5α cells and sequenced at the sequencing facility of the Cornell University Life Sciences Core Laboratories Center to ensure that no errors were introduced by recombinant PCR. The plasmids were introduced into the *Agrobacterium tumefaciens* GV3101 strain by electroporation, and *Agrobacterium* transformants were selected and grown at 28-30 ºC on LB medium supplemented with Kanamycin (50 µg/mL), Gentamycin (50 µg/mL), and Rifampicin (100 µg/mL).

Plant material, transformation, and growth conditions

The major part of the work described here was performed in *Arabidopsis thaliana* plants of the C24 ecotype. The Bay-0, L*er*-0, Kas-2, Hodja, Cvi-0, and Lz-0 ecotypes were also used for comparative analysis of the *AtS1*pr*::cYFP:SRKb + SCRb*pr*::SCRb* construct in different ecotypes. Furthermore, the *AtS1*pr*::SRKb:mC* construct was analyzed in the C24 and Cvi-0 ecotypes, and the *35S*pr*::GFP* construct (seeds obtained from Jian Hua) was analyzed in the Col-0 ecotype.

Plant transformations were performed via the floral dip method (modified from Clough & Bent 1998 and Martinez-Trujillo *et al.* 2004), using *Agrobacterium* cells, harboring the plasmid of interest, that were grown to an $O.D._{600}$ between 0.8 and 2 and resuspended in infiltration medium consisting of 5% sucrose and 0.02 or 0.005% Silwet L-77 as surfactant. The cYFP- and mC-tagged SRKb constructs were introduced into wild type plants, while the mC-tagged organelle markers were introduced into both wild type plants and plants homozygous for the cYFP-tagged SRKb constructs.

For growth of wild type and transformed *A. thaliana* plants, seeds were sterilized in 20% (v/v) bleach with vigorous shaking for 5-20 minutes, and then washed 4-5 times with sterile

Milli-Q® H_2O in a sterile hood. Using sterile toothpicks, sterilized seeds were plated on Murashige and Skoog (MS) agar medium supplemented with 1% (w/v) sucrose (pH 5.7). Wild type (untransformed) seeds were plated on medium without antibiotics. To select for the transgenes, seeds of plants transformed with pCAMBIA1300 derivatives (including each of the various FP-tagged SRKb constructs) and those transformed with the *35S::GFP* plasmid were plated on medium containing Hygromycin (60 µg/mL), while seeds of plants transformed with a pBIN+ plasmid containing *SRKb*pr*::SRKb* + *SCRb*pr*::SCRb* were plated on medium containing Kanamycin (30 µg/mL). Seeds of plants carrying the mC-tagged organelle marker transgenes were selected on medium containing Glufosinate-ammonium (10 µg/mL). Plated seeds were stratified at 4 ºC in the dark for 3-5 days and subsequently placed in growth chambers (20-25 ºC) to allow germination and seedling growth. Seedlings were transplanted to Metro-Mix® 200 (Sun Gro®) soil and returned to the same chambers. Seeds, seedlings, and mature plants were grown in either growth rooms or chambers equipped with fluorescent bulbs alone, high-pressure sodium and metal halide bulbs, or metal halide bulbs alone, and were subjected to constant light in growth rooms, or 16 hr. light / 8 hr. dark cycles in chambers. Plants were watered with water oftentimes supplemented with Nitrogen-Phosphorus-Potassium fertilizer.

Pollination assays

Pollination assays were performed to assess the functionality of FP-tagged SRKb proteins. These assays used the most mature floral buds on an inflorescence, at the −1-stage of development, which is just prior to, or at the commencement of, anthesis (or flower opening). These buds were used for two reasons: (1) their stigmas express an intense self-incompatibility (SI) response, and (2) the −1 developmental stage precedes anther dehiscence, and as a result the

stigmas of −1-stage floral buds are free of pollen. For each pollination assay, floral buds were removed at their pedicels from the inflorescence stems and placed pedicel-down in 0.4% agarose to maintain hydration of the bud tissues. Fine-tipped forceps and a stereoscope were used to pollinate the stigma of each bud using mature pollen from open flowers. After 2-4 hours, which is sufficient time to allow growth of pollen tubes in compatible pollinations, the buds were fixed in 3 parts ethanol : 1 part acetic acid at 4 ºC overnight. Fixative was then removed and buds were washed twice with H_2O. The buds were then treated with 1M NaOH and incubated at 60-65 ºC for 15-30 minutes to soften the tissue. The NaOH solution was then removed, and buds were washed twice with H_2O. The buds were subsequently treated with decolorized aniline blue solution to stain callose. The pistils of treated buds were excised and mounted on microscope slides in order to visualize pollen tubes under UV light using a Leica DM5500 epifluorescence microscope. Pollination images were captured using a color charge-coupled device (CCD) camera, ProgRes C14 acquisition software, and a UV filter cube (band-pass (BP) 340-380 excitation filter, long-pass 425 emission filter, 400 dichroic mirror).

Establishment of plant lines homozygous for a single cYFP-tagged SRKb transgene integration

To establish homozygous lines for imaging studies, plant genomic DNA was extracted, using a CTAB method (modified from Doyle & Doyle 1990), from transformants that expressed each of the cYFP-tagged SRKb proteins and exhibited a robust SI response. DNA gel blot analysis was used to determine which transformants contained single transgene integrations. Homozygous lines derived from these single-integration transformants were then identified among T_2 plants by growing T_3 seedlings on antibiotic-resistance selection media and selecting

the lines that produced only antibiotic-resistant T_3 progenies. These homozygous single-integration lines were used for the comparative confocal microscopic analyses of SRKb distribution described in this chapter.

Stereoscope fluorescence microscopy and laser scanning confocal microscopy

A stigma sample was obtained by using fine-tipped forceps to excise the −1 bud from an inflorescence and "planting" the bud by placing its pedicel into 0.4% agarose solidified in a 10 cm x 10 cm plastic petri dish. All buds needed for one experiment were placed on the plate and transported to the Plant Cell Imaging Center (PCIC) at the Boyce Thompson Institute (Ithaca, NY). Using an Olympus SZX-12 stereomicroscope and two pairs of fine-tipped forceps, the sepals, petals, and anthers were pulled away from the central pistil to expose the stigma. Pistils were then excised below the style and placed in 0.4% agarose with the stigma facing upward. Fluorescence images of excised pistils were captured with the Olympus SZX-12 stereoscope using a color CCD camera, Optronics MagnaFire acquisition software, and a BP green filter cube (480/30 excitation filter, 535/40 emission filter, 505 dichroic mirror).

For confocal microscopy, one to three excised pistils were placed in a droplet (~17-20 µL) of water (or 5% NaCl, for plasmolysis experiments) on a microscope slide and covered with a coverslip before viewing under the Leica TCS SP5 Laser Scanning Confocal Microscope at the PCIC. Teflon-printed slides were often used to minimize cell bursting because they allowed some depth between the slide and the coverslip. When standard microscope slides were used, the outer edges of the coverslip were sealed with VALAP (1 part Vaseline : 1 part Lanolin : 1 part Paraffin) to minimize the evaporation of the water, which can cause the sample to change

position while viewing. The imaging parameters used in confocal microscopy are indicated in the figure legends and throughout the text.

Protein gel blot analysis

Protein was extracted from 25 −1-stage stigmas and subjected to SDS-PAGE using a 7.5% polyacrylamide gel. Following transfer to an Immobilon PVDF membrane by semi-dry electroblotting, an α-GFP IgG1 mouse monoclonal primary antibody (Covance®) was used (1:3,000 dilution), followed by a peroxidase-conjugated α-mouse monoclonal secondary antibody (1:6,000 dilution) and the Amersham™ ECL™ Plus Western Blotting Detection kit (GE Healthcare Life Sciences) to detect the presence of the cYFP-tagged SRKb proteins.

RESULTS

Generation of transgenic plants that express functional cYFP-tagged SRKb proteins

SRK genes typically produce three different protein species as shown in Figure 1: (1) a full-length, plasma membrane (PM)-spanning SRK protein, which consists of an N-terminal extracellular S domain, a single-pass transmembrane domain, and a cytoplasmic kinase domain; (2) an extracellular soluble SRK protein, designated eSRK, which consists of only the S domain and is produced by a transcript that contains an in-frame stop codon and terminates within the first intron (Stein *et al.* 1991; Giranton *et al.* 1995); and (3) a post-translationally generated membrane-tethered protein, designated tSRK, which lacks the kinase domain and consists of the S domain, the transmembrane domain, and part of the short juxtamembrane domain located between the transmembrane and kinase domains (Shimosato *et al.* 2007).

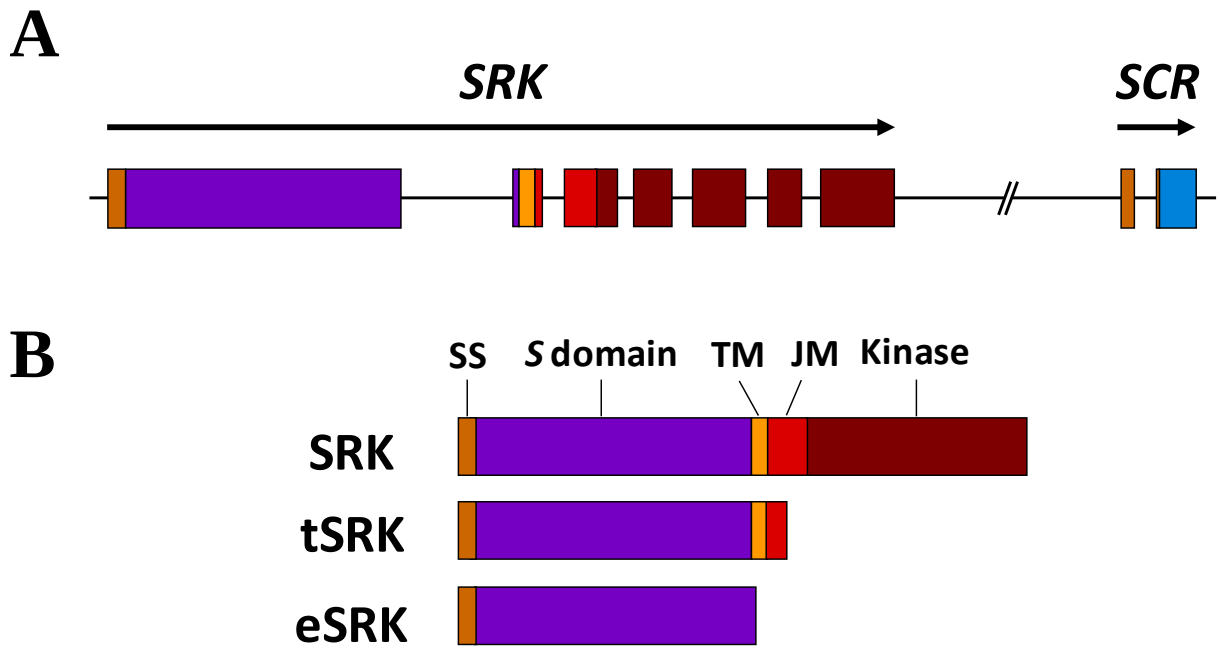

Figure 1. The *S* locus in the self-incompatible Brassicaceae.
(A) SI specificity is determined by at least two tightly-linked genes, *SRK* and *SCR*, at the *S* (*Sterility*) locus. The gene structures of *SRK* and *SCR* are indicated. Rectangles depict exons, and different colors represent regions of the genes that encode for different protein domains. Arrows above the gene structures indicate the 5' to 3' orientation of the genes. Different *S* haplotypes consist of unique *SRK* and *SCR* genes that vary in their relative orientations and physical distances (parallel slashes between the genes). **(B)** Three different proteins are produced from the *SRK* gene: full-length SRK, tSRK, and eSRK. tSRK is a membrane-anchored protein that is produced post-translationally. eSRK is a soluble protein that is produced by alternative splicing. Different protein domains are indicated above the full-length SRK protein. SS, signal sequence; TM, transmembrane domain; JM, juxtamembrane region. Relative genic and protein domains, with the exception of the intergenic region between *SRK* and *SCR* (parallel slashes), are drawn to scale for the *Arabidopsis lyrata Sb* haplotype.

In order to visualize the distribution of SRK proteins *in vivo*, several constructs designed to express the *Arabidopsis lyrata* SRKb protein tagged with the Citrine variant of yellow fluorescent protein (cYFP) were expressed in *A. thaliana* plants. As shown in Table 1, the constructs differed in the following ways: (1) the cYFP sequence was inserted within the *SRKb* coding region either directly downstream of the signal sequence (for expression of SRKb carrying an N-terminus tag, hereafter designated cYFP-SRKb) or directly upstream of the stop codon (for expression of SRKb carrying a C-terminus tag, hereafter designated SRKb-cYFP); (2) the *SRKb* coding sequence was inserted as a genomic sequence that contained introns or as a cDNA sequence that lacked introns; (3) expression of fluorescent protein (FP)-tagged SRKb was driven by either its native promoter or the *AtS1* promoter; and (4) the *SCRb* gene with its native promoter was included in some constructs. While inclusion of the *SCRb* gene allowed for a rough determination of the strength of self-incompatibility (SI) based on autonomous seed set, the other variations in the constructs were designed to ensure proper tissue localization and adequate levels of SRKb expression, and to help differentiate between FP signals derived from the various SRKb isoforms, as described below.

The choice of the native *SRKb* promoter or the *AtS1* promoter was predicated on the fact that both promoters are active in stigma epidermal cells and are able to drive SRK expression to levels sufficient for SI (Nasrallah *et al.* 2002, 2004; Boggs *et al.* 2009*b*), but they differ with respect to cell specificity and strength. A previous study had shown that the *SRKb* promoter directs GUS expression in stigma epidermal cells as well as in the transmitting tract of the style and ovary, and that *SRKb* transcripts accumulate to moderate levels in stigmas (Kusaba *et al.* 2001). In contrast, analysis of an *AtS1*pr::*GUS* reporter had shown that the *AtS1* promoter is active specifically in stigma epidermal cells (Dwyer *et al.* 1994). Additionally, microarray data

had shown that the *AtS1* gene is one of the most highly expressed genes in these cells (Tung *et al.* 2005), and the use of the *AtS1* promoter was expected to ensure that adequate levels of FP-tagged SRKb proteins are produced, especially if these proteins prove to exhibit less stability or activity than non-tagged SRKb. For their part, the use of N- or C-terminal tags and the inclusion or omission of introns was expected to allow differential visualization or production of SRKb isoforms (Table 1). Thus, a C-terminal cYFP tag should allow visualization of only the full-length SRKb protein, an N-terminal cYFP tag together with the inclusion of introns should allow visualization of all three SRK species, and the omission of introns via the use of *SRKb* cDNA should allow visualization of the full-length and tSRKb proteins in the absence of eSRKb, since eSRKb is produced from a transcript that terminates within the first intron of *SRKb* (Figure 1). Finally, the contribution of eSRK to the observed signals may be deduced from features exhibited by stigmas of *cYFP:SRKb* transformants but not by stigmas of *cYFP:SRKb*(cDNA) transformants.

All cYFP-tagged SRKb constructs were introduced into *A. thaliana* plants of the C24 ecotype. In all cases, protein gel blot analysis of total stigma protein extracts detected the expected SRKb isoforms. As shown in Figure 2A, only the full-length SRKb protein was detected in the stigmas of plants transformed with *SRKb:cYFP* transgenes, while three SRKb isoforms were detected in the stigmas of plants transformed with *cYFP:SRKb* transgenes that contained introns. Two isoforms were detected in the stigmas of plants transformed with *cYFP:SRKb* transgenes that lacked introns (not shown). Additionally, a screen of transformants by fluorescence microscopy showed that stigmas expressing cYFP-tagged SRKb proteins produced a signal that was appreciably more intense than the autofluorescence exhibited by

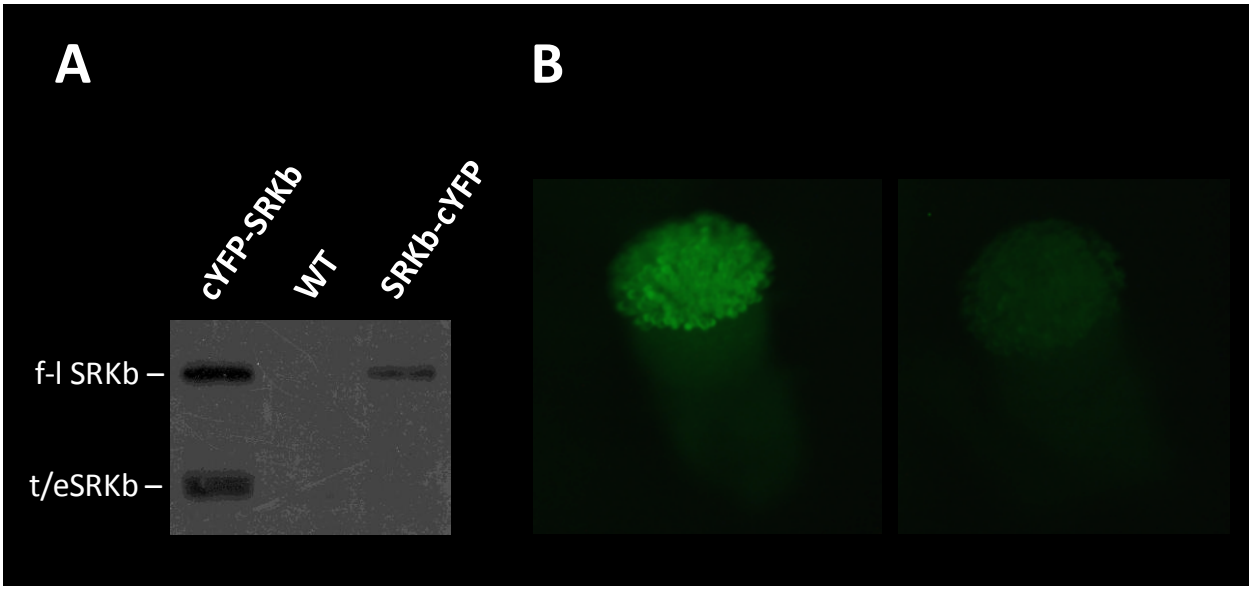

Figure 2. cYFP-tagged SRKb is expressed in transgenic *Arabidopsis thaliana* plants.
(A) Protein gel blot showing SRKb tagged with cYFP at the N terminus (cYFP-SRKb; *AtS1*pr*::cYFP:SRKb*) and at the C terminus (SRKb-cYFP; *AtS1*pr*::SRKb:cYFP*) using an α-GFP antibody against total protein from excised stigmas. Wild type (untransformed) stigmas (WT) were used as a negative control. *SRKb-cYFP* lines should have only the full-length SRKb protein tagged (f-l SRKb; ~125 kDa), while *cYFP-SRKb* lines should have all three proteins tagged (full-length SRKb, tSRKb, and eSRKb). Note that tSRKb and eSRKb (~78 kDa) in the doublet band pair cannot be definitively distinguished in this blot, and that a lower-molecular-weight cross-reactive band is apparent in the WT and SRKb-cYFP samples. **(B)** Fluorescence stereoscope images of excised stigmas of plants transformed with *AtS1*pr*::cYFP:SRKb* (left) and *SRKb*pr*::SRKb* + *SCRb*pr*::SCRb* (right) plants using a BP Green (FITC) filter cube (480/30 excitation filter; 535/40 emission filter) and identical software settings.

untransformed C24 stigmas (Figure 2B), indicating that visualization of the SRKb proteins by confocal microscopy would be feasible.

The functionality of the cYFP-tagged SRKb proteins was tested by pollination assays of stigmas from floral buds at the −1 stage of development (see Materials & Methods), which represents the stage at which a strong SI response is exhibited in all *A. thaliana* ecotypes that express SI (Nasrallah *et al.* 2004; Boggs *et al.* 2009*a*). Stigmas from plants transformed with each of the cYFP-tagged SRKb constructs were pollinated with pollen expressing SCRb or with wild type pollen (i.e., lacking SCRb) as a control. Similar to plants transformed with a construct encoding non-tagged SRKb and SCRb proteins (Figure 3A), plants transformed with each of the cYFP-tagged SRKb constructs were identified in which stigmas inhibited SCRb-expressing pollen but allowed the production of large numbers of wild type pollen tubes (Figure 3B-G). In contrast, wild type stigmas (i.e., lacking SRKb) accept pollen of both genotypes (Figure 3H). Furthermore, transformants expressing both cYFP-tagged SRKb and SCRb set very little seed, similar to transformants expressing non-tagged SRKb and SCRb proteins (not shown). These results indicate that the cYFP-tagged SRKb proteins are indeed functional *in planta*, that the location of the cYFP tag relative to the SRKb protein had no effect on SRKb function, and that the *SRKb* and *AtS1* promoters were both effective at expressing cYFP-tagged SRKb. Additionally, the fact that the *AtS1*pr::*SRKb*(cDNA) construct conferred an SI response that was as intense as that conferred by *SRKb* transgenes capable of producing eSRK demonstrates that eSRK is not required for SI, at least in the case of the *A. lyrata*-derived *Sb* specificity.

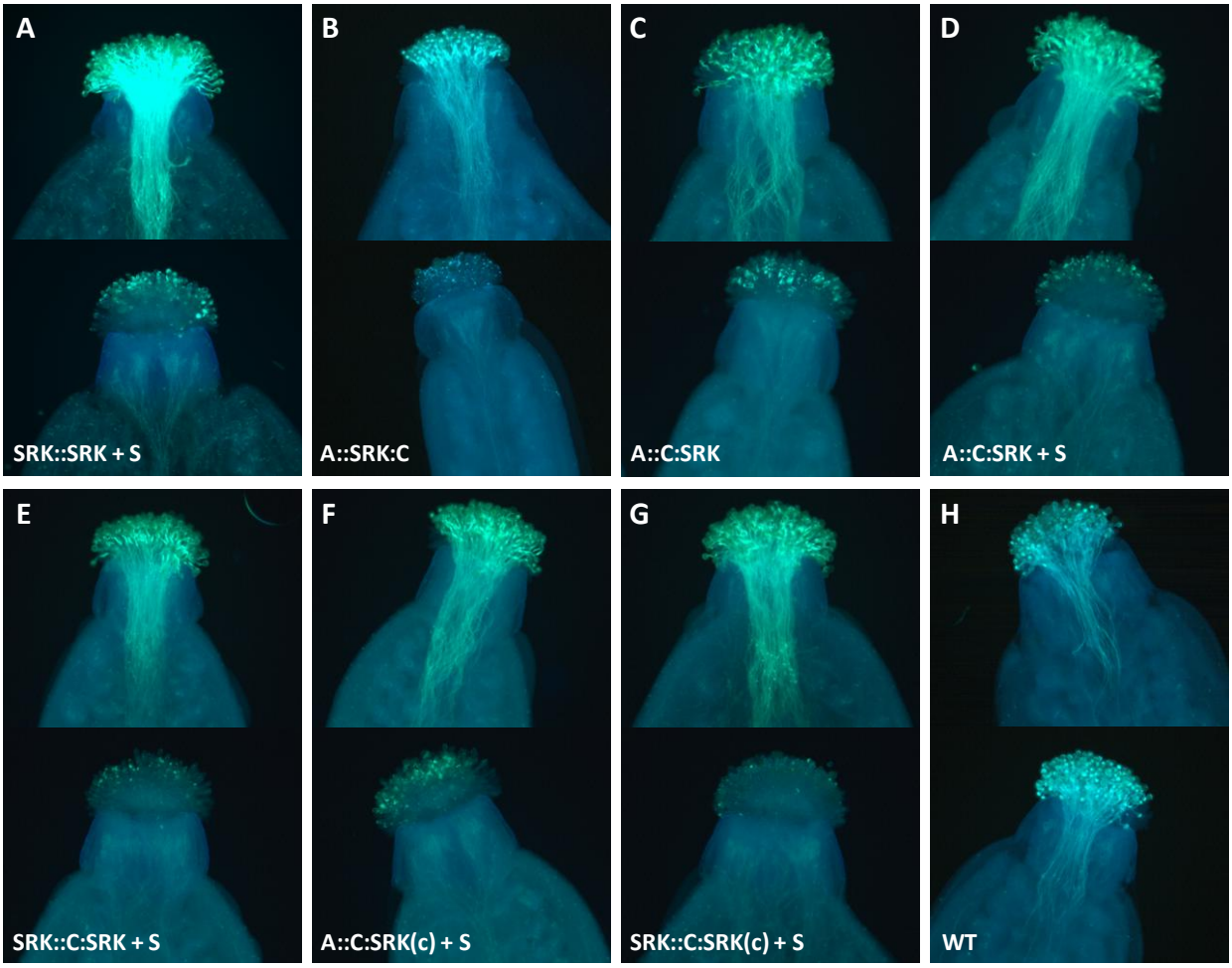

Figure 3. SRKb tagged with cYFP is functional in transgenic *Arabidopsis thaliana* plants. Pistils from −1-stage floral buds of *A. thaliana* transformed with various cYFP-tagged SRKb constructs **(B-G)** accept pollen that does not express SCRb, allowing pollen tube formation and penetration into the continuous transmitting tract of the stigma, style, and ovary (top), and reject pollen that expresses SCRb, precluding pollen tube formation (bottom); these pollination phenotypes are identical to those of *A. thaliana* transformed with untagged SRKb **(A)**, suggesting that tagging SRKb with cYFP does not interfere with its function *in planta*. Wild type (untransformed) *A. thaliana* pistils **(H)** accept both pollen without SCRb (top) and pollen with SCRb (bottom). The two positions of the cYFP tag relative to SRKb (N-terminal or C-terminal), the two promoters with activity in stigmatic tissue and driving the expression of the *SRKb* gene (*SRKb*pr and *AtS1*pr), and the presence or absence of *SCRb* in the same construct do not influence pollination phenotypes: pistils from *A. thaliana* plants transformed with *SRKb*pr*::SRKb* + *SCRb*pr*::SCRb* **(A)**, *AtS1*pr*::SRKb:cYFP* **(B)**, *AtS1*pr*::cYFP:SRKb* **(C)**, *AtS1*pr*::cYFP:SRKb* + *SCRb*pr*::SCRb* **(D)**, *SRKb*pr*::cYFP:SRKb* + *SCRb*pr*::SCRb* **(E)**, *AtS1*pr*::cYFP:SRKb*(cDNA) + *SCRb*pr*::SCRb* **(F)**, *SRKb*pr*::cYFP:SRKb*(cDNA) + *SCRb*pr*::SCRb* **(G)**. Pollen tubes are revealed with callose staining. Top and bottom images of **A-H**, respectively, represent the same genotype, and respective pollinations, treatments, and imaging were performed concurrently.

Establishing optimal parameters for visualizing FP-tagged SRKb by confocal microscopy of stigma epidermal cells

Confocal microscopic analysis of the homozygous cYFP-tagged SRKb transformants required extensive troubleshooting to establish the optimal parameters for generating high-quality, interpretable, and meaningful images. It was first established, using the Leica Application Suite Advanced Fluorescence (LAS AF) software, that the fluorescence emission spectra obtained from confocal images of stigma epidermal cells expressing cYFP-tagged SRKb generally approximated the emission spectrum and peak value of 529 nm expected for the cYFP protein (Griesbeck *et al.* 2001) (Figure 4). Multiple analyses using several different regions of interest (ROIs) from several images revealed that the peak emission value occasionally shifted to 532 nm, as shown for the *AtS1*pr*::cYFP:SRKb* + *SCRb*pr*::SCRb* transformant in Figure 4. Occasional peak shifts in the spectra can be expected when a single ROI is considered (as in Figure 4), because the true spectrum for cYFP is theoretically made up of a combination of all possible ROIs. In addition, the fluorescence values in Figure 4 were determined every 3 nm, the spectral length of the step size chosen for the lambda scan, which ignores the values in between and cannot produce the smooth curve expected for the true cYFP emission spectrum.

Autofluorescence of stigma epidermal cells was a potentially problematic issue that was investigated in this study. Under the imaging parameters typically used for confocal imaging of cYFP, and consistent with the fluorescence images shown in Figure 2B, wild type stigma epidermal cells were found to exhibit autofluorescence at their periphery (Figure 5A), specifically within the cell wall as determined by the plasmolysis experiments described later. The autofluorescence peak fell at the approximate spectral position of the peak in the cYFP spectrum, but it was broader and more red-shifted than the cYFP peak (Figure 4), which could be

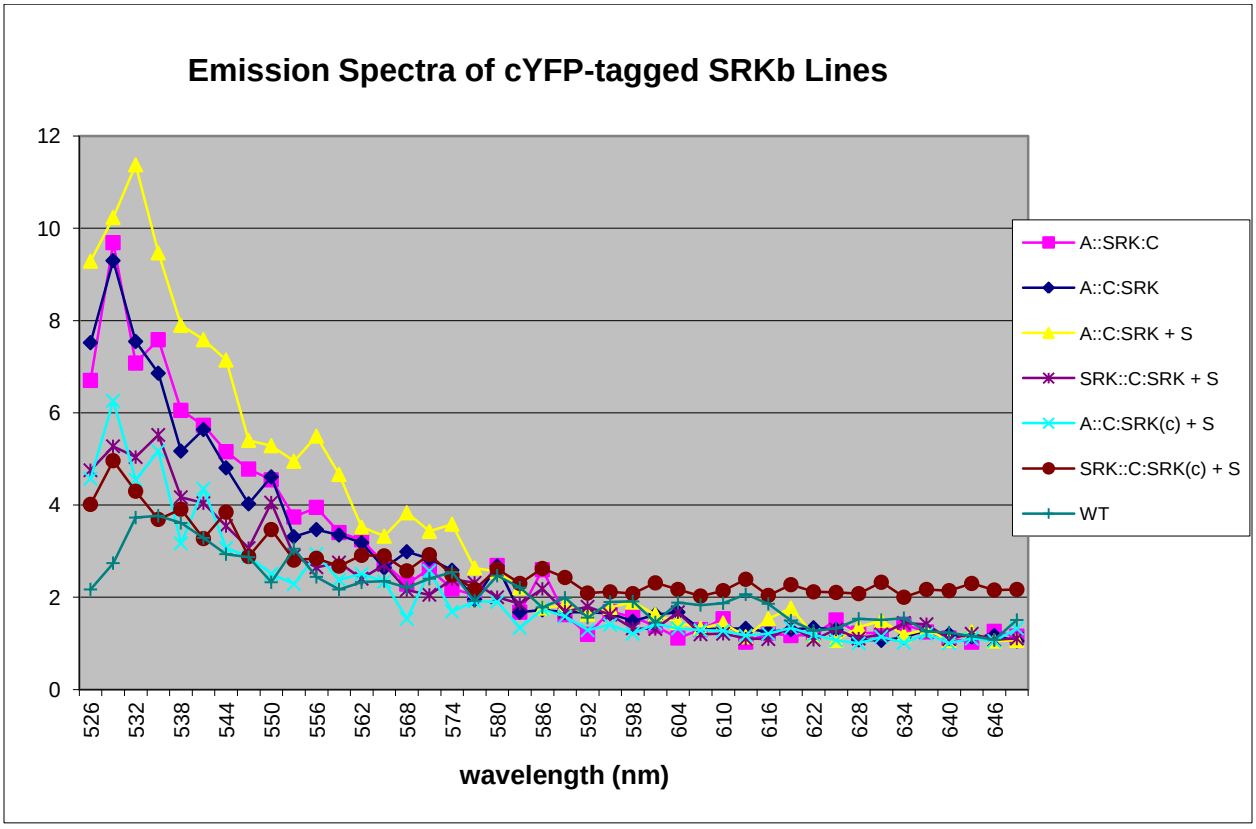

Figure 4. Emission spectra of cYFP-tagged SRKb lines.
Representative fluorescence emission spectra of the cYFP-tagged SRKb lines, obtained experimentally by performing confocal microscopy lambda scans of the stigma epidermis from a −1-stage floral bud of a homozygous, *Arabidopsis thaliana* transformant, each transformed separately with the various constructs. All images were captured with identical parameters, including the gain value, such that differences in signal levels could be compared (25% Argon laser power; 49% 514 nm laser line intensity; 1 line-averaging; 1061 V gain; lambda scan: 526-649 nm range (123 nm total), 5 nm bandwidth, 42 steps, 3 nm stepsize). An untransformed wild type (WT) sample was included for comparison. The region of interest selected to obtain arbitrary fluorescence values (Y-axis) for analysis was the same size and shape for each sample, and was positioned strategically over a small area at the cell periphery, devoid of chloroplasts, where fluorescence was visible. A::SRK:C, *AtS1*pr*::SRKb:cYFP*; A::C:SRK, *AtS1*pr*::cYFP:SRKb*; A::C:SRK + S, *AtS1*pr*::cYFP:SRKb* + *SCRb*pr*::SCRb*; SRK::C:SRK + S, *SRKb*pr*::cYFP:SRKb* + *SCRb*pr*::SCRb*; A::C:SRK(c) + S, *AtS1*pr*::cYFP:SRKb*(cDNA) + *SCRb*pr*::SCRb*; SRK::C:SRK(c) + S, *SRKb*pr*::cYFP:SRKb*(cDNA) + *SCRb*pr*::SCRb*.

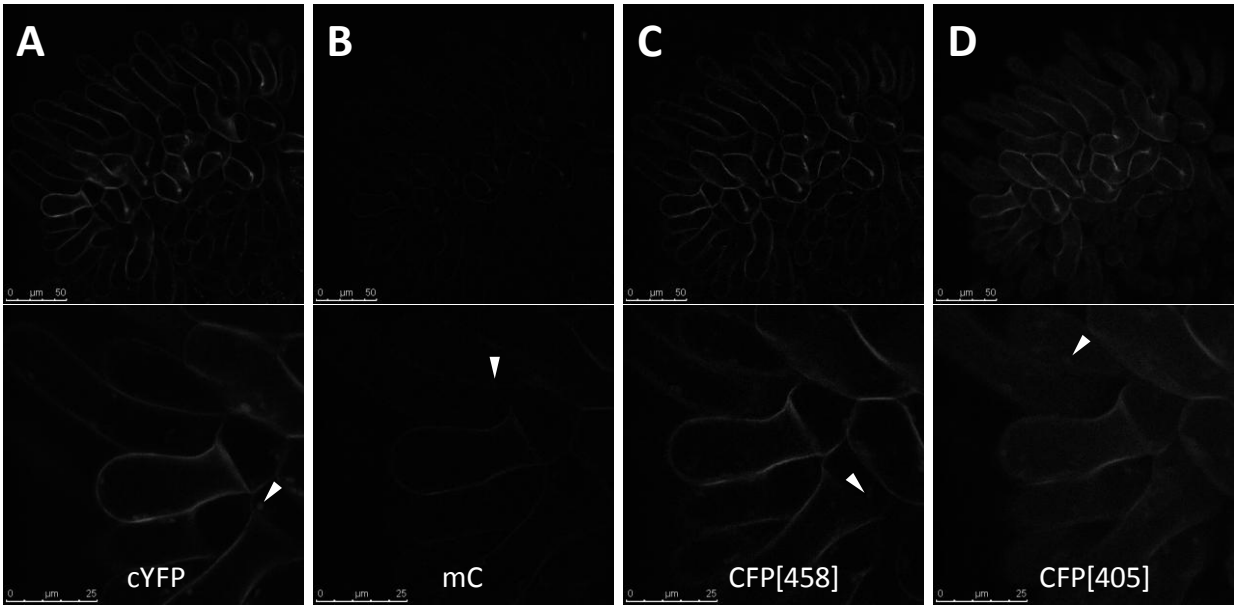

Figure 5. Autofluorescence of the *Arabidopsis thaliana* stigma epidermis seen with confocal microscopy imaging parameters used for different fluorescent proteins.
Under all confocal microscopy imaging parameters used for visualizing various fluorescent proteins, some autofluorescence of the stigma epidermal cells is evident. For best comparison of the autofluorescence visualized using the different fluorescent protein parameters, the same wild type C24 stigma sample was imaged under each set of confocal imaging parameters for cYFP (**A**, 25% Argon laser power; 49% 514 nm laser line intensity; 522-550 nm emission), mC (**B**, 50% 561 nm DPSS laser line intensity; 592-629 nm emission), and CFP (**C** (CFP[458]), 25% Argon laser power; 50% 458 nm laser line intensity; 466-491 nm emission & **D** (CFP[405]), 50% 405 nm Near UV Diode laser line intensity; 466-491 nm emission). Images were captured sequentially at 1X (top) and 3X (bottom) zoom values, and in consecutive order, as represented in the figure (**A** (top, followed by bottom), **B** (top, followed by bottom), etc.). Autofluorescence of the cell walls and chloroplasts (arrowheads) of the stigma epidermal cells can be seen for each set of imaging parameters. Note that because a live sample was used and the images were captured sequentially, the position of the chloroplasts has changed from one image to the next.

due to the combined signal produced by cYFP and the autofluorescence of a cell wall-localized molecule, such as lignin (Chapman *et al.* 2005).

To determine if the autofluorescence of stigma epidermal cells could be minimized or eliminated, wild type untransformed stigmas were examined for autofluorescence using confocal imaging parameters for the commonly used FPs, mCherry (mC) and cyan fluorescent protein (CFP), as well as cYFP. The following parameters were utilized: for cYFP, 25% Argon laser power, 49% 514 nm laser line intensity, 522-550 nm emission (Figure 5A); for mC, 50% 561 nm DPSS laser line intensity, 592-629 nm emission (Figure 5B); and for CFP, two sets of parameters: CFP[458], 25% Argon laser power, 50% 458 nm laser line intensity, 466-491 nm emission (Figure 5C); and CFP[405], 50% 405 nm Near UV Diode laser line intensity, 466-491 nm emission (Figure 5D). In order to visualize most clearly the potential autofluorescence under these imaging parameters, gain levels were increased beyond what would be required for highly-expressed FPs. For best comparison of the autofluorescence produced using the various imaging parameters, the same stigma sample was imaged using each set of parameters. Under all imaging parameters tested, some autofluorescence of the stigma epidermal cells was evident (Figure 5).

All sets of parameters caused autofluorescence of both the cell walls and chloroplasts of stigma epidermal cells (Figure 5). However, cell wall autofluorescence was most apparent with cYFP and CFP[458] parameters, and chloroplast autofluorescence was most apparent with the cYFP parameters (Figure 5). Unlike all other parameters, CFP[405] parameters caused autofluorescence of the whole stigma epidermal cell, suggesting that imaging of CFP in this cell type would be best accomplished with the 458 laser line. The mC parameters caused the least amount of autofluorescence, with the stigma epidermal cell and chloroplasts being barely visible, indicating that mC and other RFPs would be the best option for tagging a protein in *A. thaliana*

stigma epidermal cells. However, multiple FP tags are often used simultaneously, as in co-localization studies, and some bleed-through of autofluorescence signal is therefore unavoidable in stigma epidermal cells. It would be interesting to identify the molecule or molecules causing the autofluorescence of the stigma epidermal cells, which seems to be a unique feature of this particular cell type.

The autofluorescence signal produced by stigma epidermal cell walls and chloroplasts is much lower than that of cYFP-tagged SRKb under the established cYFP imaging parameters. This is exemplified by the use of different laser lines to image stigmas of plants expressing cYFP-tagged SRKb. Unlike use of the established cYFP parameters with the 514 laser line (Figure 6A), use of the 488 laser line (another option for exciting cYFP) caused chloroplasts to be readily apparent (Figure 6B). Therefore, use of the established cYFP imaging parameters should prevent autofluorescence from interfering with the detection of cYFP-tagged SRKb in stigma epidermal cells.

The fact that the 488 laser line increased chloroplast autofluorescence is useful for locating the positions of chloroplasts relative to other organelles or proteins. Lambda scans using either the 488 or the 514 laser line revealed that the resulting chlorophyll emission spectra were identical (not shown). However, because the 514 laser line caused more cell wall autofluorescence (Figure 7A), the 488 laser line was best for exciting chlorophyll in stigma epidermal cells (Figure 7B).

Taken together, these results suggest that in stigma epidermal cells, (1) cYFP fluorescence signal is best imaged using the 514 nm Argon laser line for excitation and a 522-550 nm emission collection range, (2) chloroplast autofluorescence signal is best imaged using the 488 nm Argon laser line for excitation and a 665-700 nm emission collection range, and (3) it

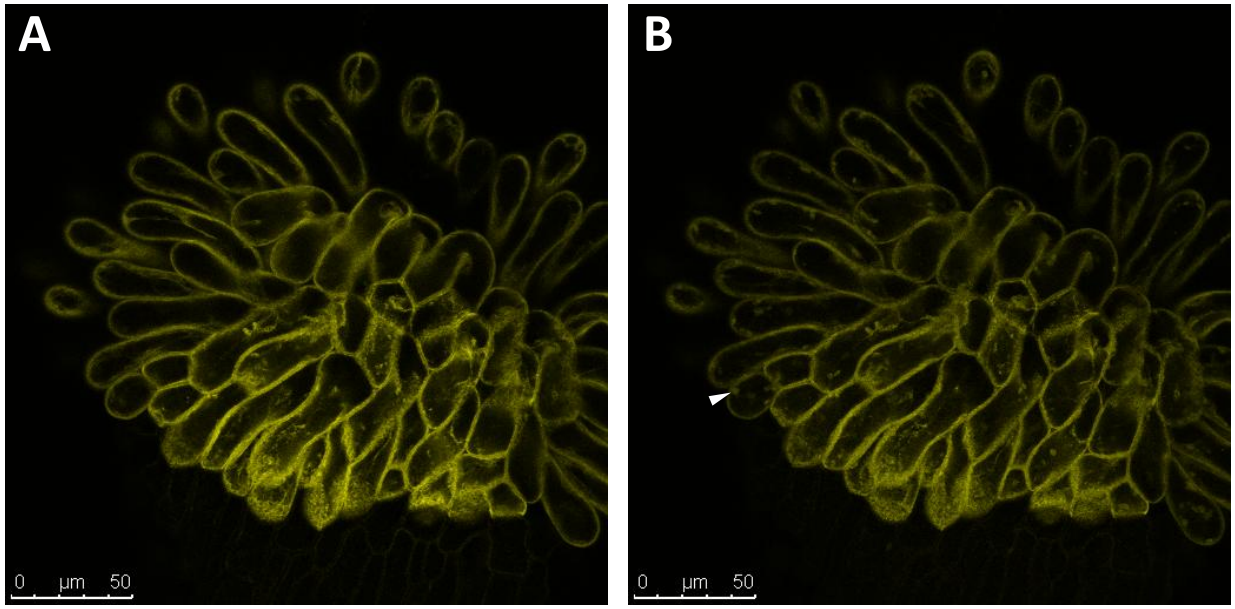

Figure 6. cYFP in the *Arabidopsis thaliana* epidermis is best imaged using the 514 Argon laser line.
Confocal microscopy images showing the stigma epidermis and part of the style from a −1-stage floral bud of an *A. thaliana* plant transformed with *AtS1*pr*::cYFP:SRKb* excited with only the 514 Argon laser line **(A)** and only the 488 Argon laser line **(B)**. All other parameters were kept constant. Both images were collected with a 522-550 nm emission range. cYFP can be imaged with either the 514 or the 488 laser line; however, images of stigmas transformed with cYFP-tagged SRKb reveals that the chloroplast autofluorescence is not nearly as noticeable when excited with the 514 laser line **(A)**, as compared to when excited with the 488 laser line **(B)**. These results suggest that the 514 laser line is the optimal choice for imaging cYFP in *A. thaliana* stigmas. The arrowhead denotes the fluorescence signal from an assumed chloroplast. The two images were captured sequentially (**A**, followed by **B**).

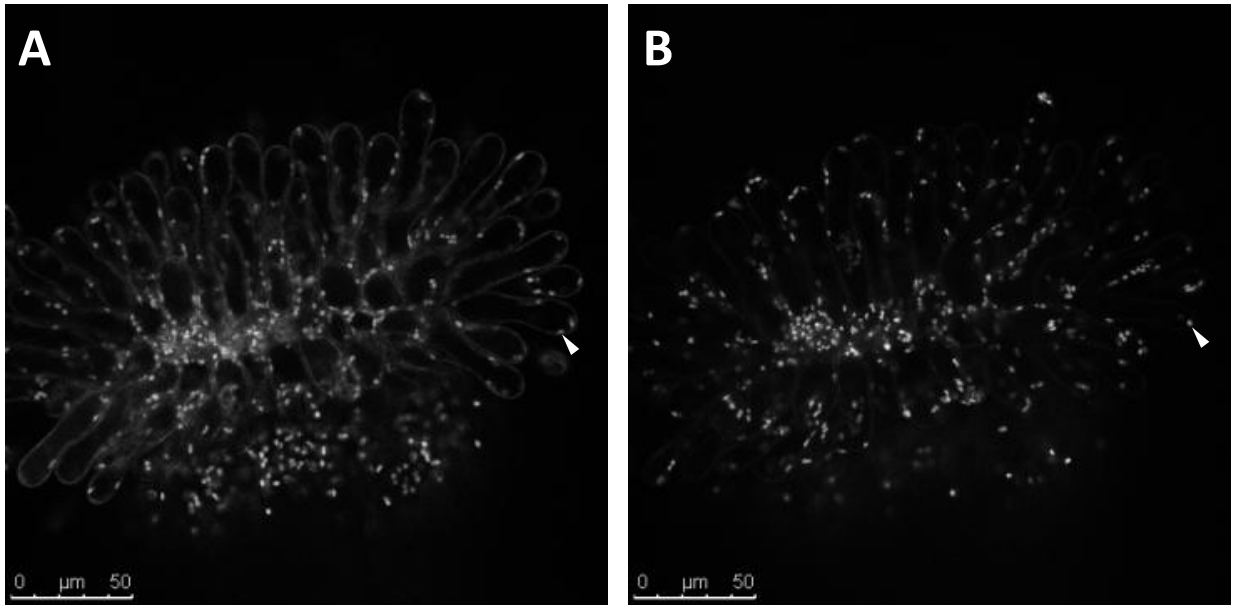

Figure 7. Chloroplast autofluorescence in the *Arabidopsis thaliana* epidermis is best imaged using the 488 nm Argon laser line.
Confocal microscopy images showing the stigma epidermis and part of the style from an *A. thaliana* −1-stage floral bud excited with only the 514 nm Argon laser line **(A)**, at 49% intensity, and only the 488 nm Argon laser line **(B)**, at 50% intensity. All other parameters, except the gain value (915.1 V **(A)** versus 835.7 V **(B)**), were kept constant (25% Argon laser power; 665-700 nm emission; 8 line-averaging). Both images were collected with a 665-700 nm emission range best for capturing chloroplast autofluorescence. While both imaging parameters reveal chloroplast (arrowheads) autofluorescence, more stigma epidermal cell wall autofluorescence is revealed with the 514 nm laser line **(A)** than with the 488 nm laser line **(B)**. These results indicate that the 488 nm laser line is best for capturing confocal images of chloroplast autofluorescence from *A. thaliana* stigmas. Note that because a live sample was used and the two images were captured sequentially (**A**, followed by **B**), the positions of the chloroplasts have changed from one image to the next.

is possible to use these two sets of parameters for simultaneous imaging of cYFP and chloroplasts, which is useful for co-localization studies and determining the physical relationships among subcellular signals.

Visualization of cYFP-tagged SRKb by confocal microscopy

The homozygous cYFP-tagged SKRb transformants were analyzed for the subcellular distribution of SRKb using the cYFP confocal imaging parameters established in this study. In all transformants, SRKb signal in the stigma epidermal cells was localized to the outer edge of the cell and to various degrees depending on the construct, in cytoplasmic (transvacuolar) strands (Figure 8). Careful analysis revealed that as compared to the other cYFP-tagged SRKb transformants, *AtS1*pr*::SRKb:cYFP* transformants exhibited the sharpest and most uniform localization of SRKb at the cell periphery and the lowest signal in transvacuolar strands (Figure 8A). The level of SRKb signal at the cell periphery as compared to that in transvacuolar strands is relatively equivalent in all other transformants (Figure 8B-F). Because the *AtS1*pr*::SRKb:cYFP* construct is unique in that the only SRKb protein species tagged with cYFP is the full-length SRKb (Table 1), these subcellular localization patterns suggest that in stigma epidermal cells, the full-length SRKb protein is localized predominantly at the cell periphery. These results also suggest that SRKb signal in the transvacuolar strands is almost exclusively contributed by the tSRKb and/or the eSRKb protein species. Additionally, because the *cYFP:SRKb*(cDNA) constructs lack the eSRKb protein (Table 1), most of the SRKb signal in the transvacuolar strands is likely contributed by the tSRKb protein.

To help pinpoint the subcellular localization of cYFP-tagged SRKb, excised stigmas were treated with 5% NaCl, which caused stigma epidermal cell protoplasts to retract from their cell

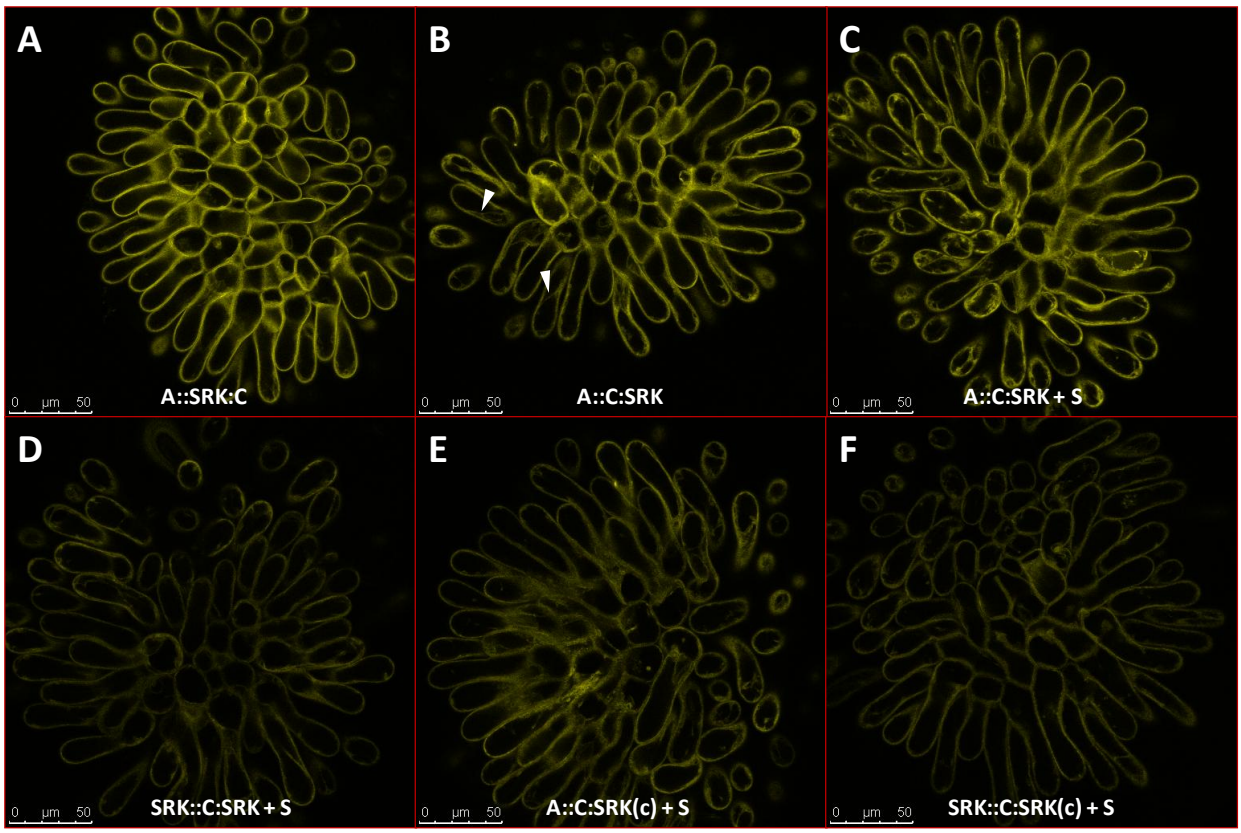

Figure 8. *Arabidopsis thaliana* stigma epidermal cells expressing cYFP-tagged SRKb from various constructs.
Representative confocal microscopy images of the stigma epidermis from a −1-stage floral bud of a homozygous *A. thaliana* transformant, each transformed separately with *AtS1*pr*::SRKb:cYFP* **(A)**, *AtS1*pr*::cYFP:SRKb* **(B)**, *AtS1*pr*::cYFP:SRKb* + *SCRb*pr*::SCRb* **(C)**, *SRKb*pr*::cYFP:SRKb* + *SCRb*pr*::SCRb* **(D)**, *AtS1*pr*::cYFP:SRKb*(cDNA) + *SCRb*pr*::SCRb* **(E)**, and *SRKb*pr*::cYFP:SRKb*(cDNA) + *SCRb*pr*::SCRb* **(F)**. The genotypes/lines used were identical to those used in Figure 4. All images were captured with identical parameters, including the gain value, such that differences in localization pattern and signal levels could be compared (25% Argon laser power; 49% 514 nm laser line intensity; 522-550 nm emission; 8 line-averaging; 1061 V gain). SRKb signal in all transformants appears to be localized to the cell periphery and to various degrees depending on the construct, in transvacuolar strands (arrowheads).

walls within 15 minutes of treatment (Figures 9 & 10). These plasmolysis experiments revealed that autofluorescence is localized to the stigma epidermal cell walls (Figure 9). Autofluorescence signal, as visualized by confocal microscopy with the cYFP parameters (Figure 9A), is localized to both chloroplasts (Figure 9B) and cell walls, which were distinguished from retracted protoplasts with transmitted light images using the 514 laser line (Figure 9C). Simultaneous capturing of the three images, using the sequential scanning LAS AF software setting to avoid potential cross-talk caused by spectral overlap interference, permitted their merging (Figure 9D) and confirmed the localization of stigma epidermal cell autofluorescence. Plasmolysis experiments also showed that full-length SRKb is indeed localized to the PM, since *AtS1*pr*::SRKb:cYFP* transformants exhibited SKRb signal in Hectian strands, which are stretched portions of the PM that form upon retraction of the protoplast from the cell wall following plasmolysis (Figure 10A). Punctate spots of SRKb signal were seen directly beneath the cell wall, particularly at sites where Hechtian strands connect to the PM (Figure 10A). These patterns are characteristic of PM-localized proteins following plasmolysis (Oparka 1994; Sardar *et al.* 2006). In stigma epidermal cells of plants transformed with all other cYFP-tagged SRKb transgenes (Figure 10B-F), the majority of SRKb signal remained in the protoplast following plasmolysis, with very faint and only occasional localization in Hechtian strands (Figure 10D&E).

SRKb localization in subcellular compartments of stigma epidermal cells

For a detailed characterization of SRK subcellular distribution in stigma epidermal cells, it is important to have a good understanding of the subcellular architecture of this cell type. However, stigma epidermal cells have been used only rarely for confocal microscopic studies,

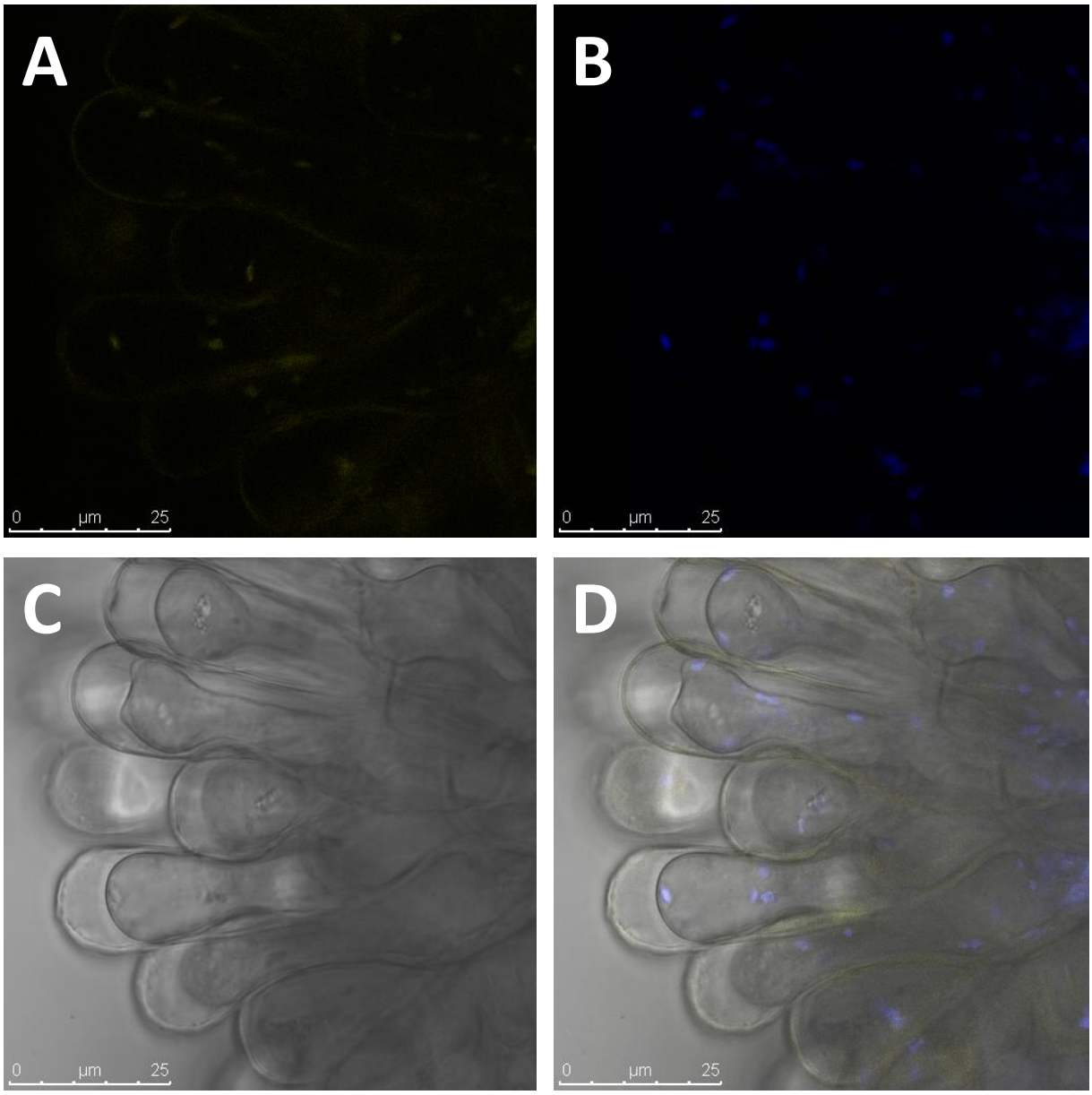

Figure 9. Autofluorescence of *Arabidopsis thaliana* stigma epidermal cells with the established cYFP imaging parameters is localized to the cell wall.
Plasmolyzed stigma epidermal cells of a −1-stage floral bud from a plant transformed with untagged SRKb shows that autofluorescence under the established cYFP imaging parameters is localized to the cell wall. Autofluorescence using cYFP imaging parameters **(A)**, chloroplast autofluorescence **(B)**, transmitted light **(C)**, and merged **(D)** images of the same field of view. Plasmolysis was accomplished by using 5% NaCl, rather than H_2O, as the mounting medium. Stigma epidermal cells were observed to plasmolyze within the first 15 minutes after placement of the cover slip. Stigma epidermal cell autofluorescence is not localized to the plasma membrane, as indicated by the lack of signal in the outlines of the retracted protoplasts. Some chloroplast autofluorescence is also seen with the cYFP imaging parameters, as the dots of fluorescence **(A)** perfectly co-localize **(D)** with the chloroplast autofluorescence **(B)**.

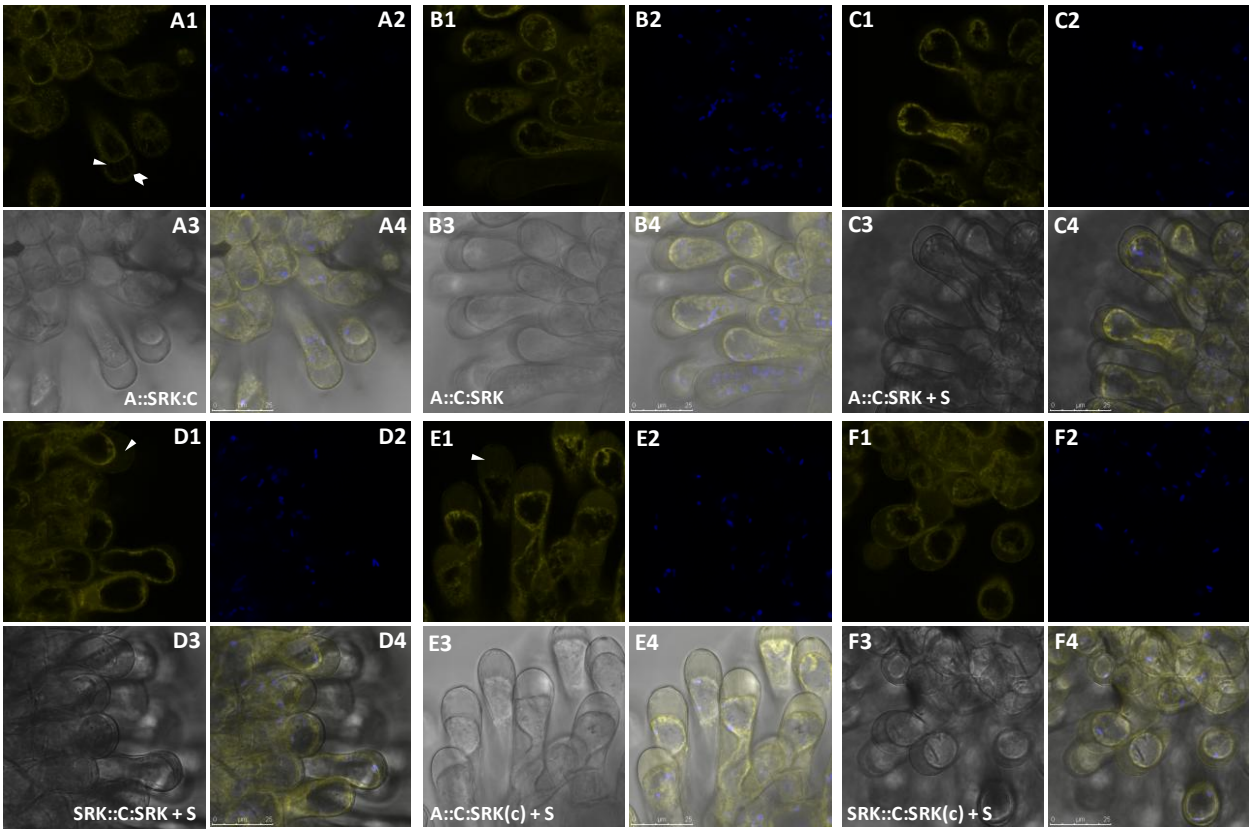

Figure 10. SRKb localization in plasmolyzed stigma epidermal cells of plants transformed with cYFP-tagged SRKb.

Confocal microscopy images of the plamolyzed stigma epidermal cells from a −1-stage floral bud of *A. thaliana* plants, each transformed separately with *AtS1*pr*::SRKb:cYFP* **(A)**, *AtS1*pr*::cYFP:SRKb* **(B)**, *AtS1*pr*::cYFP:SRKb* + *SCRb*pr*::SCRb* **(C)**, *SRKb*pr*::cYFP:SRKb* + *SCRb*pr*::SCRb* **(D)**, *AtS1*pr*::cYFP:SRKb*(cDNA) + *SCRb*pr*::SCRb* **(E)**, and *SRKb*pr*::cYFP:SRKb*(cDNA) + *SCRb*pr*::SCRb* **(F)**. The genotypes/lines used were identical to those used in Figures 4 and 8. cYFP imaging parameters **(1)**, chloroplast autofluorescence **(2)**, transmitted light **(3)**, and merged **(4)** images of the same field of view. Plasmolysis was accomplished by using 5% NaCl, rather than H_2O, as the mounting medium. Stigma epidermal cells were observed to plasmolyze within the first 15 minutes after placement of the cover slip. SRKb signal can be seen in Hechtian strands (arrowheads) and punctate areas (chevron) beneath the cell wall in *AtS1*pr*::SRKb:cYFP* transformants **(A1 & A4)**, whereas only faint signal in Hectian strands was occasionally observed **(D & E)** in *cYFP-SRKb* transformants **(B-F)**.

and their subcellular architecture is not as well described as that of other epidermal cell types such as pavement cells of the leaf epidermis. Many large, differentiated epidermal cells contain a large central vacuole that is traversed by transvacuolar strands consisting of cytosol with organelles such as peroxisomes, mitochondria, chloroplasts, Golgi, and ER. To determine if stigma epidermal cells have a similar organization, soluble green fluorescent protein (GFP) was used as a marker for the cytosol. Although a previous GUS reporter study had concluded that the CaMV *35S* promoter is not active in the stigma epidermal cells of *A. thaliana* plants of the C24 ecotype (Wilkinson *et al.* 1997), analysis of *35S*pr*::GFP* transformants of the Col-0 ecotype demonstrated that *35S* promoter activity was strong enough to drive expression of GFP in these cells (Figure 11). Thus, these plants could be used to visualize the cytosol in stigma epidermal cells and to compare its localization to that of the cytosol in other epidermal cell types. However, co-localization of the soluble, cytosolic GFP with cYFP-tagged SRKb could not be assessed due to the large overlap in the excitation and emission spectra of GFP and cYFP.

Confocal microscopy of the *35S::GFP* transformants demonstrated the presence of transvacuolar strands in both stigma epidermal cells (Figure 11A) and leaf pavement cells (Figure 11C). In both cell types, soluble GFP was also detected in the nucleus but not in the nucleoli (Figure 11A). This subcellular localization pattern is the same as that previously described for GFP expressed under the control of the CaMV *35S* promoter in cotyledon mesophyll and root tip cells of *A. thaliana* seedlings of the C24 ecotype (Haseloff & Amos 1995). Stigma epidermal cells also exhibited GFP signal in spots that perfectly co-localized with chloroplasts (Figure 11A), indicating that the GFP imaging parameters (488 nm Argon laser line excitation, 498-522 nm emission) caused autofluorescence of chloroplasts. This conclusion was confirmed by the detection of chloroplast signal in non-GFP-expressing stigma epidermal cells

Figure 11. Soluble GFP serves as a marker for the cytosol and the nucleus of *Arabidopsis thaliana* stigma epidermal cells.
Expression of soluble GFP in *A. thaliana* Col-0 plants transformed with *35S*pr*::GFP*, as seen with confocal microscopy imaging parameters appropriate for GFP (488 nm Argon laser line excitation, 498-522 nm emission), highlights the location of the cytosol and the nucleus in stigma epidermal cells of a −1-stage floral bud **(A1)**. Cytoplasmic (transvacuolar) strands (arrowheads) can be seen traversing the large central vacuole, which, as in pavement cells of the leaf epidermis **(C)**, occupies most of the volume of stigma epidermal cells. Note the absence of GFP signal in the nucleoli (chevron; **A1 & A3**). Additionally, spots of signal that are the same size and shape of chloroplasts **(A1)** co-localize perfectly with chloroplasts **(A2 & A3)**, indicating that the parameters used for imaging GFP reveal chloroplast autofluorescence. This observation is supported by images of stigma epidermal cells from −1-stage floral buds of *A. thaliana* Col-0 plants transformed with *SRKb*pr*::SRKb + SCRb*pr*::SCRb*, a transgene that does not encode a fluorescent protein, which show only chloroplast autofluorescence with the GFP imaging parameters **(B1-B3)**. GFP imaging parameters **((A/B)1)**, chloroplast autofluorescence parameters **((A/B)2)**, and merged **((A/B)3)** images of the same field of view. In a non-expressing sibling **(D)** of the homozygous *35S*pr*::GFP* line used for visualizing GFP localization **(A, C, & E)**, only stomatal aperture wall (arrow) and chloroplast (pentagon) autofluorescence could be seen in the leaf epidermis using the GFP imaging parameters **(D)**. Retraction of the protoplast from the cell wall upon plasmolysis of stigma epidermal cells expressing soluble GFP **(E1-4)** reveals that localization of GFP is exclusively in the protoplast. GFP imaging parameters **(E1)**, chloroplast autofluorescence **(E2)**, transmitted light **(E3)**, and merged **(E4)** images of the same field of view. Because GFP signal is not localized to the cell wall, plasmolysis reveals that the stigma epidermal cell wall does not exhibit autofluorescence with these parameters **(E1-E4)**. "Expressing": images of plants expressing GFP; "non-expressing": images of plants not expressing GFP.

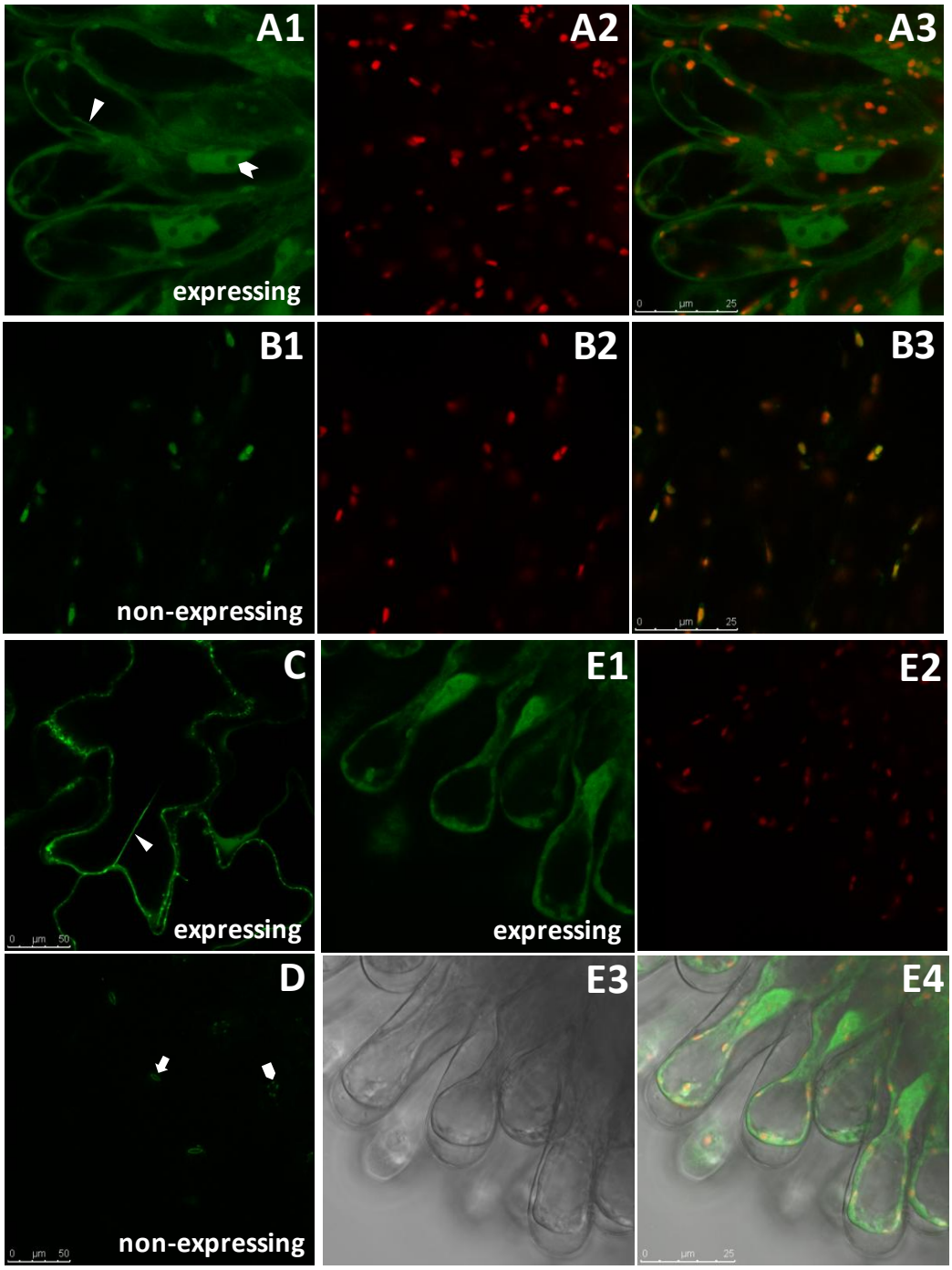
A1
A2
A3
expressing
0 µm 25
B1
B2
B3
non-expressing
0 µm 25
C
E1
E2
expressing
expressing
0 µm 50
D
E3
E4
non-expressing
0 µm 50
0 µm 25

(Figure 11B) and stomatal guard cells (Figure 11D), but not in leaf pavement cells, which do not contain chloroplasts. Plasmolysis of stigma epidermal cells revealed that, as expected, soluble GFP is found neither in the PM, as no Hechtian strands were detected, nor in the cell wall (Figure 11E). The lack of signal in the cell wall also indicated that the GFP imaging parameters did not cause autofluorescence of the stigma epidermal cell walls.

Tracking the movement of chloroplasts through the transvacuolar strands and along the edges of stigma epidermal cells revealed the highly dynamic nature of this cell type, especially when compared to the less visibly dynamic sub-epidermal cells of the style (Figure 12). The transvacuolar strands themselves are also highly dynamic, as their positions in the stigma epidermal cells changed over time (Figure 12). Furthermore, the cYFP signal was observed to move steadily through transvacuolar strands, especially in plants expressing cYFP-SRKb (Figures 8 & 12).

Additional SRKb subcellular localization patterns were observed in some surface-view confocal microscopy images of stigma epidermal cells (Figure 13). In these surface-view images, SRKb was detected in tiny vesicle-like structures along the edges of stigma epidermal cells of *AtS1*pr*::SRKb:cYFP* transformants (Figure 13A&B). On the other hand, similar images of *AtS1*pr*::cYFP:SRKb* transformants revealed a reticulate pattern of the cYFP signal (Figure 13C&D). In other surface-view images, diffraction is presumed to cause the cYFP signal to appear as concentric rings at the site of a stigma epidermal cell (Figure 13B2, bottom).

Co-localization of SRKb with organelle markers

In an attempt to identify the subcellular compartments to which SKRb is localized in stigma epidermal cells, co-localization studies with various organelle markers were performed.

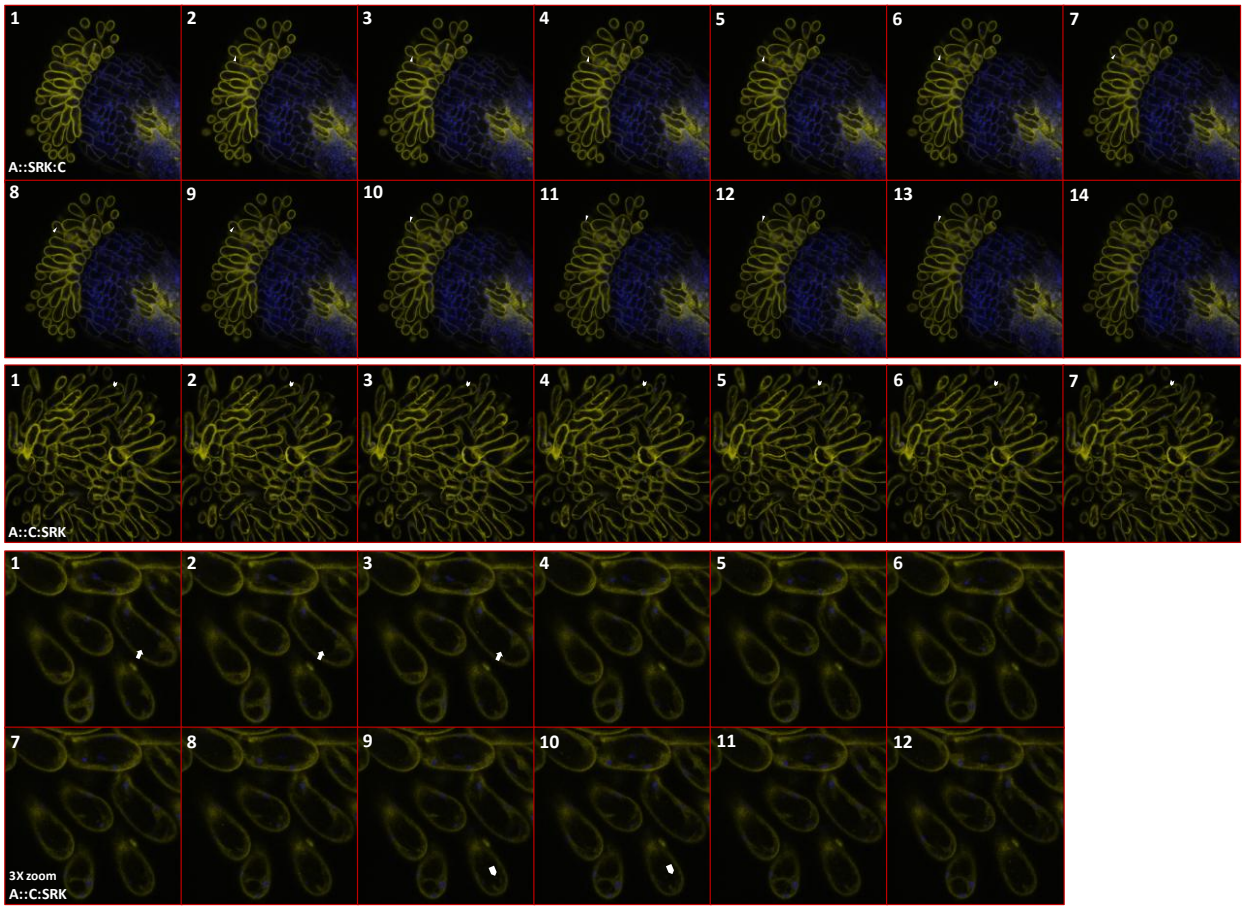

Figure 12. Stigma epidermal cells are highly dynamic.
Time lapse series of confocal microscopy images of stigma epidermal cells from plants transformed with *AtS1*pr*::SRKb:cYFP* (top row) or *AtS1*pr*::cYFP:SRKb* (bottom two rows). Frames of images are ordered consecutively, and within a set of images, each frame is separated by the same duration of time. Each frame is shown as a merged cYFP (yellow) and chloroplast autofluorescence (blue) image. The top row shows images of the side view of a stigma from a plant transformed with *AtS1*pr*::SRKb:cYFP*. Each frame is separated by 10.48 seconds. The faint, but present, transvacuolar strands, as visualized with cYFP-tagged SRKb, change position over time. Chloroplasts can be seen moving along these transvacuolar strands, and therefore, their positions also change over time. For example, one chloroplast appears in frame 2, and its movement can be tracked over time until it disappears by frame 14 (arrowheads). Transvacuolar strands are more easily visualized in the stigma epidermal cells of plants transformed with *AtS1*pr*::cYFP:SRKb* (bottom two rows) than with *AtS1*pr*::SRKb:cYFP* (top row; also compare B to A, Figure 8). The bottom row is made up of 3X zoom images of the same top view of the stigma epidermis shown in the middle row. Each frame for both sets of images is separated by 2.62 seconds. A transvacuolar strand can be seen changing position over time (chevron) in the middle row. A close-up view of the stigma epidermal cells (bottom row) reveals the presence of small vesicle-like structures that can be seen moving in and out of the optical plane of section. One of them appears in frame 1 (arrow), changes position in frames 2 and 3, and disappears by frame 4. Another comes into view in frame 9 (pentagon) and disappears by frame 11.

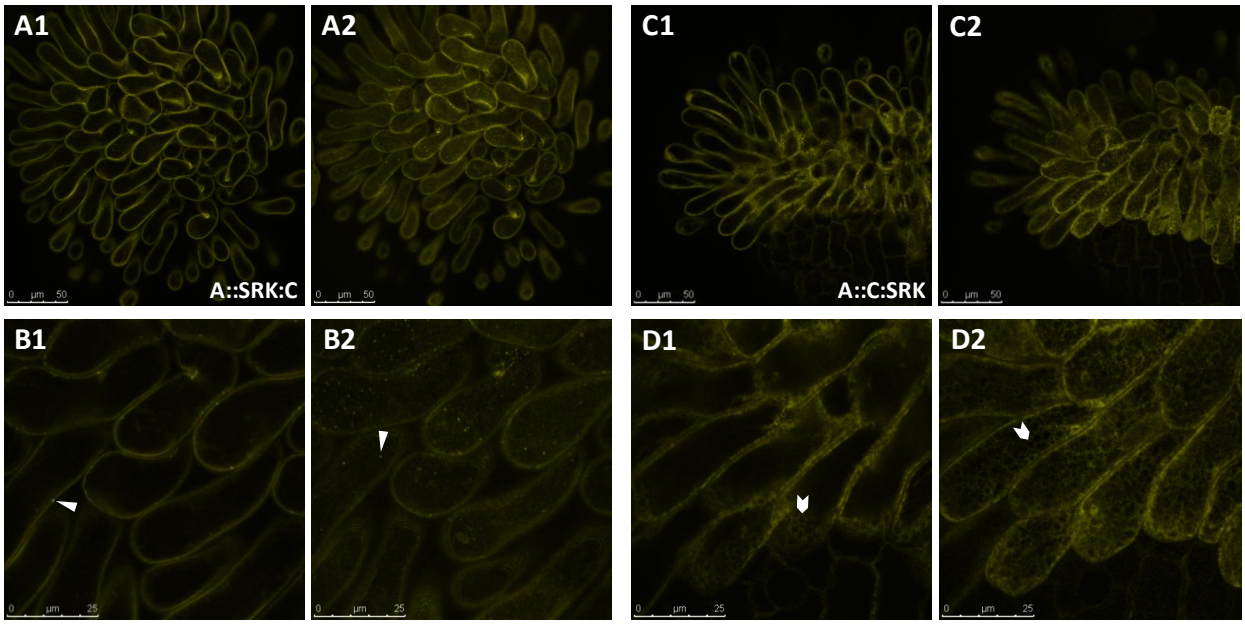

Figure 13. Detailed subcellular localization patterns of SRKb in stigma epidermal cells of *Arabidopsis thaliana* plants transformed with *AtS1*pr*::SRKb:cYFP* or *AtS1*pr*::cYFP:SRKb*. Confocal microscopy images showing subcellular patterns of SRKb in stigma epidermal cells that are most easily seen in cell-surface-view optical sections. Optical cross-sections **(1)** and surface-view sections **(2)** of the stigma epidermal cells of plants transformed with *AtS1*pr*::SRKb:cYFP* **(A & B)** and *AtS1*pr*::cYFP:SRKb* **(C & D)**. **B** and **D** show 3X zoom images of **A** and **C**, respectively. SRKb signal is visible in tiny vesicle-like structures (arrowheads) in *AtS1*pr*::SRKb:cYFP* stigma epidermal cells, and in a reticulate pattern that resembles cortical ER with a network of signal interspersed with voids of signal (chevrons) in *AtS1*pr*::cYFP:SRKb* stigma epidermal cells.

Constructs containing chimeric genes in which expression of mC-tagged markers for the PM, endoplasmic reticulum (ER), vacuolar membrane (tonoplast), Golgi, peroxisomes, and mitochondria were driven by the CaMV *35S* promoter were obtained (Nelson *et al.* 2007). To ensure that these markers would be expressed at high enough levels for visualization in stigma epidermal cells, the *35S* promoter was replaced with the *AtS1* promoter. These constructs were then transformed into *AtS1*pr*::SRKb:cYFP* or *AtS1*pr*::cYFP:SRKb* transformants for co-localization studies, and into wild type C24 plants as controls. In addition, the original constructs that used the *35S* promoter were transformed into wild type C24 plants for comparative studies of leaf and stigma epidermal cells. For simultaneous imaging of cYFP, mC, chlorophyll, and transmitted light in the same frame, the established imaging parameters for each setting were used in conjunction with the sequential scanning function of the LAS AF software, such that cross-talk among fluorescence spectra was avoided.

cYFP-tagged SRKb (Figure 14A) co-localized with the mC-tagged PM marker (Figure 14B) in stigma epidermal cells of *AtS1*pr*::SRKb:cYFP* plants, as seen when images of these two proteins in the same stigma epidermal cells are merged (Figure 14C). This result suggests that full-length SRKb is localized to the PM, consistent with the result obtained from the plasmolysis experiment in which cYFP-tagged SRKb from *AtS1*pr*::SRKb:cYFP* plants localized to Hechtian strands in stigma epidermal cells (Figure 10A). Interestingly, some SRKb-containing vesicle-like structures also co-localized with the mC-tagged PM marker (Figure 14).

Expression of the PM marker in both stigma and leaf epidermal cells revealed that it exhibited some localization patterns that are unexpected for a marker described as being exclusively localized to the PM. In surface-view images of stigma epidermal cells, the PM marker signal was sometimes seen as uneven spots that varied in size and shape and that co-

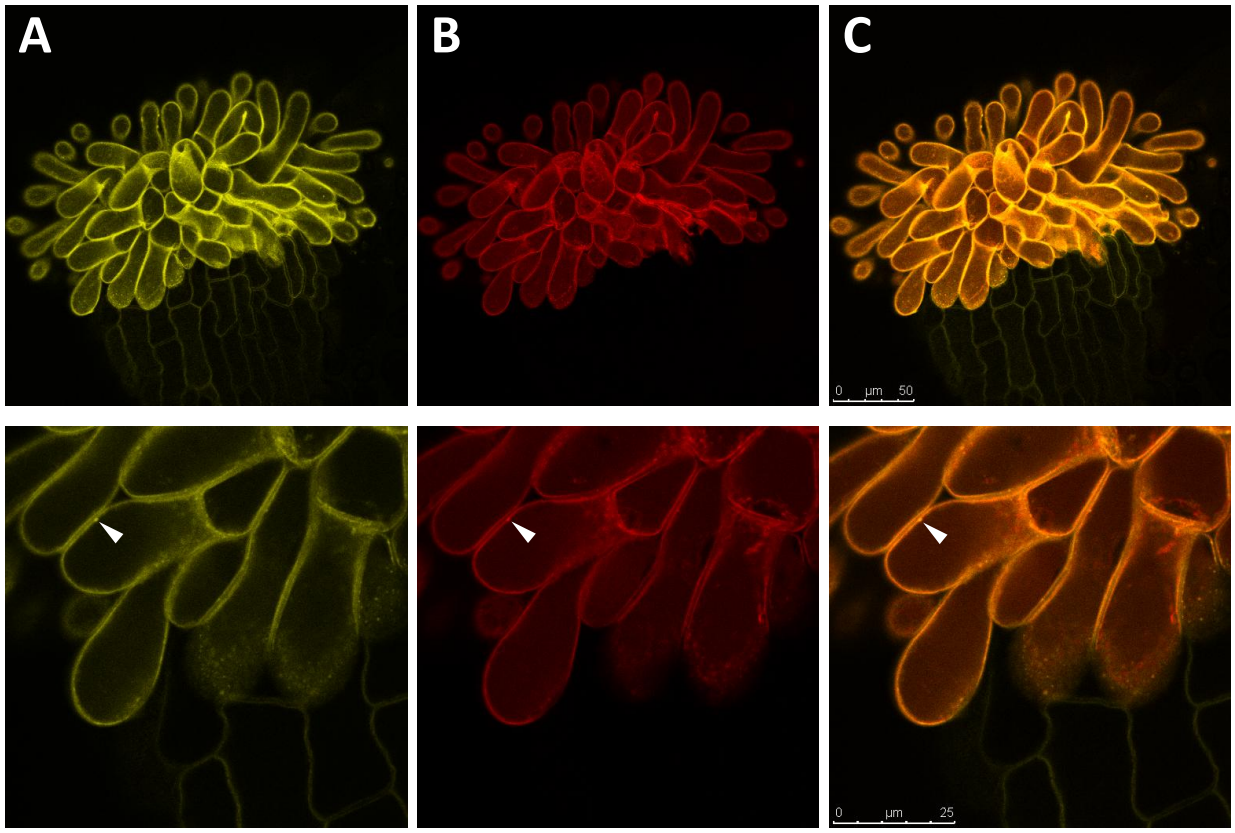

Figure 14. Vesicle-like structures containing full-length SRKb co-localize with the plasma membrane marker, and none of the organelle marker proteins driven by the *AtS1* promoter exhibit style epidermal cell localization.
Confocal images of a stigma of a plant co-transformed with *AtS1*pr*::SRKb:cYFP* and the plasma membrane (PM) marker tagged with mC and driven by the *AtS1* promoter. The bottom row shows 3X zoom images of the same stigma seen in the top row. cYFP **(A)**, mC **(B)**, and merged images **(C)** of the same field of view. Full-length SRKb, as represented by the cYFP signal from the *AtS1*pr*::SRKb:cYFP* construct **(A)**, co-localizes well with the PM marker **(B)** along the edges of the stigma epidermal cells **(C)**. Other membranous structures that are also marked by the PM marker (**B**; see also Figure 15) seem to include the vesicle-like structures (arrowhead) containing full-length SRKb (**A**; Figure 13). In contrast to the localization of SRKb when driven by the *AtS1* promoter (**A**; Figure 21A-C&E), localization of the PM marker, and of all other organelle (ER, tonoplast, Golgi, peroxisome, and mitochondria) markers used in this study, was never seen in style epidermal cells **(B)**.

localized with a few voids of SRKb signal in *AtS1*pr*::SRKb:cYFP* transformants (Figure 15A) and curiously co-localized nearly perfectly with the voids of SRKb signal in *AtS1*pr*::cYFP:SRKb* transformants (Figure 15B). These PM marker spots could also be seen in optical sections as uneven spots along the edges of cells, both in stigma (not shown) and leaf (Figure 15F) epidermal cells. PM marker signal was also sometimes seen in other membranous structures that outlined the nucleus and chloroplasts and were found within transvacuolar strands (Figure 15C). These results were unexpected for a PM marker, especially since this PM marker was reported to exhibit an even distribution along the edges of cells (Nelson *et al.* 2007). In some cases, the PM marker signal was observed in the expected location, at the cell periphery in both stigma (Figure 15D) and leaf (Figure 15E) epidermal cells, but even in these cases, some of the cells also exhibited signal surrounding the nucleus, possibly in the nuclear membrane (Figure 15E1). In contrast, the full-length SRKb protein, as seen in *AtS1*pr*::SRKb:cYFP* transformants, was found to localize to the PM but not to the sites of unexpected PM marker localization (Figure 15A&C). Thus, SRKb:cYFP may serve as a better, more consistent marker of the PM, at least in stigma epidermal cells.

Surface-view confocal microscopy images of stigma epidermal cells revealed that the mC-tagged ER marker did not co-localize with cYFP-tagged SRKb in *AtS1*pr*::SRKb:cYFP* plants (Figure 16A). However, the mC-tagged ER marker and cYFP-tagged SRKb both exhibited a reticulate pattern and co-localized in *AtS1*pr*::cYFP:SRKb* plants (Figure 16B). These results suggest that tSRKb and/or eSRKb, but not full-length SRKb, are localized to the ER. The reticulate pattern was similar to that observed for the ER marker in leaf epidermal cells of the midrib and other areas of the leaf blade (Figures 16C-E), and to the pattern obtained with the same ER marker by Nelson *et al.* (2007) and with another ER marker by Cutler *et al.* (2000). The

Figure 15. Expression of a plasma membrane marker in stigma and leaf epidermal cells of *Arabidopsis thaliana*.
Confocal images showing localization of the plasma membrane (PM) marker tagged with mC **(A3, B3, C3, D3, E1, & F)**. The PM marker driven by the *AtS1* promoter was co-transformed into *A. thaliana* plants transformed with *AtS1*pr*::SRKb:cYFP* **(A & C)** or *AtS1*pr*::cYFP:SRKb* **(B & D)**, and the same PM marker driven by the *35S* promoter was transformed into wild type plants **(E & F)** for comparison. **A-D** show cYFP **(1)**, chloroplast autofluorescence **(2)**, mC **(3)**, and merged images **(4)** of the same field of view. Cell-surface optical sections **(A & B)** and optical cross-sections **(C & D)** for each of the co-transformed genotypes are shown, where PM marker localization can sometimes be seen as spots of signal **(A3 & B3)**, sometimes in transvacuolar strands **(C3)**, and sometimes as a sharp outline of the cell periphery **(D3)**. The voids of SRKb signal seen in *AtS1*pr*::cYFP:SRKb* transformants **(B1)** hypothesized to be ER lacunae (arrowheads) co-localize almost perfectly with the spots of PM marker signal **(B4)**. Sometimes, the PM marker shows the expected subcellular localization, with signal almost exclusively found along the edges of the cells, typical for a plasma-membrane-localized protein **(D3)**. At other times, PM marker signal is found in transvacuolar strands, where it appears to localize to membrane compartments other than the PM **(C3)**, as is apparent by observing membranous structures surrounding the nucleus (pentagon) and surrounding chloroplasts (arrow). In epidermal cells of leaf blades seen in optical cross-section **(E & F)**, the PM marker protein appears along the edges of leaf epidermal cells **(E1)**, as expected, but it can also be seen surrounding the nucleus (arrow) and as spots of signal (chevron; **F**) that are reminiscent of those seen in optical cross-section views of stigma epidermal cells (Figure 18) known to have spots of signal in cell-surface views **(A3 & B3)**, as well. **E** shows mC **(1)**, chloroplast autofluorescence **(2)**, transmitted light **(3)**, and merged images **(4)** of the same field of view. Note that unlike cYFP-tagged SRKb driven by the *AtS1* promoter **(A1)**, the PM marker driven by the *AtS1* promoter does not show localization in style epidermal cells **(A3)**.

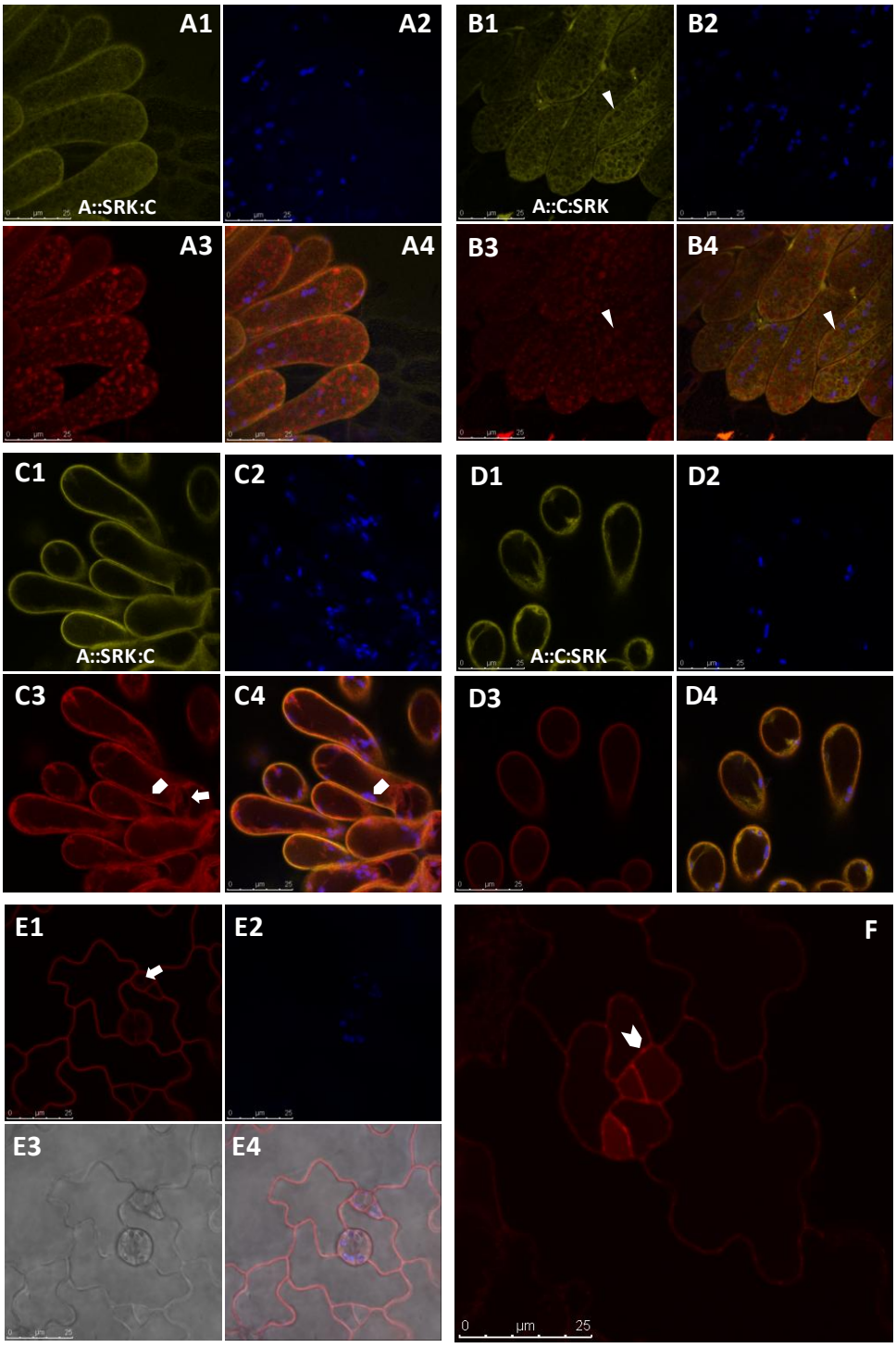
A1
A2
A::SRK:C
B1
B2
A::C:SRK
A3
A4
B3
B4
C1
C2
A::SRK:C
D1
D2
A::C:SRK
C3
C4
D3
D4
E1
E2
E3
E4
F
0 µm 25

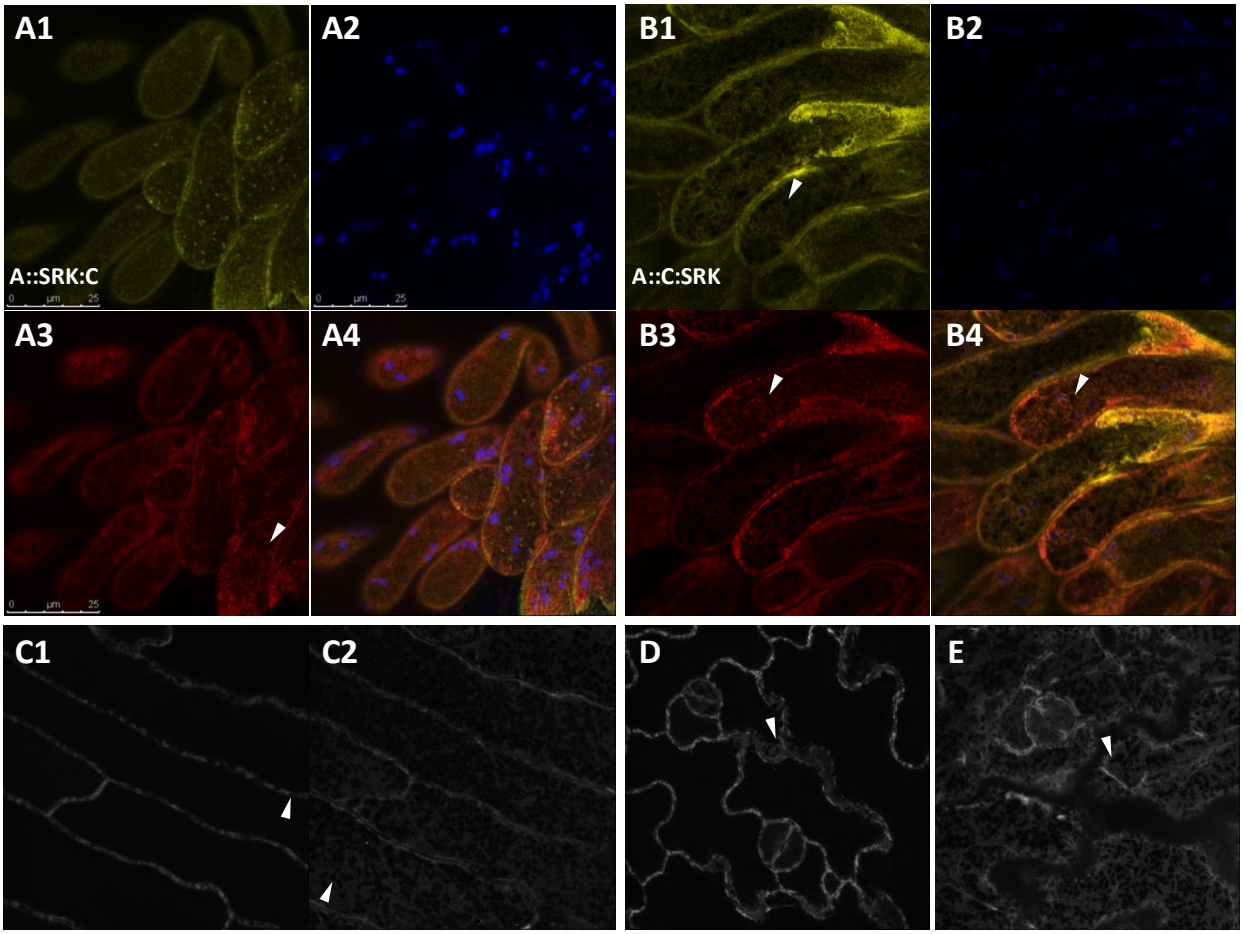

Figure 16. Expression of an ER marker in stigma and leaf epidermal cells of *Arabidopsis thaliana* reveals that tSRKb and/or eSRKb is likely localized in the ER.
Confocal images showing localization of the ER marker tagged with mC **(A3, B3, C, D, & E)**. The ER marker driven by the *AtS1* promoter was co-transformed into *A. thaliana* plants with *AtS1*pr*::SRKb:cYFP* **(A)** and *AtS1*pr*::cYFP:SRKb* **(B)**, and the same ER marker driven by the *35S* promoter was transformed into wild type C24 plants **(C-E)** for comparison. **A** and **B** show cYFP **(1)**, chloroplast autofluorescence **(2)**, mC **(3)**, and merged images **(4)** of the same field of view. Full-length SRKb, as represented with the *AtS1*pr*::SRKb:cYFP* transgene **(A1)**, co-localizes poorly **(A4)** with the ER marker **(A3)**, while tSRKb and/or eSRKb, as represented with the *AtS1*pr*::cYFP:SRKb* transgene **(B1)**, co-localizes almost perfectly **(B4)** with the ER marker **(B3)**, in stigma epidermal cell-surface optical sections. SRKb signal appears more diffuse than ER marker signal, perhaps because the former is represented by more than one protein species that may be localized to multiple subcellular compartments. Voids of signal (arrowheads), as seen with the ER marker and the SRKb protein from the *AtS1*pr*::cYFP:SRKb* transgene, are likely to be ER lacunae. Leaf epidermal cells expressing the ER marker **(C-E)** exhibited the same reticulate pattern observed in stigma epidermal cells, as represented in midrib **(C)** and blade **(D & E)** surface-view **(C2 & E)** and optical cross-section **(C1 & D)** images. **C1** and **C2** are images of the same area of the midrib. Note that a faint line devoid of signal, the area of plasma membrane and cell wall localization, can be seen between adjacent cells in **C1**.

fact that the reticulate pattern was observed, not only in surface-view images (Figure 16C2&E), but also in some optical cross sections of leaf epidermal cells, where it was located along the edges of cells (Figure 16C1&D), indicates that it represents the network of cortical ER, which is typically located directly below the PM in plant cells. The areas that lacked mC or cYFP signal likely represent spaces between the ER network called ER lacunae, since they were variable in size and more numerous than the few chloroplasts that coincided with the areas that lacked signal (Figure 16A&B). Further support for the lack of overlap between the signals derived from full-length SRKb and tSRK/eSRK is provided by the fact that in *AtS1*pr*::SRKb:cYFP* stigma epidermal cells, the areas lacking cYFP signal differed in size and shape from those observed for the signal derived from the mC-tagged ER marker (Figure 16A).

The mC-tagged ER marker and cYFP-SRKb also co-localized in the transvacuolar strands of stigma epidermal cells as revealed by optical cross-section images (Figure 17), demonstrating that tSRKb/eSRKb localize to the motile non-cortical ER found in these strands. However, as in the surface-view images (Figure 16), the SRKb signal seems to be more diffuse than the ER marker signal (Figure 17). This difference may be due to a difference in the imaging properties of the cYFP and mC proteins themselves. Alternatively, tSRKb/eSRKb might localize to several physically overlapping subcellular locations in the cell, which would obscure the distinction among various intracellular compartments such as those of the endomembrane system, including the ER, Golgi, vacuole, and endosomes.

To determine if SRKb signal in transvacuolar strands represents the vacuolar membrane itself, co-localization of the tonoplast marker was performed with cYFP-tagged SRKb from each of the *AtS1*pr*::SRKb:cYFP* and *AtS1*pr*::cYFP:SRKb* constructs. In transvacuolar strands, the tonoplast marker appeared to co-localize with the faint SRKb signal in *AtS1*pr*::SRKb:cYFP*

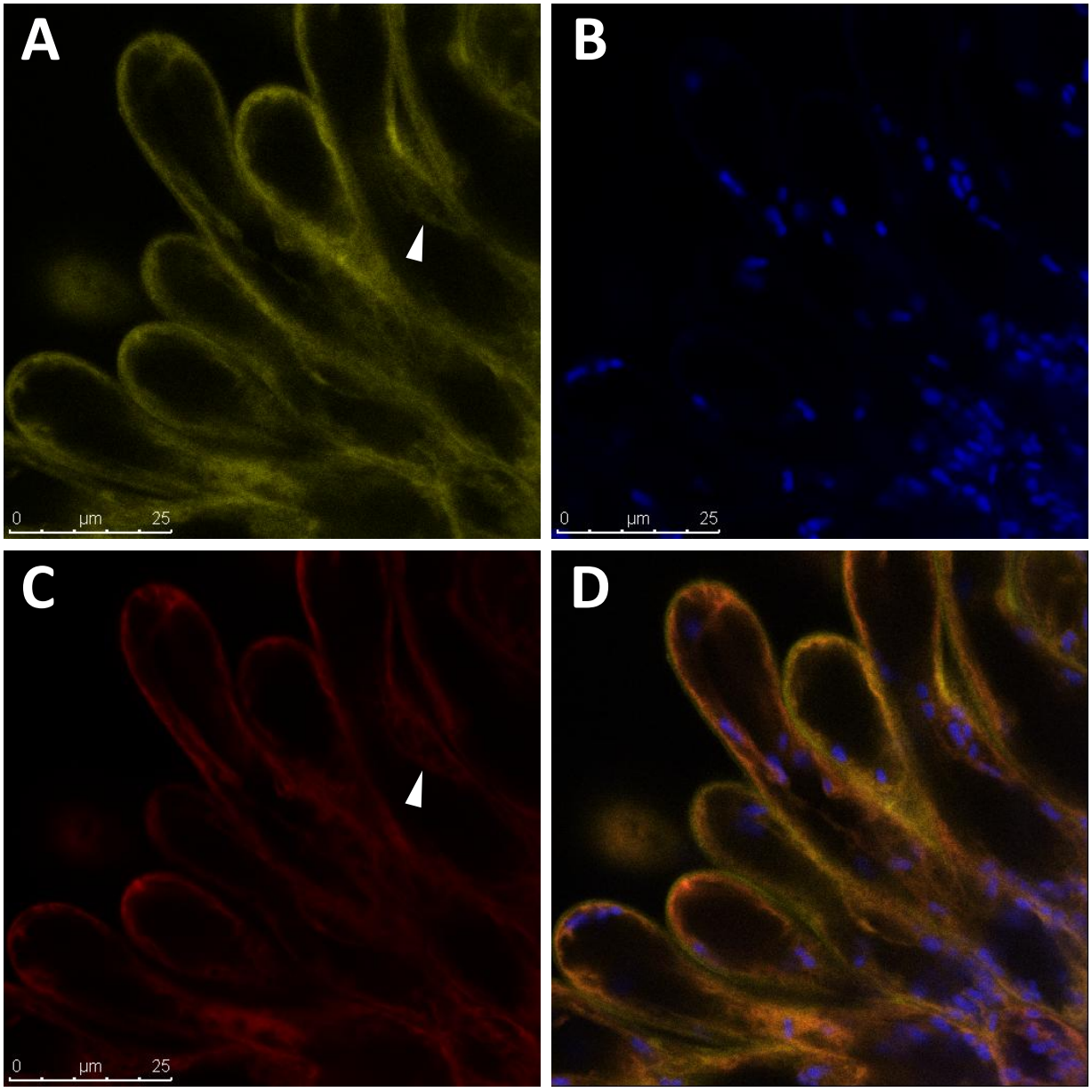

Figure 17. SRKb signal in transvacuolar strands may be co-localized to non-cortical ER found in transvacuolar strands.
Optical cross-sections of stigma epidermal cells of *Arabidopsis thaliana* co-transformed with the *AtS1*pr*::cYFP:SRKb* construct and the ER marker driven by the *AtS1* promoter reveal relative co-localization of SRKb and the ER. cYFP **(A)**, chloroplast autofluorescence **(B)**, mC **(C)**, and merged images **(D)** of the same field of view. Although SRKb signal **(A)** appears to be more diffuse than ER signal **(C)**, the areas of signal appear to co-localize **(D)**. Note that signal can be seen surrounding the nucleus (arrowhead), which could represent either ER membrane or nuclear membrane.

transformants and the strong SRKb signal in *AtS1*pr*::cYFP:SRKb* transformants (Figure 18A&B). The tonoplast marker was also found to localize to membranous material surrounding both chloroplasts (Figure 18B) and the nucleus (Figure 18C&E). Interestingly, the tonoplast marker exhibited localization patterns reflecting distinct tonoplast characteristics in leaf epidermal cells that were not observed in stigma epidermal cells, such as small bulges projecting inward from cell edges (Figure 18D), lack of contact with outwardly-projecting cell lobes (Figure 18F), and "bulbs" (i.e., mobile tonoplast structures of spherical shape; Saito *et al.* 2002; Figure 18G).

Co-localization experiments with the *AtS1*pr*::SRKb:cYFP* construct revealed that although they are similar in size, neither peroxisomes nor mitochondria co-localized with the vesicle-like structures containing full-length SRKb in stigma epidermal cells (Figure 19A&B). Additionally, unlike SRKb-containing vesicle-like structures that are most visible in surface-view images (Figure 13A&B), peroxisomes and mitochondria were easily seen in both surface-view and optical cross-section images (not shown). Golgi stacks also do not co-localize with the SRKb-containing vesicle-like structures (Figure 19C&D). Golgi are also larger and are easily seen in optical cross-section images (Figure 19C&D).

Whether expressed alone or together in *A. thaliana* C24 plants, the characteristic localization pattern exhibited by each of the mC-tagged organelle proteins or the cYFP-tagged SRKb proteins was identical in stigma epidermal cells. These results indicate that the presence of one type of FP-tagged protein did not have an influence on the localization of another type of FP-tagged protein used in this study, and supports the assumption that cross-talk among fluorophores was avoided with the sequential scanning function and therefore was not responsible for any observed co-localization.

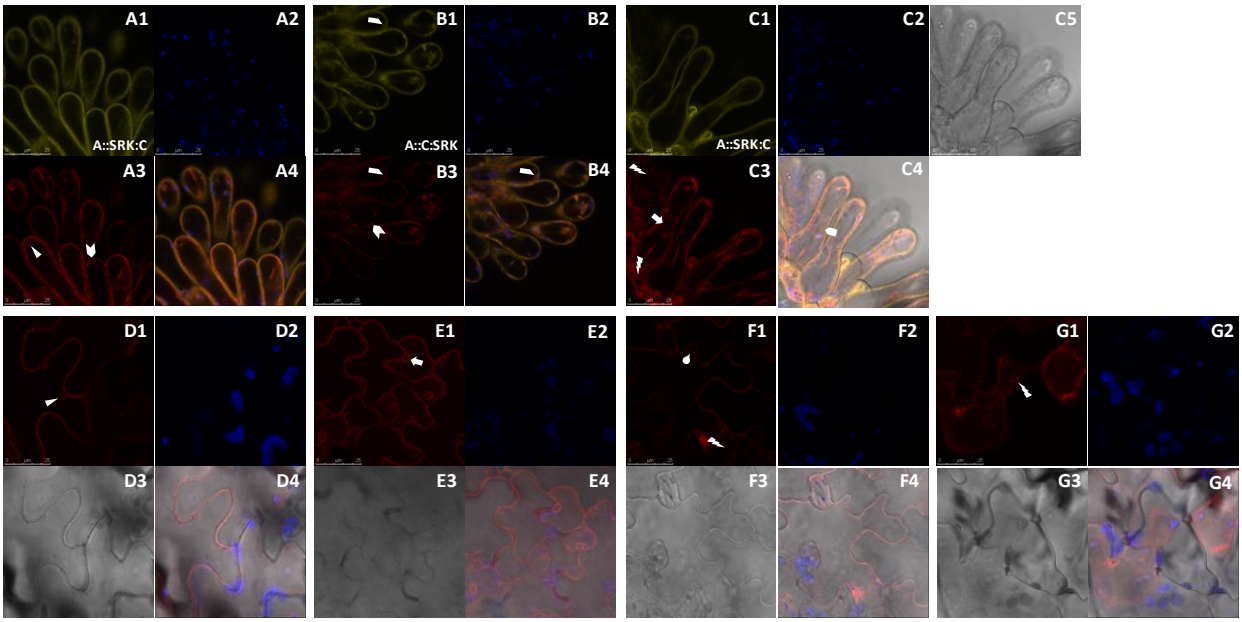

Figure 18. Expression of a vacuole membrane marker in stigma and leaf epidermal cells of *Arabidopsis thaliana*.

Confocal images showing localization of the vacuole membrane (tonoplast) marker tagged with mC **(A3, B3, C3, D1, E1, F1, & G1)**. The tonoplast marker driven by the *AtS1* promoter was co-transformed into *A. thaliana* plants transformed with *AtS1*pr*::SRKb:cYFP* **(A & C)** and *AtS1*pr*::cYFP:SRKb* **(B)**, and the same ER marker driven by the *35S* promoter was transformed into wild type plants **(D-G)** for comparison. **A** and **B** show cYFP **(1)**, chloroplast autofluorescence **(2)**, mC **(3)**, and merged images **(4)** of the same field of view. In **C**, a transmitted light image **(C5)** was added. **D-G** show mC **(1)**, chloroplast **(2)**, transmitted light **(3)**, and merged images **(4)** of the same field of view. In leaf epidermal cells, the vacuole marker is localized in membranous structures **(D1)** that bulge inward from the edge of the cell (arrowhead), although this localization pattern was rarely seen, if at all, in stigma epidermal cells **(A3)**. The arrowhead in **A3** points to a putative bulge. As expected, the vacuole appears to be pulled away (teardrop) from pavement cell lobes with a sharp turn **(F1)**, a pattern that was not seen in stigma epidermal cells, likely because the shape of the cells does not allow for such a pattern. The SRKb signal in transvacuolar strands appears to co-localize with the tonoplast marker **(A-C)**, although it cannot be ruled out that SRKb signal in transvacuolar strands is alternatively or additionally found in ER that moves within transvacuolar strands. As with the PM (Figure 15) and ER (Figure 17) markers, the tonoplast marker appears to surround the nucleus (arrows) in both stigma **(C3)**, as evidenced by the nucleolus (pentagon; **C4**), and leaf **(E1)** epidermal cells, and in chloroplasts (trapezoid; **B**). As with the PM marker, uneven spots of signal (chevron) can be seen along the edges of some stigma epidermal cells **(A3 & B3)**. "Bulbs" of tonoplast (lightning bolts) were sometimes seen nearest the pavement cell wall facing the subadjacent mesophyll cells **(G1)**. Similar structures were seen in broken cell debris likely resulting from the mechanical bursting of the cell during slide preparation **(C & F)**. It should be noted that the inward bulges **(D1)** and the hypothesized nucleus **(E1)** in the pavement cells may truly be "bulbs." Because most distinguishing features of the tonoplast marker are seen nearest the pavement cell wall facing the mesophyll cells, the chloroplasts seen in **D-G** are from the underlying mesophyll cells.

Figure 19. Vesicle-like structures containing full-length SRKb do not co-localize with peroxisomes, mitochondria, or Golgi stacks.
Confocal images showing localization of a peroxisome (px) marker **(A3)**, mitochondria (mt) marker **(B3)**, or Golgi marker **(C3 & D3)** tagged with mC, each driven by the *AtS1* promoter and co-transformed separately into *A. thaliana* plants transformed with *AtS1*pr*::SRKb:cYFP*. cYFP **(1)**, chloroplast autofluorescence **(2)**, mC **(3)**, and merged images **(4)** of the same field of view. **A** and **B** are surface-view optical sections highlighting SRKb-containing vesicle-like structures in stigma epidermal cell apices. **C** shows 3X zoom images of **D**, where some vesicle-like structures are visible (arrowhead). Note that unlike cYFP-tagged SRKb driven by the *AtS1* promoter **(C1 & D1)**, the Golgi marker driven by the *AtS1* promoter does not exhibit localization in style epidermal cells **(C3 & D3)**.

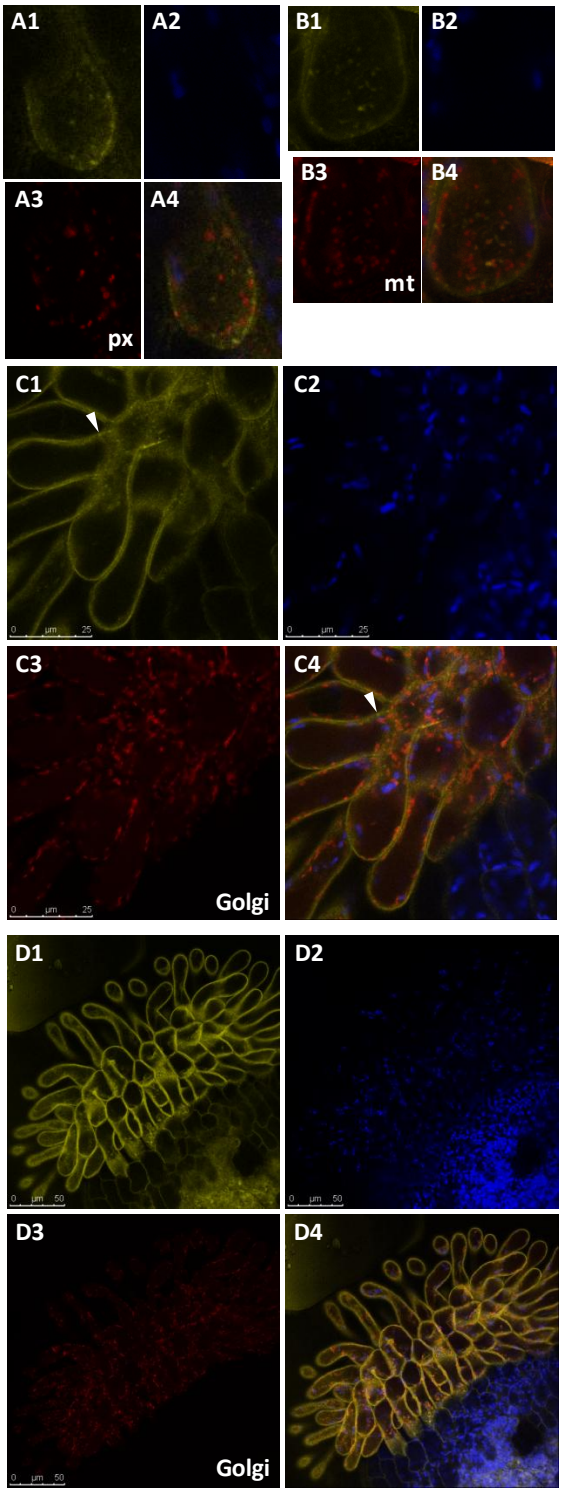
A1
A2
B1
B2
A3
px
A4
B3
mt
B4
C1
C2
C3
Golgi
C4
D1
D2
D3
Golgi
D4

SRKb subcellular distribution following pollination

In order to determine if ligand-induced changes in the subcellular localization of SRKb occur, −1-stage stigmas from *A. thaliana* plants transformed with cYFP-tagged SRKb were pollinated with pollen expressing SCRb or with wild type pollen. Stigmas were subjected to confocal microscopy at various time points between 10 and 60 minutes after pollination. Neither the pollination time nor the presence or absence of the SCRb ligand in pollen appeared to have any clear effect on the subcellular distribution of SRKb (Figure 20). In other words, SRKb expression patterns in stigma epidermal cells were indistinguishable among unpollinated stigmas, stigmas pollinated with pollen expressing SCRb, and stigmas pollinated with wild type pollen (Figures 13A&B & 20).

SRKb signal in non-stigma epidermal cells

Confocal microscopy images of side views of excised pistils revealed that all cYFP-tagged SRKb transformants exhibited SRKb signal in both stigma epidermal cells and, unexpectedly, in style epidermal cells (Figures 12, 13C&D, 14A, 15A1, 19C1&D1, 20A1, & 21A-F). Because some of the constructs used to express cYFP-tagged SRKb were driven by the *AtS1* promoter (Figure 21A-C&E) and others by the native *SRKb* promoter (Figure 21D&F), this pattern is not promoter-dependent. The pattern is also not promoter-specific, since all of the mC-tagged organelle marker proteins were expressed under the control of the *AtS1* promoter, and yet all of these proteins exhibited signal in stigma, but not style, epidermal cells (Figures 14B, 15A3, & 19C3&D3). The difference in localization between the organelle marker proteins and SRKb proteins is also not dependent on the FP tag, since both cYFP- and mC-tagged SRKb exhibit an identical localization pattern in stigma and style epidermal cells (Figure 22). Although SRKb

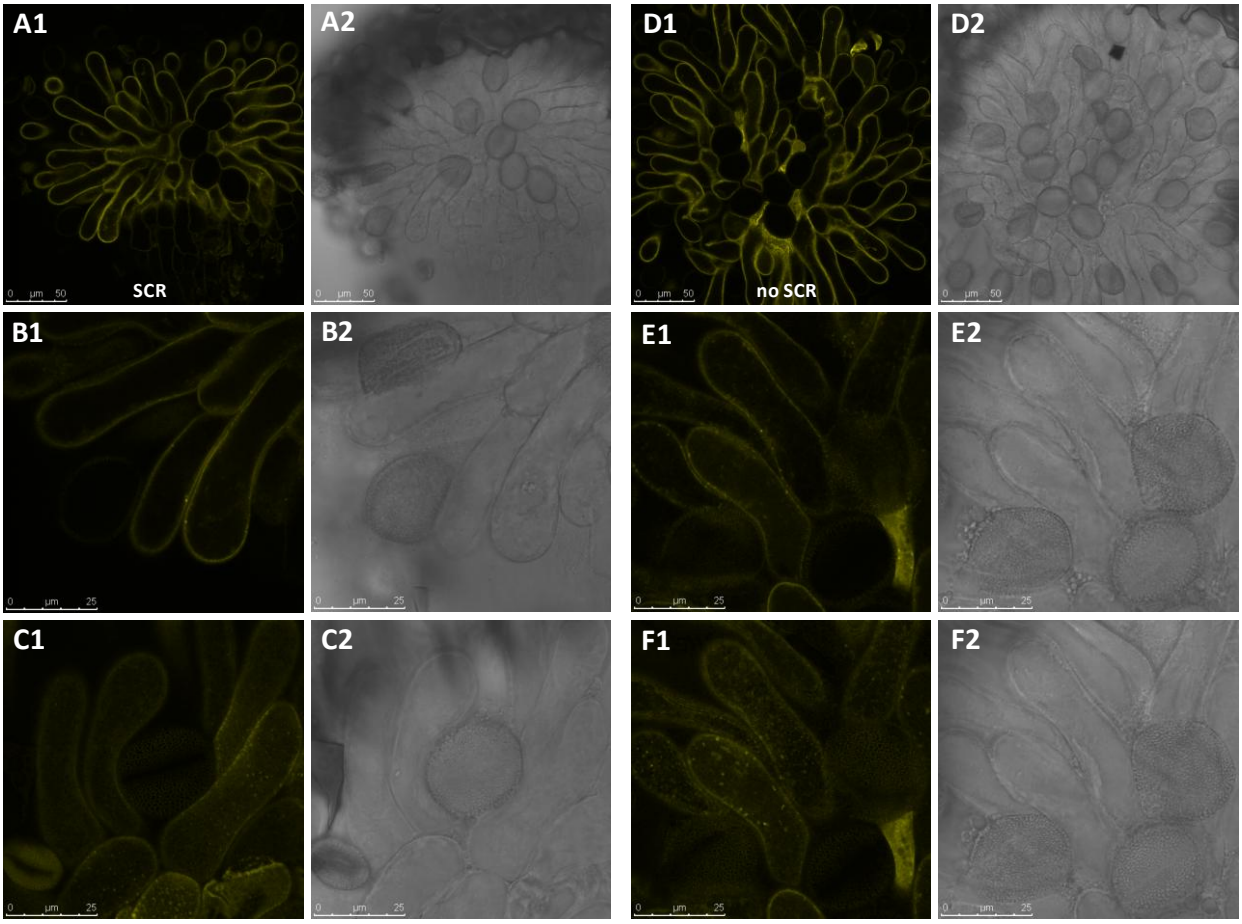

Figure 20. Pollinated stigmas from *Arabidopsis thaliana* plants transformed with cYFP-tagged SRKb show no detectable changes in the subcellular distribution of SRKb.
Confocal images of −1-stage *A. thaliana* stigmas transformed with *AtS1*pr*::SRKb:cYFP* after pollination with either pollen expressing SCRb (left) or wild type pollen (right) show no detectable differences between either each other or unpollinated stigmas (Figure 13A&B) in the subcellular distribution of SRKb. Pollination incubation periods between 10 minutes and 1 hour before imaging also had no detectable effect on SRKb distribution. Similar results were also obtained for all other tested plants transformed with cYFP-tagged SRKb constructs. cYFP **(1)** and transmitted light **(2)** images of the same field of view. Optical cross-section views **(A, B, D, & E)** and epidermal cell-surface views **(C & F)** are shown. **B** depicts 3X zoom images of the stigma shown in **A**, and **C** depicts images of another stigma at the same magnification as that used in **B**. **E** and **F** depict the same 2-dimensional view, 3X zoom images of the stigma shown in **D**. Pollen grains, which exhibit autofluorescence with the cYFP imaging parameters, can be seen in all images.

Figure 21. *Arabidopsis thaliana* plants transformed with each of the cYFP-tagged SRKb constructs exhibit SRKb localization in both stigma and style epidermal cells.
Representative confocal microscopy images of the side view of the stigma and style epidermis from a −1-stage floral bud of an *A. thaliana* plant, each transformed separately with *AtS1*pr*::SRKb:cYFP* **(A)**, *AtS1*pr*::cYFP:SRKb* **(B)**, *AtS1*pr*::cYFP:SRKb* + *SCRb*pr*::SCRb* **(C)**, *SRKb*pr*::cYFP:SRKb* + *SCRb*pr*::SCRb* **(D)**, *AtS1*pr*::cYFP:SRKb*(cDNA) + *SCRb*pr*::SCRb* **(E)**, and *SRKb*pr*::cYFP:SRKb*(cDNA) + *SCRb*pr*::SCRb* **(F)**, or untransformed **(G)**. All images were captured with all the same parameters (25% Argon laser power; 49% 514 nm laser line intensity; 522-550 nm emission; 8 line-averaging; 1061.2 V gain), except for wild type (WT; **G**), whose parameters differed only in gain value (maximum, 1250 V). Fluorescence signal is present in the style epidermal cells (arrowhead) of all cYFP-tagged SRKb transformants **(A-F)**, but not of WT plants **(G)**, indicating that this signal is due to SRKb, and not autofluorescence of the style epidermal cell walls.

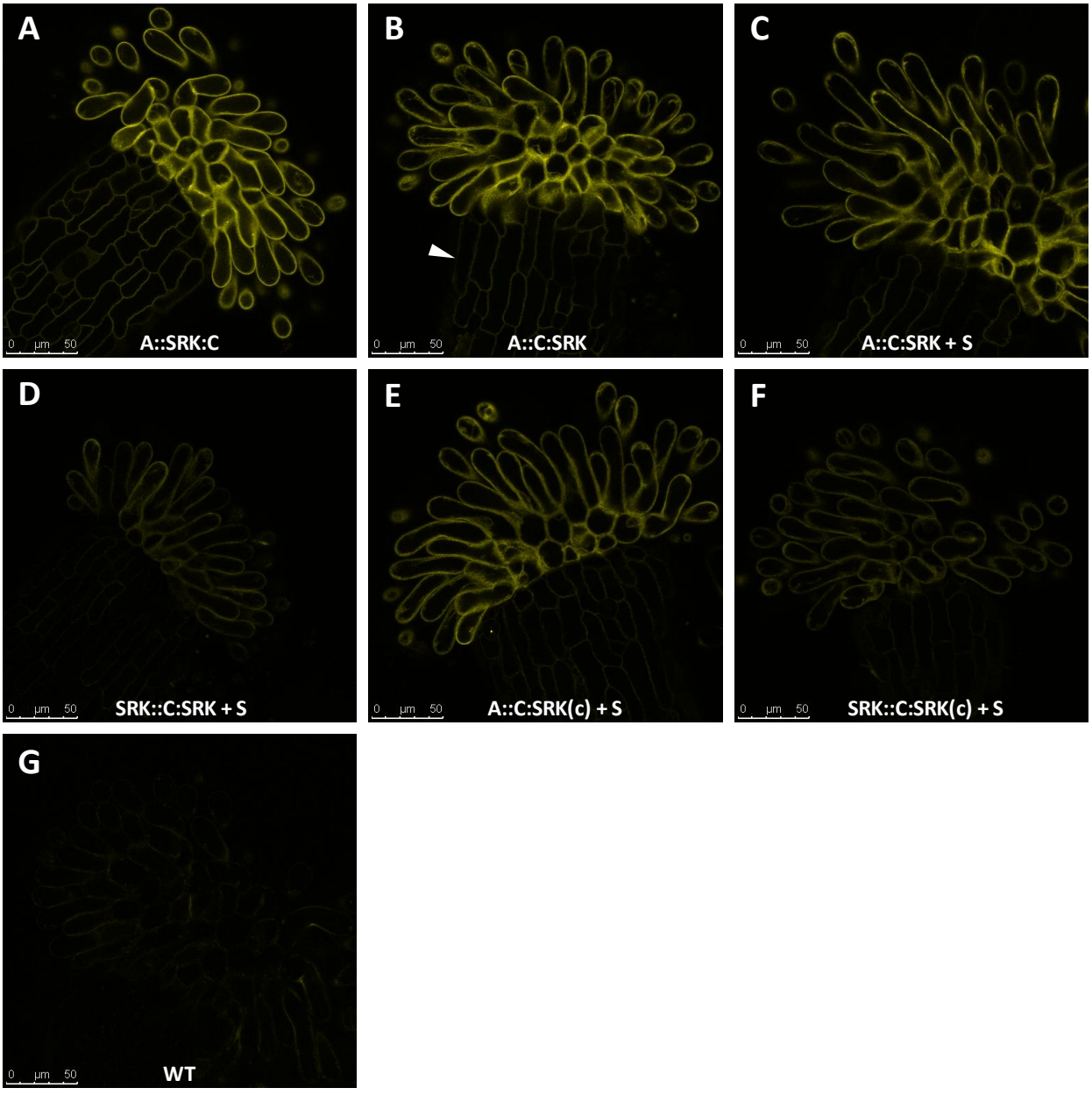
A
0 µm 50
A::SRK:C
B
0 µm 50
A::C:SRK
C
0 µm 50
A::C:SRK + S
D
0 µm 50
SRK::C:SRK + S
E
0 µm 50
A::C:SRK(c) + S
F
0 µm 50
SRK::C:SRK(c) + S
G
0 µm 50
WT

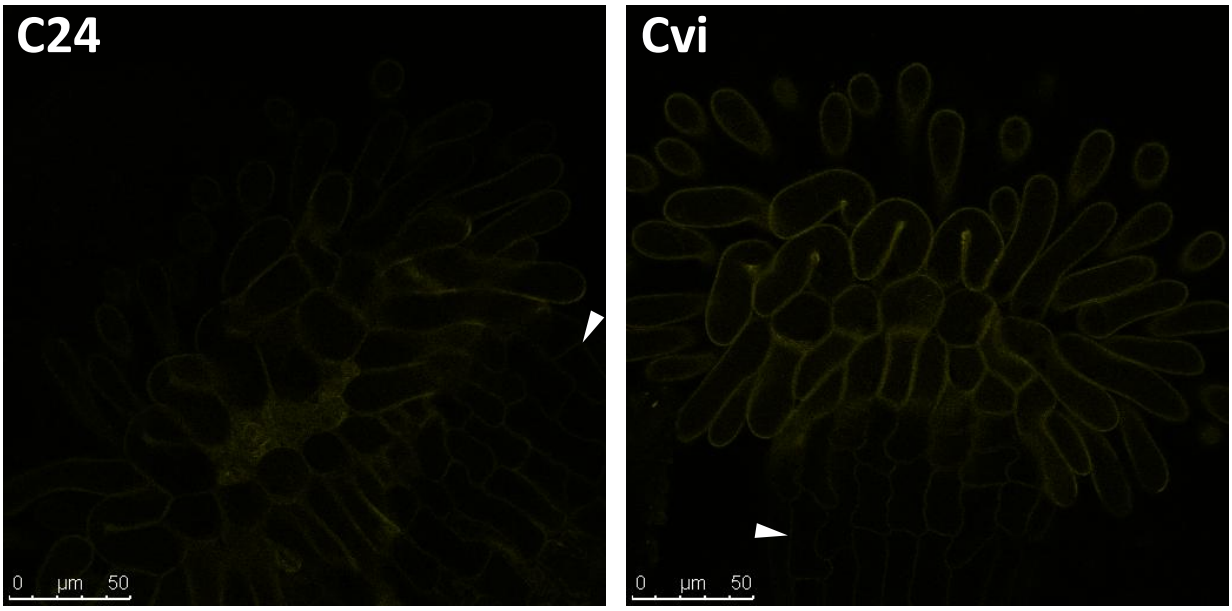

Figure 22. *Arabidopsis thaliana* plants expressing mC-tagged SRKb exhibit the same SRKb localization pattern in both the stigma and style epidermal cells as plants expressing cYFP-tagged SRKb.
C24 (left) and Cvi-0 (right) ecotypes of *A. thaliana* transformed with *AtS1*pr*::SRKb:mC* exhibit SRKb localization in both stigma and style (arrowheads) epidermal cells, just as in the various ecotypes transformed with the various cYFP-tagged SRKb constructs, and exhibit the same appearance of subcellular localization as that obtained from plants transformed with the *AtS1*pr*::SRKb:cYFP* construct. Because the sequences of cYFP and mC are different, these results suggest it is unlikely that the FP tag influences the SRKb localization pattern. Fluorescence signal from mC was false-colored yellow, as was done for the fluorescence signal from cYFP, in order to facilitate visual comparison of signal between the two FPs. Both images were captured with the same confocal imaging parameters (50% 561 nm DPSS laser line intensity; 592-629 nm emission; 8 line-averaging; 1250 V gain).

signal was much lower in the style than in the stigma epidermal cells, this pattern cannot be attributed to autofluorescence, since the wild type sample lacked fluorescence signal in style epidermal cells, even at the maximum gain value (Figure 21G). Close inspection revealed that as in stigma epidermal cells (Figure 8), the SRKb signal in style epidermal cells of plants transformed with the *AtS1*pr*::SRKb:cYFP* construct (Figure 21A) appeared sharper than that in plants transformed with all of the other constructs, the latter of which looked indiscernible from one another in subcellular localization pattern (Figure 21B-F).

SRKb signal in the style epidermis was found to extend to the entire pistil epidermis (Figure 23A-F). Sub-epidermal optical sections of the pistil revealed that SRKb signal was also present in the septum, the tissue located between the two fused carpels that make up the pistil (Figure 23B&C). It is unclear if SKRb expression was present in the entire septum, or only part of the septum, such as the transmitting tract or the medial vascular bundle (Gu *et al.* 1998; Ferrándiz *et al.* 1999). Equivalent images of wild type −1-stage pistils showed that the only signal present was due to the autofluorescence of the stigma epidermal cell walls and of chloroplasts in the stigma, style, and ovary (Figure 23G-I).

SRKb signal was also found in all other −1-stage floral bud organs of plants expressing cYFP-tagged SRKb (Figure 24A-G). SRKb signal in stamens was found in both adaxial and abaxial epidermal cells and in the presumed vascular strand (Figure 24A-E). The vascular strand signal was most obvious in the deeper optical section of the stamen where the abaxial epidermis is facing upward (Figure 24D), likely because the vascular strand is situated nearest the abaxial surface (Scott *et al.* 2004). SRKb signal was also seen in the epidermal cells of petals and sepals (Figure 24F&G). Equivalent images of wild type floral organs revealed only occasional

Figure 23. *Arabidopsis thaliana* plants expressing cYFP-tagged SRKb exhibit SRKb localization in epidermal cells of the entire pistil.
Shown are confocal microscopy images of a −1-stage pistil from a plant transformed with *AtS1*pr*::cYFP:SRKb* **(A-F)** and one from an untransformed (wild type) plant **(G-I)** for comparison. Images captured with a 20X objective show that the apical **(A)** and basal **(D)** portions of the pistil exhibit SRKb localization in the epidermal cells. Deeper optical sections through the same apical region of the pistil **(B, C)** reveal that SRKb signal is also present in the septum (arrowheads) between the two fused carpels that make up the pistil, and may be present specifically in the transmitting tract. Magnified images captured with a 63X objective show the epidermis of the stigma and style **(E)**, and the epidermis of the ovary apex **(F)** where it connects to the style, of the same pistil. The colored squares surrounding the images **(E & F)** represent the areas demarcated by the equivalent colored squares from the pistil apex image **(A)**. Equivalent 20X-objective images of the apical epidermis **(G)** and a deeper optical section **(I)**, and a 63X-objective image of the epidermis and style **(H)**, of a wild type (WT) pistil show only faint autofluorescence of the stigma epidermal cell walls and of chloroplasts in the stigma, style, and ovary. No signal was found in the presumed septum in WT pistils **(I)**. All images were captured with the same confocal imaging parameters (25% Argon laser power; 49% 514 nm laser line intensity; 522-561 nm emission; 1 line-averaging, with 20X images captured at 1005V gain and 63X images captured at 1101 V gain).

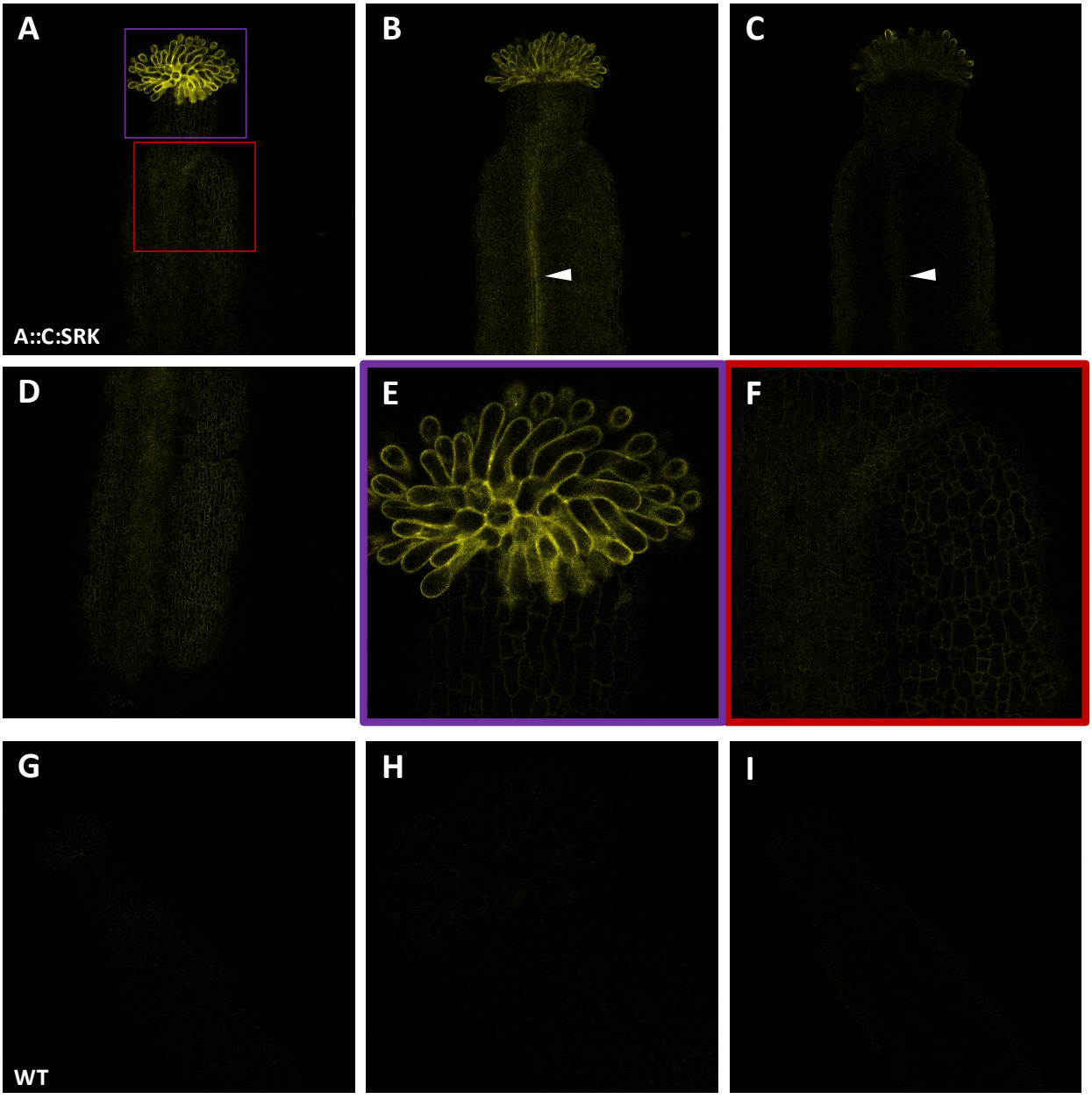
A
A::C:SRK
B
C
D
E
F
G
WT
H
I

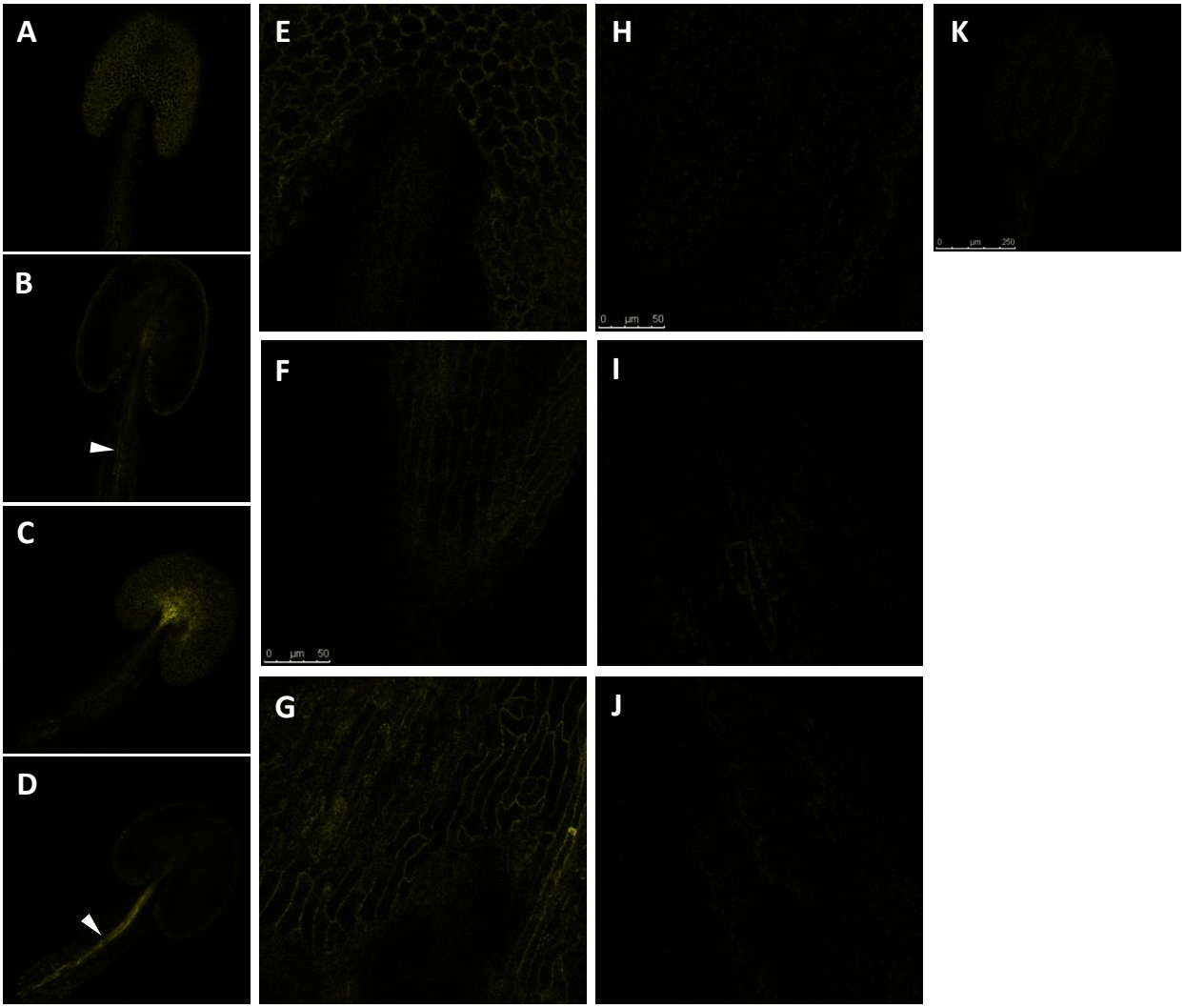

Figure 24. *Arabidopsis thaliana* plants expressing cYFP-tagged SRKb exhibit SRKb localization in epidermal cells of all floral organs.
Shown are confocal images of stamens, petals, and sepals from −1-stage floral buds from a plant transformed with *AtS1*pr*::cYFP:SRKb* **(A-G)** and from an untransformed (WT) plant **(H-K)** for comparison. Images captured with a 20X objective reveal SRKb localization in both the adaxial **(A)** and abaxial **(C)** epidermis, and in the presumed vasculature, of stamens from transformed plants, which cannot be seen in WT stamens **(K)**. The vasculature is seen more definitively as a central strand of signal (arrowheads) in the filament of deeper optical sections of the stamens **(B & D)**. The vasculature strand is most obvious in the deeper optical section of the stamen where the abaxial epidermis is facing upward **(D)**. Magnified images captured with a 63X objective show SRKb localization in the adaxial epidermis of the stamen at the anther-filament junction **(E)**, the epidermis of the petal **(F)**, and the epidermis of the sepal **(G)**, unlike in equivalent WT images (**H**, **I**, and **J**, respectively). All images were captured with the same confocal imaging parameters (25% Argon laser power; 49% 514 nm laser line intensity; 522-561 nm emission; 1 line-averaging, with 20X images captured at 1005V gain and 63X images captured at 1101 V gain).

autofluorescence of a few epidermal cells (Figure 24I) and of chloroplasts in sub-epidermal tissue (Figure 24H-K).

The localization of SRKb in all epidermal cells of the pistil does not seem to be dependent on the genetic background of the C24 ecotype. Other *A. thaliana* ecotypes transformed with the *AtS1*pr*::cYFP:SRKb* + *SCRb*pr*::SCRb* construct also exhibited SRKb signal in epidermal cells, although the levels and stigma-to-style ratios of signal differed (Figure 25). The images shown in Figure 25 were captured to highlight both the SRKb signal and the autofluorescence of stigma epidermal cells, and to compare signal levels between transformed and untransformed samples. Therefore, the gain values among the images are different, and the images do not necessarily reflect the relative SRKb signal levels among the various transformed ecotypes. However, when gain values were considered, SRKb signal levels among ecotypes could be approximated, and are depicted in order of increasing signal level in stigma epidermal cells in Figure 25 (i.e., Bay-0, L*er*-0, Kas-2, Hodja, C24, Cvi-0, Lz-0). Generally, there was a positive correlation between the strength of SI (not shown) and the level of SRKb signal in the stigma, as determined by confocal microscopy (Figures 25 & 26) and by protein gel blot (not shown) analyses. All ecotypes were also found to exhibit cell wall autofluorescence of stigma epidermal cells, but not of style epidermal cells, as shown in images of excised stigmas from untransformed plants (Figure 25). Additionally, all transformed ecotypes were found to exhibit SRKb signal in the style epidermal cells (Figure 25). Therefore, every transformed ecotype expressed SRKb to some extent, which would have been difficult to conclude by analyzing only the stigma epidermal cells of moderately-expressing ecotypes, since autofluorescence could have impeded detection of SRKb signal. Interestingly, the Bay-0 ecotype exhibited a unique SRKb localization pattern in the style epidermis, where the SRKb signal level decreased basipetally

Figure 25. Different ecotypes of *Arabidopsis thaliana* expressing cYFP-tagged SRKb exhibit unique levels and ratios of SRKb signal in stigma and style epidermal cells.
Various ecotypes of *A. thaliana* transformed with the *AtS1*pr*::cYFP:SRKb + SCRb*pr*::SCRb* construct exhibit their own, signature localization pattern with regard to the levels of SRKb signal in both the stigma epidermis and the style epidermis. Representative confocal microscopy images of the side view of an excised stigma from a −1-stage floral bud of a transformed (top) and an untransformed (bottom) plant of each ecotype are shown. All images were captured with 25% Argon laser power, 49% 514 nm laser line intensity, 522-561 nm emission, and 1 line-averaging, except the transformed and untransformed L*er*-0 images, which were captured with 522-550 nm emission and 8 line-averaging. The gain values used were as follows: Bay-0, 1250 V; L*er*-0, 1250 V; Kas-2, 1250 V; Hodja, 1040.1 V transformed, 1041.2 V untransformed; C24, 1061.7 V transformed, 1250 V untransformed; Cvi-0, 1103.9 V transformed, 1250 V untransformed; Lz-0, 991 V transformed. Starting from left to right, top to bottom, the ecotypes are ordered in the figure according to their estimated, approximate increasing order of SRKb signal level seen in the stigma epidermal cells (i.e., Bay-0, L*er*-0, Kas-2, Hodja, C24, Cvi-0, Lz-0). All ecotypes exhibit autofluorescence of the stigma epidermal cells, but not of the style epidermal cells (bottom).

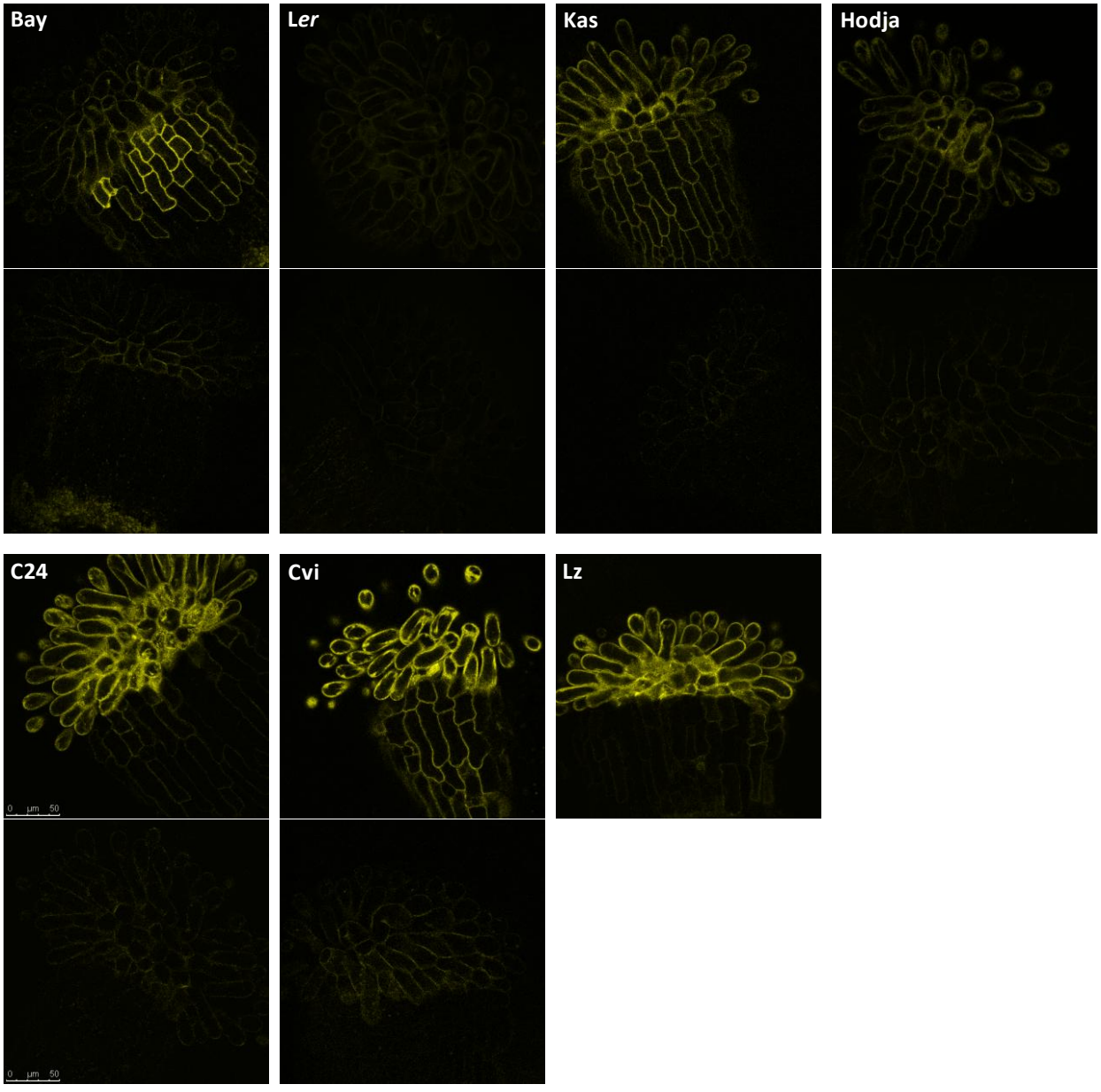
Bay
Ler
Kas
Hodja
C24
Cvi
Lz
0 µm 50
0 µm 50

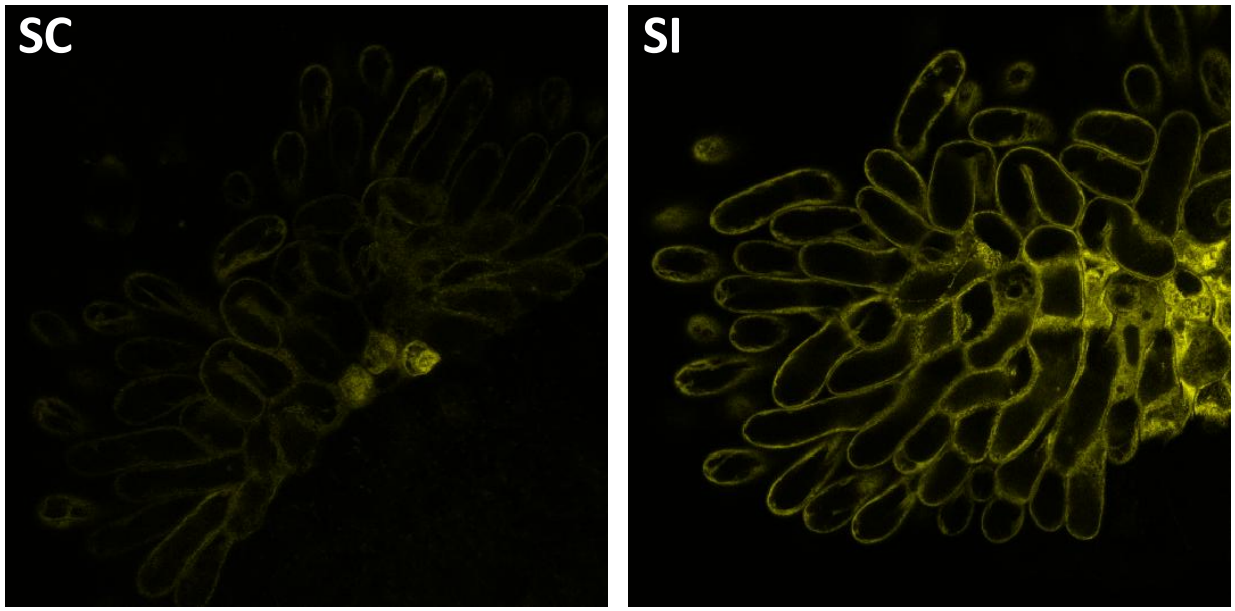

Figure 26. Self-incompatibility strength positively correlates with SRKb signal level. Confocal images showing localization of SRKb in stigmas of two *Arabidopsis thaliana* F_2 plants of the same family, resulting from a cross between a plant of the Cvi-0 ecotype transformed with the *AtS1*pr*::cYFP:SRKb + SCRb*pr*::SCRb* construct and a wild type plant of the L*er* ecotype. The F_2 plants segregated for the self-compatibility phenotype. A self-compatible (SC) plant (left) and a self-incompatible (SI) plant (right) show low and high levels of SRKb signal, respectively, indicating that the strength of incompatibility positively correlates with SRKb signal level. Both images were captured with identical cYFP imaging parameters.

(Figure 25). Differences among the tested ecotypes in the stigma-to-style and overall SRKb signal levels can likely be attributed to the effects of the different genetic backgrounds among the ecotypes on SRKb signal levels.

SRKb signal throughout floral development

In order to determine if levels of SRKb signal correlate with developmental maturity of the floral bud and/or the stigma epidermal cells, and/or with the strength of incompatibility, consecutive buds and flowers from an inflorescence stem were numbered in reference to the −1 bud and their excised stigmas were imaged by confocal microscopy (Figures 27 & 28).

Signal produced by full-length SRKb, only, throughout floral development can be analyzed in *A. thaliana* plants transformed with *AtS1*pr*::SRKb:cYFP* (Figure 27). In stigma epidermal cells of these plants, fluorescence signal was barely visible in the −5-stage stigma, became apparent by the −4 stage, and progressively increased in developmentally more mature stigmas until it appeared to reach a maximum level at the −2 stage that persisted until the +2 stage (Figure 27). This signal began to diminish at the +3 stage, and was undetectable once the stigma epidermal cells were dead at the +4 stage (Figure 27), at which time the ovary had begun to elongate, an indication that fertilization had occurred and seed development was commencing. Maximum levels of signal in stigma epidermal cells correlated both with the competency of the stigma epidermal cells to receive pollen and permit pollen tube growth at a high and efficient level, and with the ability of the stigma to reject self-incompatible pollen.

Signal produced by all three forms of the SRKb protein, namely, full-length SRKb, tSRKb, and eSRKb, on the other hand, can be analyzed throughout floral development in *A. thaliana* plants transformed with *AtS1*pr*::cYFP:SRKb* (Figure 28). The appearance of SRKb

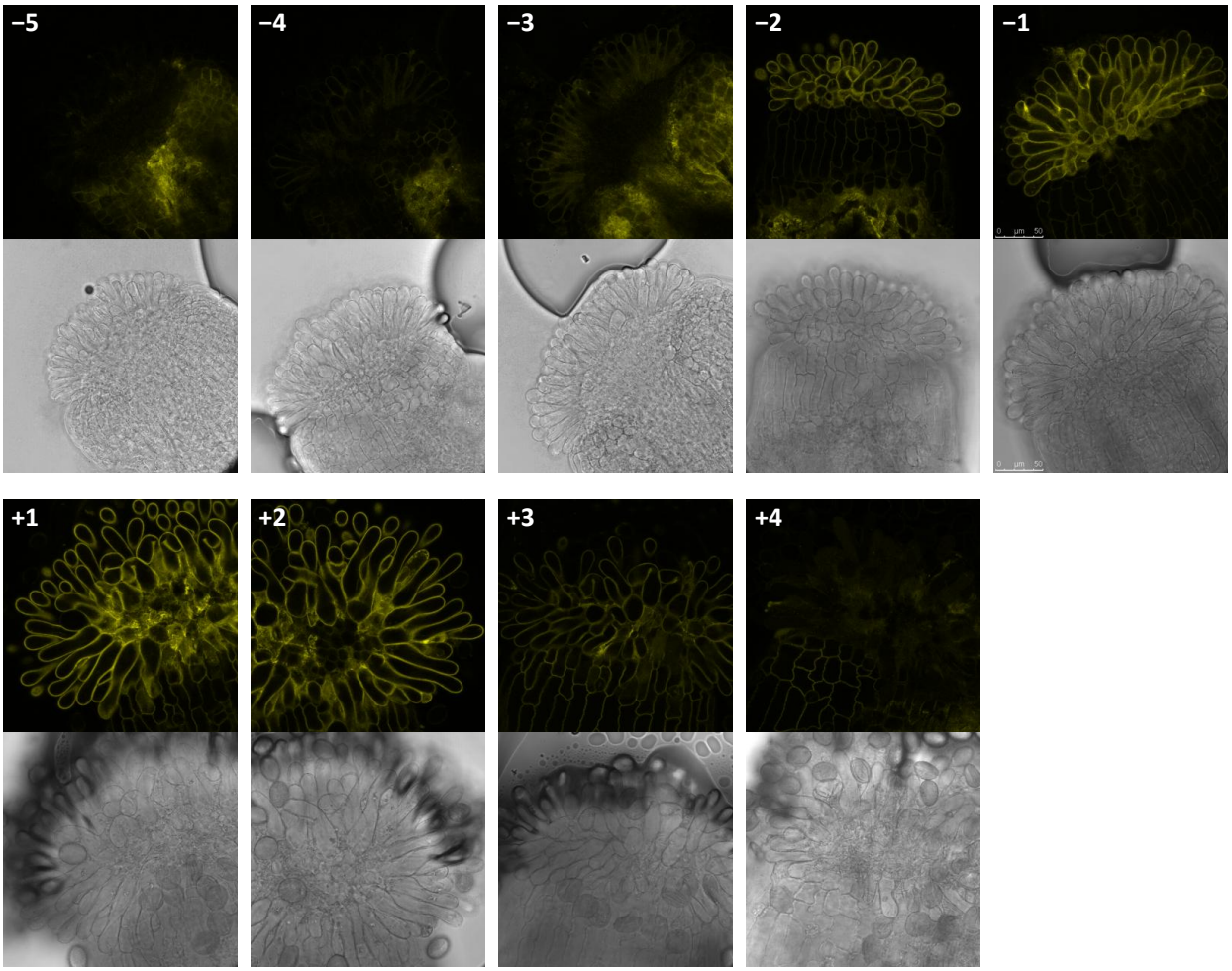

Figure 27. Localization of SRKb throughout floral development in excised pistils of *Arabidopsis thaliana* transformed with *AtS1*pr*::SRKb:cYFP*.
Shown are confocal microscopy images of excised pistils from consecutive buds and flowers found on one inflorescence stem, which were excised at one time and numbered in reference to the −1 bud. Buds at progressively younger developmental stages were labeled −2, −3, −4, and −5, and are shown on the top row. Open flowers, or those undergoing anthesis, at progressively older developmental stages were labeled +1, +2, +3, +4, and +5, and are shown in the bottom row. Within a row, fluorescence images using cYFP imaging parameters are shown at the top, and corresponding transmitted light images of the same field of view are shown at the bottom. Pollen that was naturally shed from anthers and deposited onto the stigma epidermal cells from the same flower can be seen in the images of excised pistils of all open flowers (bottom row).

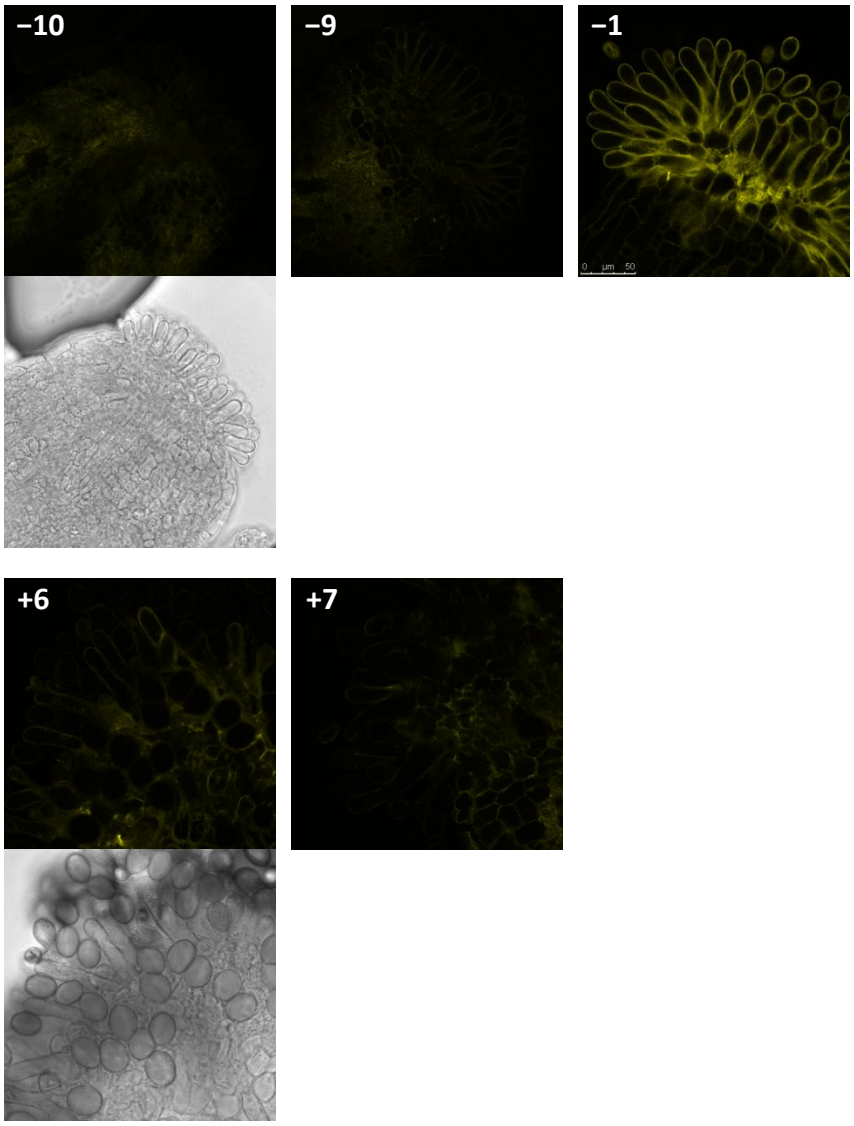

Figure 28. Localization of full-length SRKb, tSRKb, and eSRKb at transitional stages of signal levels in excised pistils of *Arabidopsis thaliana* transformed with *AtS1*pr*::cYFP:SRKb.*

Shown are confocal microscopy images of excised pistils from buds and flowers found on one inflorescence stem, which were excised at one time and numbered in reference to the −1 bud. Buds at younger developmental stages are shown on the top row, and those at older developmental stages are shown in the bottom row. Within a row, fluorescence images using cYFP imaging parameters are shown at the top, and corresponding transmitted light images of the same field of view (if applicable) are shown at the bottom. For simplicity, only excised stigmas of buds and flowers at the transitional stages, or those representing the stages between the presence and absence of signal, and the −1 bud, are shown, since the gradual rise and decline of signal at intermediate stages follows the same pattern as that seen with the *AtS1*pr*::SRKb:cYFP* transformants (Figure 27).

signal in the stigma epidermal cells occurred at an earlier stage of development in these plants than in the *AtS1*pr*::SRKb:cYFP* transformants, with the first detectable signal appearing in the −9-stage stigma (Figure 28) and the −4-stage stigma (Figure 28), respectively. Although the developmental stage at which the onset of signal in stigma epidermal cells occurred varied slightly within a genotype, that stage was consistently developmentally more immature in the *AtS1*pr*::cYFP:SRKb* genotype than in the *AtS1*pr*::SRKb:cYFP* genotype.

In contrast with the expression of SRKb in stigma epidermal cells, expression in style epidermal cells was persistent throughout development, even at developmentally immature bud stages when signal was absent in stigma epidermal cells (−5, *AtS1*pr*::SRKb:cYFP* [Figure 27]; −10, *AtS1*pr*::cYFP:SRKb* [Figure 28]), and at mature stages when stigma epidermal cells were dead (+4, *AtS1*pr*::SRKb:cYFP* [Figure 27]; +7, *AtS1*pr*::cYFP:SRKb* [Figure 28]).

DISCUSSION

This study employed live-cell confocal microscopy to visualize the subcellular localization and dynamics of cYFP-tagged SRKb in the stigmas of transgenic *Arabidopsis thaliana*. By manipulating the placement of the cYFP tag at the N- or C-terminus of the SRKb protein and by using genomic or cDNA *SRKb* sequences, it was possible to visualize within individual stigma epidermal cells different complements of the three SRKb protein species, full-length SRKb, tSRKb, and eSRKb: only full-length SRKb (C-terminal tag), all three SRKb protein species (N-terminal tag inserted in the *SRKb* genomic sequence), or only full-length SRKb and tSRKb (N-terminal tag inserted in the *SRKb* cDNA sequence). Significantly, neither the cYFP tag, irrespective of its placement at the N- or C-terminus of SRKb, nor the choice of promoter used to drive expression of SRKb in sigma epidermal cells affected SRKb function,

since a strong SI response was conferred by all chimeric genes used in this study. Notably, even the chimeric gene constructed with *SRKb* cDNA, which does not produce the eSRKb protein, conferred SI. This result demonstrates that the eSRK is not required for SI, at least in the case of *Sb* specificity. This observation resolves the long-standing question of whether the eSRK isoform functions in SI.

Subcellular localization of SRKb in stigma epidermal cells

The confocal microscopy study described here revealed that SRKb was localized to the cell periphery and in transvacuolar strands. This pattern can be expected in large, specialized, and highly differentiated epidermal cells of plants, which tend to have a very large central vacuole that makes up the majority of the cell volume. Pinpointing the localization of proteins to the cytosol, plasma membrane (PM), endoplasmic reticulum (ER), or vacuolar membrane (tonoplast) using fluorescent protein (FP) tags can sometimes be difficult given the large central vacuole of plant epidermal cells. Identification of the putative organelles to which SRKb is localized should provide clues as to how SRKb is regulated.

Because only a faint signal was seen in transvacuolar strands of *SRKb-cYFP* transformants, it is likely that almost all of the full-length SRKb is localized to the PM. Therefore, the signal produced by *cYFP-SRKb* transformants in the cortical ER and in as-yet-unidentified membrane-containing structures in transvacuolar strands that likely represent ER, must de derived from tSRKb and/or eSRKb. Because the tSRKb and eSRKb protein species could only be visualized with a tag placed at the N terminus of the *SRKb* sequence, the hypothesized localizations of these protein species to the PM, in the case of tSRKb, or in the cell wall, in the case of eSRKb, may be obscured. It is therefore possible that the signal visualized in

cYFP-SRKb transformants represents the location of these proteins on their journey through the secretory pathway. However, it cannot be ruled out that tSRKb and eSRKb are more abundant in the ER than in the PM and cell wall, respectively, where they may be involved in signaling subsequent to binding and recognition of SCRb by SRKb at the PM.

Because SRKb in transvacuolar strands appears to co-localize with the PM, ER, and tonoplast markers, it will be difficult to conclude definitively with co-localization methods that any or all of these subcellular compartments represent the true localization of SRKb in transvacuolar strands. This difficulty is confounded by the observation that these three markers sometimes appeared to localize to membranous material surrounding chloroplasts and the nucleus. Although Nelson *et al.* (2007) reported that the tonoplast marker does not surround the nucleus on the side facing the cell edge, this conclusion cannot be easily made in some of their images of leaf epidermal cells, where the tonoplast marker signal can be visualized in membranous material surrounding the nuclei. Interestingly, another γ-TIP (tonoplast intrinsic protein) marker (Saito *et al.* 2002) was reported to exhibit localization around nuclei in root apex cells, which was hypothesized to represent ER membrane. If true, this would support the hypothesis that the PM, ER, and tonoplast markers used in this study (Nelson *et al.* 2007) overlap in the membrane compartments to which they are localized, which may be a concern for use in co-localization studies where these compartments must be distinguished.

Another difficulty confounding the determination of the transvacuolar structures to which SRKb is localized is that many of the distinguishing features of the vacuole in pavement cells of the leaf epidermis do not seem to be useful in distinguishing the vacuole from other subcellular compartments in stigma epidermal cells. For example, due to the sinuous nature of pavement cells, extreme lobing of the cell margins often prevents the vacuole from directly abutting the

lobe edges in this cell type (Figure 18F). Additionally, distinctive bulges of tonoplast that project inward from the cell edge can be seen in pavement cells (Figure 18D). Furthermore, a particularly distinctive feature of this (Nelson *et al.* 2007) and another (Saito *et al.* 2002) γ-TIP marker is the presence of tonoplast "bulbs," relatively spherical intracellular structures that are continuous with the tonoplast and are motile. "Bulbs" were seen in pavement cells, usually nearest the wall facing the subjacent mesophyll cells (Figure 18G). It cannot be ruled out that in pavement cells, the structures bulging inward from cell edges (Figure 18D) and the structure hypothesized to be the nucleus (Figure 18E) are truly "bulbs." None of these features were observed, at least not readily, in stigma epidermal cells. Spheres similar in appearance to "bulbs" were seen in broken stigma epidermal cell debris (Figure 18C&F), but are unlikely to represent "bulbs," as these structures were otherwise never found in stigma epidermal cells. "Bulbs" were reportedly found mainly in rapidly expanding cells (Saito *et al.* 2002), which may explain why stigma epidermal cells, highly differentiated at the −1 stage at which these images were captured, were never found to exhibit these structures.

Other than testing and utilizing organelle markers that may be more specifically and stably targeted to their appropriate destinations in the cell, another potentially helpful approach to identifying the vesicle-like compartments and those within the transvacuolar strands to which SRKb localizes would be to incubate live stigmas with FM4-64 dye and subject them to confocal microscopy analysis. FM-dyes are amphiphilic styryl dyes that are thought to be taken up by cells via endocytosis, and can be used to progressively stain various components of the endomembrane system over time, beginning with the PM (Bolte *et al.* 2004). FM-dyes have been used in animal, fungal, and plant cells for this purpose (Bolte *et al.* 2004). Use of the FM4-64 dye with *A. thaliana* plants transformed with the various cYFP-tagged SRKb constructs would

potentially supplement the data obtained from co-localization studies, which could help to identify the precise subcellular compartments to which each SRKb species, full-length SRKb, tSRKb, and eSRK, is localized.

Subcellular localization of the plasma membrane marker, mC-tagged AtPIP2A

It is unclear why the PM marker exhibited signal in subcellular locations other than the PM, such as in membranous material surrounding nuclei and chloroplasts (Figure 15). The PM marker is AtPIP2A (*Arabidopsis thaliana* plasma membrane intrinsic protein 2A), which is an aquaporin, or water channel, reported to exhibit PM localization by both Nelson *et al.* (2007) and Cutler *et al.* (2000). PM marker signal was also detected in cell surface-localized spots (Figure 15). Similar unexpected patterns occasionally occurred with the tonoplast marker (Figure 18), γ-TIP (tonoplast intrinsic protein), which like the PM marker, is an aquaporin. Unlike the other markers in this set, which were based on known signal sequences that target proteins to their appropriate organelle, the PM and tonoplast markers were full-length proteins (Nelson *et al.* 2007). Therefore, the unexpected localization patterns may be due to a feature inherent to aquaporins. These unexpected patterns cannot be due to some inherent property of stigma epidermal cells, since some of the cells exhibited the expected PM localization pattern (Figure 15D), and the unexpected patterns were also sometimes observed in leaf epidermal cells (Figure 15E&F). Interestingly, the uneven spots of surface-localized PM marker signal were not observed in every epidermal cell, even within the same stigma or leaf sample. These results may suggest that unexpected localization patterns of the PM and tonoplast markers are induced by some physical means or stress, such as cell damage.

The cell surface-localized spots of PM marker signal are particularly peculiar, and appear to be present in the same optical section plane as the cortical ER. It may be that they represent areas of labeled membranous material seen in the cytoplasm through the ER lacunae. Alternatively, the spots may represent lipid rafts, which are sphingolipid-rich microdomains of the PM that include particular PM-associated proteins and exclude others. The spotty expression pattern is reminiscent of that of proteins found to reside in lipid rafts in a green alga (Grossmann *et al.* 2006) and in tomato (Raffaele *et al.* 2009). Because the cortical ER is subjacent to the PM, lipid rafts may bulge slightly into the cell, making it possible for the cortical ER to surround the potential aquaporin-associated lipid rafts. Support for this hypothesis comes from studies in mammals, in which aquaporins were found to localize to lipid rafts (Zheng & Bollag 2003; Ishikawa *et al.* 2006). One aquaporin was found to co-localize with caveolin in these lipid rafts (Zheng & Bollag 2003). Interestingly, caveolin is found in caveolae, which are often seen as invaginations of the PM (Anderson 1998). A recent study found that GFP-AtPIP2A is localized to lipid rafts in *A. thaliana* (Col) root epidermal cells (Li *et al.* 2011). Although these and other lipid rafts (Grossmann *et al.* 2006; Raffaele *et al.* 2009) appeared smaller than the AtPIP2A PM marker spots seen in this study (Figure 15A&B), salt stress induced the formation of large cell surface-localized patches of GFP-AtPIP2A signal that projected inward, and labeling of intracellular structures in a few of the cells (Li *et al.* 2011). FM4-64 dye staining of these cells indicated that the PM remained intact, and a different PM marker did not exhibit these localization patterns following salt treatment (Li *et al.* 2011). These findings support the hypothesis that the cell surface-localized spots of AtPIP2A PM marker signal seen in stigma epidermal cells are lipid raft-like structures that may be induced by stress. This stress may be

caused by the difference in osmolarity between the stigma epidermal cell and the water in which the sample was placed.

Ligand-induced effects on receptor subcellular localization

cYFP-tagged SRKb localization in stigma epidermal cells does not appear to change upon pollination, either with pollen expressing the SCRb ligand, or with wild type pollen (Figure 20). In *A. thaliana*, other plant receptor-like kinases (RLKs) such as FLS2 (FLAGELLIN SENSING 2), BRI1 (BRASSINOSTEROID-INSENSITIVE 1), and CLV1 (CLAVATA 1), have been studied in context with their respective ligands via live-cell confocal imaging. Like full-length SRKb, they are localized to the PM and endosomes, although not under all conditions (Robatzek *et al.* 2006; Geldner *et al.* 2007; Nimchuk *et al.* 2011). All three receptors, like SRK, are single-pass transmembrane proteins with a cytoplasmic serine/threonine kinase domain, but unlike SRK, they have a leucine-rich repeat (LRR) extracellular domain. As with SRK, interaction of each of these receptors with its respective ligand induces some subcellular change that culminates in some cellular response. However, FLS2, BRI1, and CLV1 are each involved in very different processes and exhibit different localization patterns and trafficking behaviors upon ligand binding.

For example, FLS2 is involved in basal immunity against pathogens. In the absence of ligand, FLS2 is localized to the PM, and in the presence of bacteria-derived flg22 ligand, becomes exclusively localized to vesicles and is eventually degraded (Robatzek *et al.* 2006). BRI1, in contrast, is involved in regulating plant growth and development and localizes simultaneously to the PM and endosomes, both in the presence and absence of the brassinolide ligand (Russinova *et al.* 2004; Geldner *et al.* 2007). Interestingly, BRI1 signaling was found to

occur in endosomes (Geldner *et al.* 2007). CLV1 is involved in maintaining shoot meristem size. Like FLS2, CLV1 localizes to the PM in the absence of its CLV3 ligand and becomes endocytosed in the presence of CLV3 (Nimchuk *et al.* 2011). However, unlike FLS2 and BRI1, CLV1 gets trafficked to the lytic vacuole following endocytosis (Nimchuk *et al.* 2011).

While studies with these three receptors are useful for comparisons with this study because the receptors are similar in structure to SRK and were studied in *A. thaliana* by live-cell imaging, comparisons can also be made with an immunocytochemistry study on the subcellular distribution and dynamics of SRK_3 in *Brassica oleracea*. SRK_3 was found to localize preferentially to endosomes and at barely detectable levels to the PM (Ivanov & Gaude 2009). SRK_3 internalization occurred subsequent to binding at the PM of an antibody that mimicked the SCR_3 ligand, suggesting that signaling occurs at the PM and not in endosomes (Ivanov & Gaude 2009). Interestingly, self-pollination (or binding of SCR_3 to SRK_3) caused some degradation of SRK_3, but neither self- nor cross-pollination altered the localization of SRK_3 (Ivanov & Gaude 2009).

Although SRK_3 localization to the PM and endosomes may be expected, the preference for SRK_3 localization to endosomes is not expected, since different SRK haplotypes have been shown to localize to the PM in a heterologous system and to be present in PM-enriched fractions (Stein *et al.* 1996; Cabrillac *et al.* 1999). More importantly, these results are in conflict with the results from this study, which indicate that while SRKb is localized to vesicle-like structures, it is preferentially localized to the PM. Although it may be argued that SRKb is expressed in a heterologous system in this study, *A. thaliana* is a member of the same family as *Brassica* species, and clearly the SI system is functional in *A. thaliana* once *SRKb* and *SCRb* from *A. lyrata* are introgressed into the genome. In addition, this study demonstrates the first instance of

live-cell imaging of an SRK protein in the cells where it is known to act. It is interesting that when not exposed to their respective ligands, FLS2, BRI1, and CLV1 are all localized predominantly to the PM, and not to endosomes, in contrast with SRK_3. Although Ivanov & Gaude (2009) hypothesize that the difference in subcellular preference in the case of SRK_3 reflects the unique ability of one stigma epidermal cell to manifest two different outcomes simultaneously depending on the presence or absence of the ligand, the difference may alternatively be due to something inherent with the immunocytochemistry technique, which was not employed for studying localization and dynamics of the other plant RLKs.

Despite the difference in the preference of SRK localization in the PM versus endosomes, the lack of an effect of incompatible or compatible pollination on SRK localization was found both in this study and in the Ivanov & Gaude (2009) study. This finding is also similar to that of BRI1, the localization of which is not dependent on the presence of ligand. In contrast to BRI1, however, SRK_3 signaling does not appear to be transduced from endosomes. If all the SCR-induced SRK signaling occurs at the PM, there would be no expected change in the amount of SRK in endosomes following ligand binding. The presence of SRK in endosomes could simply reflect a continual intermediate step of normal recycling of SRK to and from the PM before it is degraded in the vacuole. Although it is possible that signaling via endosomes occurs in the case of SRKb, it is difficult to imagine that such a mechanism would allow for a single stigma epidermal cell to simultaneously reject an incompatible pollen grain and accept a compatible pollen grain, as the endosomes would likely be free to move around in the cell. However, the fact that exocytosis can occur in localized regions of a single cell, as in tip-growing cells such as pollen tubes, may suggest that localized endocytosis could effect a localized intracellular change in response to signaling. In any case, if a stigma epidermal cell comes in contact with an

incompatible pollen grain, it would only make sense to rid of the SRK at the PM subtending the site of pollen contact by endocytosis and degradation, rather than the entire pool of SRK, since the stigma epidermal cell may quickly and subsequently come in contact with another incompatible pollen grain at a different site on the same stigma epidermal cell, after which it must faithfully manifest an SI response against that pollen grain. Therefore, localized endocytosis of SRK at the PM subtending the site of pollen contact is plausible. Nevertheless, more data are needed to determine whether SRKb localization changes upon pollination with SCRb-expressing pollen. It is possible that in order to visualize any detectable change, ligand concentrations need to be increased and/or spread evenly over the stigma surface, ensuring that almost all of the epidermal cells are exposed to ligand. This problem could potentially be overcome by applying purified SCRb ligand, rather than SCRb-expressing pollen, to the stigma surface.

If anything, there may be a slight change in the localization of SRKb in response to wild type pollen, although more data are needed (Figure 20). The vesicle-like structures may be more numerous, larger, and more irregularly shaped after pollination with wild type pollen (Figure 20). If this pattern of expression is reproducible, it may be related to the finding in *B. rapa* that cross-pollination increased, and self-pollination decreased, the number of actin filaments in stigma epidermal cells (Iwano *et al.* 2007). Actin bundles localized preferentially to the site of contact between the pollen grain or pollen tube and the stigma epidermal cell, and actin polymerization was required for hydration and germination of pollen on stigma epidermal cells (Iwano *et al.* 2007). Therefore, the possible increase in the SRKb-containing vesicle-like structures upon pollination with wild type pollen may reflect a consequence of increased trafficking of vesicles (some of which happen to contain SRKb) that carry molecules that are necessary for pollen

hydration and germination, due to the increased formation of actin filaments upon cross-pollination. Future studies using *A. thaliana* transformed with cYFP-tagged SRKb will likely prove useful in determining how SRK is regulated and trafficked throughout the stigma epidermal cells.

SRKb localization in non-stigmatic tissues

It is clear that the SRKb-cYFP construct imparts a unique subcellular localization pattern of SRKb that differs from all other constructs (Figures 8, 10, & 21). In contrast, all of the various constructs impart identical tissue-specific localization patterns of SRKb, namely, localization in the presumed transmitting tract and in epidermal cells of all floral organs, with predominant expression in the stigma epidermal cells. Thus, this pattern was observed irrespective of whether the *SRKb* or the *AtS1* promoter was used to drive the expression of cYFP-tagged SRKb.

The presence of cYFP-tagged SRKb protein signal in the stigma epidermis and the transmitting tract, with predominant signal in the stigma epidermis, could be expected when the *SRKb* gene is driven by the *SRKb* promoter, as the SRKb protein tissue-specific localization pattern mirrors the location and relative stigma epidermal cell to transmitting tract ratio of activity for both the non-functional pseudo-*SRK* (ψ*SRK*) gene promoter of the *A. thaliana* Col ecotype (Kusaba *et al.* 2001) and the *SRKb* gene promoter itself (Strickler *et al. in preparation*), when either is analyzed in the C24 ecotype via β-glucuronidase (GUS) staining.

The presence of SRKb signal in the epidermis of the style and ovary of the pistil, and in the stamens, the petals, and the sepals, on the other hand, is not expected. Strickler *et al.* (*in preparation*), however, detected *SRKb* RNA in stamens and petals. Although leaves were not examined for *SRKb* expression in this study, Prigoda *et al.* (2005) reported that while RNA

expressed from some *A. lyrata*-derived *SRK* alleles is present in both buds and leaves, *SRKb* RNA is only present in buds. Because all of the various constructs impart SRKb localization in non-stigma epidermal cells, this tissue-specific localization pattern is not construct-dependent, and must be due to some element found in all of the constructs. Curiously, this excludes an effect of the promoter, since some constructs utilize the *SRKb* promoter and others utilize the *AtS1* promoter, the sequences of which are very divergent from each other. A BLAST (Basic Local Alignment Search Tool, http://www.ncbi.nlm.nih.gov/) pairwise alignment between the two promoter sequences yielded no significant alignment: the longest contiguous stretch of sequence identity was only 16 nucleotides, with the next longest stretch being 9 nucleotides (not shown). It may be hypothesized, however, that both of the promoters exhibit the same pattern of activity, but this has not been found to be the case. The *AtS1* promoter is strictly active in the stigma epidermal cells in both C24 and Col ecotypes, as shown with GUS staining (Dwyer *et al.* 1994; Strickler *et al. in preparation*). Furthermore, neither the *SRKb* promoter nor the *AtS1* promoter has been found to exhibit non-stigma epidermal cell activity. It is possible that the GUS staining technique is not sensitive enough to reveal low levels of promoter activity that may be reflected by the SRKb protein localization in non-stigma epidermal cells, as revealed with confocal microscopy. Support for this hypothesis comes from the fact that no activity is seen in stigma epidermal cells when the *SRKb* promoter is analyzed in the Col-0 ecotype via GUS staining, although RT-PCR performed on stigmatic tissue preparations from these plants revealed that the *uidA* gene for GUS is indeed present in the plants, but at very low levels (Strickler *et al. in preparation*). However, this reasoning is likely moot, at least for the case of the *AtS1* promoter, since confocal microscopy analysis revealed that all 6 different organelle (PM, ER, tonoplast, Golgi, peroxisome, and mitochondria) markers driven by the *AtS1* promoter exhibited mC

protein tag signal exclusively in the stigma epidermal cells (Figures 14, 15A, 19C&D, & not shown). This result supports the conclusion that SRKb signal in non-epidermal cells cannot be due to the promoter, since all cYFP-tagged SRKb constructs, including the four utilizing the *AtS1* promoter, impart SRKb signal in non-stigma epidermal cells (Figures 12, 13, 14, 15, 20, 21, 22, 23, 24, 25, 27, & 28).

The presence of SRKb signal in non-stigma epidermal cells also cannot be due to ecotypic variation, as all of the ecotypes transformed with the *AtS1*pr*::cYFP:SRKb* + *SCRb*pr*::SCRb* construct exhibited SRKb signal in style epidermal cells (Figure 25). It also cannot be due to an effect of the transgene integration site, and therefore, the influence of the same unknown, nearby gene, as every line examined with confocal microscopy (19 C24 lines, total) exhibited this expression pattern, and DNA hybridization blots (not shown) indicated that each independent line had its own unique integration site. It is also unlikely to be due to an effect of an element in the *cYFP* sequence, since like cYFP-tagged SRKb, mC-tagged SRKb exhibited signal in the style epidermis (Figure 22), and cYFP and mC are different proteins derived from different sources: cYFP (Heikal *et al.* 2000; Griesbeck *et al.* 2001) is a distant derivative of GFP from *Aequorea victoria*, and mC (Shaner *et al.* 2004) is a distant derivative of DsRed from a *Discosoma* species. Although a BLAST pairwise alignment between cYFP and mC protein sequences revealed that they share 29% identity, their gene sequences do not show significant alignment: only a few regions between 12 and 22 nucleotides show perfect alignment (not shown). Nonetheless, it is unlikely that foreign animal-specific gene sequences encoding FPs would regulate a plant-specific gene *in planta*, and if they did, that it would happen to correspond to the few regions of the gene sequence that are identical between *cYFP* and *mC*.

It is more likely that an element common to all of the constructs is influencing the tissue-specific location of SRKb. This common element could be sequences derived from the pCAMBIA 1300 backbone, specifically the area between the left and right borders, which, along with the chimeric gene sequences, becomes the transgene. These sequences would potentially be excluded from the organelle marker transgenes because they were not derived from the pCAMBIA 1300 vector. Alternatively, the most obvious element common to all of the constructs, the *SRKb* sequence itself, may be regulating the *SRKb* gene and, in turn, the SRKb protein. This hypothesized element would be contained in the *SRKb* exons, since the cDNA constructs do not contain the *SRKb* introns. It is possible that at least one sequence element in one or several exons of the *SRKb* gene acts as a promoter element that drives the *SRKb* gene's own expression. This idea is not far-fetched, as the proposed molecular mechanism exists in the case of the CD28 gene, which encodes a T-cell surface receptor in humans (Lin & Tam 2001). The promoter element was found in exon 1 of the CD28 gene, and is a guanosine-rich sequence (GGGGAGGAGGGG) of only 12 bp in length, spanning position +181 to position +192 (Lin & Tam 2001). A BLAST pairwise alignment between the CD28 promoter element and either the *SRKb* genomic or cDNA sequence did not reveal any significant alignment (not shown), although this does not exclude the possibility that a promoter element with a different, unique sequence that performs a similar function as the promoter element of the CD28 exists in the *SRKb* gene sequence.

The possibility that part of the *SRKb* coding sequence could act as a promoter element that regulates its own expression, as is the case for a T-cell receptor gene, provides yet another link between self-incompatibility and defense/immunity. It is interesting that both SRKb and CD28 are cell surface receptors. Clearly, SRKb expression is highest in the stigma epidermal

cells, the location where it is known and expected to act. Lower, yet significant, expression of SRKb in the epidermis of the style, ovary, and of other floral organs could represent a remnant of evolutionary history, as it would support the theory that the self-incompatibility pathway was recruited from a more ancient pathogen defense pathway, since receptors involved in immunity would need to be expressed in most epidermal cells in order to be effective against pathogen invasion. It would be interesting to determine whether cell surface receptors involved in pathogen defense in plants, such as FLS2, are expressed in both the stigma and non-stigma epidermal cells if they were transformed into *A. thaliana*, tagged with an FP, and had their gene sequences driven by the *AtS1* promoter. Perhaps an exon-derived promoter element is common among cell surface receptors, or specifically, those involved in defense/immunity.

Whether or not SRKb can function in manifesting an SI response in non-stigma epidermal cells is irrelevant, as even mature WT pollen cannot adhere, germinate, and penetrate the ovary, anthers, petals, and sepals of WT (SRKb-lacking) −1-stage buds (Kandasamy *et al.* 1994), which represent the stage at which SI is strong, irrespective of SI-expressing *A. thaliana* ecotype (Nasrallah *et al.* 2004; Boggs *et al.* 2009*a*). In fact, it has been found that pollen can penetrate non-stigma sub-epidermal floral tissues only at very early bud stages, before developmental maturity, the oldest of which is represented by a −9-stage bud (Kandasamy *et al.* 1994). This is likely due to the very minimal amount of cutin present in undifferentiated cells, as pollen is even able to penetrate leaves, but only when they are immature (Wolters-Arts *et al.* 1998) or if they express cutinase (Sieber *et al.* 2000). It would be interesting to determine if SRKb could function in cutinase-expressing non-stigma epidermal cells of −1-stage buds to prevent penetration of SCRb-expressing pollen, in spite of its low expression in these cells.

SRKb localization in non-stigma epidermal cells may, however, reflect its role in pistil elongation, a role that was revealed in an *rdr6* mutant background in *SRKb-SCRb A. thaliana* plants (Tantikanjana *et al.* 2009). The mutation both enhances SI and causes stigma exsertion in these plants (Tantikanjana *et al.* 2009), providing a link between SI and development. These results suggest that signaling components may be shared between SI in the Brassicaceae and more ancestral pathways in plants.

Developmental stage-dependent SRKb signal in pistils

The pattern of SRKb localization throughout floral development is likely a reflection of both the age and function of the cells. Irrespective of the precise stage at which SRKb signal appears, it is clear that SRKb signal appeared at a later stage of bud development in stigma epidermal cells than it did in style epidermal cells (Figures 27 & 28). Because the non-stigma epidermal cells form before stigma epidermal cells, the appearance of SRKb signal could merely reflect cell age. This hypothesis would be supported by the localization pattern of an old flower where SRKb signal was absent in the dead epidermal cells, but present in the style epidermal cells of the same flower (+4, Figure 27; +7, Figure 28). The style epidermal cells of this old flower are still alive, likely because they, along with the ovary cells that must continually expand and divide (Gu *et al.* 1998) to allow elongation of the ovary, will form the silique during seed formation. Stigma epidermal cells begin to form at a stage represented by a −9-stage bud, at the latest (Kandasamy *et al.* 1994). Only then, of course, would it be possible for SRKb to be expressed in the stigma epidermal cells. Interestingly, this is the precise age at which SRKb signal was detected in *AtS1*pr*::cYFP:SRKb* stigmas, although it can be seen that stigma epidermal cells have formed prior to this stage, as they were visible at the −10-stage (Figure 28).

Full-length SRKb signal, however, was not detected in the stigma epidermal cells until the −4 stage (Figure 27). This difference may reflect the presence of more cYFP-tagged SRKb protein species in the *AtS1*pr*::cYFP:SRKb* transformants. It is possible that tSRKb, eSRKb, or both species are expressed earlier, or in greater abundance, than full-length SRKb at these early stages. Testing of this hypothesis would require careful, methodical protein gel blot analyses on stigma protein extracts from floral buds at multiple developmental stages, in addition to the identification of, and the distinction between, the tSRK and eSRK proteins on these blots.

It cannot be ruled out that the detectable signal is from autofluorescence of the cell wall, which would also be an indicator of cell age. Comparisons to wild type (untransformed) plants at these same developmental stages, and plasmolysis experiments on stigmas from wild type plants and from plants transformed with the cYFP-tagged SRKb constructs at various developmental stages younger than those at the −1 stage would help to support or refute this hypothesis.

It is interesting, however, that the −4 stage approximately coincides with the developmental stage of floral buds (approximately 5 days prior to anthesis) from *Brassica oleracea* plants expressing the S_6 haplotype at which RNA from the *S* locus is first detected via *in situ* hybridization analysis (Nasrallah *et al.* 1988). The gradual rise to maximum levels of RNA signal in *B. oleracea* stigmas at 1 day prior to anthesis and the gradual decline of signal in older flowers also mirrors the fluorescence signal of cYFP-tagged full-length SRKb protein in transgenic *A. thaliana* stigmas (Figure 27). Therefore, changes in the level of SRKb signal throughout floral development may reflect the ability of the stigmas to manifest an SI response as a function of SRKb signal level. As compared to epidermal cells of the style and ovary, which are likely to be mainly used for a structural function, stigma epidermal cells are highly specialized for a signaling function: the acceptance and rejection of pollen to either permit or

prevent fertilization. Thus, it would make sense that the SRKb expression in the stigma epidermal cells is more short-lived than in the style and ovary epidermal cells. Nevertheless, a combination of cell age and function are likely to contribute to the pattern of SRKb signal throughout development.

Benefits of live-cell imaging of stigma epidermal cells with fluorescent proteins

In addition to providing insight into the regulation of SRK in the SI response, the live-cell imaging of transgenic *A. thaliana* stigmas has described the subcellular features of stigma epidermal cells, which will aid in future interpretations of SI and other signaling processes that occur in these cells.

For example, familiarity with (1) the size and distribution of chloroplasts and other organelles, (2) general features, and (3) the best imaging parameters for visualizing FPs in stigma epidermal cells, as determined in the present study, could have aided in the live-cell imaging of *A. thaliana* stigma epidermal cells in a study by Samuel *et al.* (2009). In this study, the authors attempted to determine the subcellular localization of the Exo70 protein found to be involved in both the acceptance of compatible pollen in *Brassica* and *A. thaliana*, and the rejection of incompatible pollen in self-incompatible *Brassica*. However, evidence exists (not shown) that the RFP used in the Samuel *et al.* (2009) study may be both truncated and non-functional, and therefore, interpretation of the visualization of the RFP-tagged Exo70 may not be accurate. Support for this hypothesis comes from several observations. Firstly, the protein gel blots performed to detect the presence of the RFP-BnExo70 protein with an anti-RFP antibody in transgenic *Brassica* stigmas did not include untransformed stigmas as a negative control to show that the protein band does not appear in these plants (Samuel *et al.* 2009). Secondly, the authors

indicated that RFP-tagged Exo70 was detected in the PM and in intracellular dots, concluded to be Golgi, in transgenic *A. thaliana* stigma epidermal cells. However, the dots of signal are just as easily apparent in the style cells. This result is unexpected, since the RFP-tagged Exo70 is driven by the *SLR1* promoter, the gene of which is the *Brassica* ortholog of the *A. thaliana AtS1* gene. The promoters of these two genes have been shown to exhibit activity exclusively in the stigma epidermal cells (Dwyer *et al.* 1994). Furthermore, the present study indicates that FPs driven by the *AtS1* promoter are exclusively expressed in stigma epidermal cells (Figures 14, 15A, & 19C&D). Additionally, while the dots of signal are apparent in the style, the cell periphery signal is not, suggesting that the stigma epidermal cell periphery signal may represent cell wall autofluorescence. The PM localization was also not confirmed, either with plasmolysis or co-localization with a PM marker. The authors stated that a PM marker did not show up well in the stigma. Most striking is the size and distribution of the spots of signal in the stigma epidermal cells (Samuel *et al.* 2009), which look extremely similar to chloroplasts, thoroughly imaged in the present study, in these cells. These spots do not appear to be the correct size and distribution of Golgi in stigma epidermal cells, as Golgi stacks are smaller than chloroplasts and are much more numerous in this cell type (Figure 19C&D). Although it was concluded that the Exo70 spots co-localized with Golgi (Samuel *et al.* 2009), the Golgi marker was tagged with GFP. The parameters determined in the present study to be best for imaging GFP also caused autofluorescence of chloroplasts (Figure 11). It is likely that both the Golgi and PM markers did not express well in the stigma epidermal cells because the promoter used was not very active in this cell type. Even the *35S* promoter, which is known to be very strong and constitutive, is not highly active in stigma epidermal cells. Taken together, data from the present study suggest that what was thought to be signal from RFP-tagged Exo70 in the Samuel *et al.* (2009) study is

actually autofluorescence of the stigma epidermal cell wall combined with autofluorescence of chloroplasts, similar to what would be visualized with cYFP imaging parameters (Figure 7A).

Knowledge of stigma epidermal cell architecture as compared to other cell types in plants may be helpful in other future studies. For example, while it was known from transmission electron microscopy of *A. thaliana* stigma epidermal cells that these cells contain chloroplasts (Hisada *et al.* 2001), the size and distribution of the chloroplasts throughout the stigma epidermal cells was not determined. Organelles can vary in size depending on the cell type in which they reside. Plastids, for example, vary in size depending on the cell type, but are relatively uniform in size within a cell (Nelson *et al.* 2007). Chloroplasts of leaf mesophyll cells, for example, are much larger than those of the stigma epidermal cells, which may be a reflection of the major role of mesophyll cells in photosynthesis. The large mesophyll chloroplasts were seen in optical cross-section images of leaf pavement cells captured nearest the wall facing the subjacent mesophyll cells, and because pavement cells do not have chloroplasts, only mesophyll chloroplasts were visualized (Figure 18D-G).

Another interesting observation is that the architecture of the central vacuole, as visualized with the γ-TIP marker, appeared different in stigma versus leaf epidermal cells (Figure 18). Many of the features that can be used to distinguish the tonoplast from the PM or the ER in pavement cells were not observed in stigma epidermal cells. For example, due to the sinuous nature of the pavement cell walls, the tonoplast does not become appressed to some of the walls, unlike in stigma epidermal cells. “Bulbs” were also not seen in stigma epidermal cells, which may be due to the state of differentiation at the −1 stage, as “bulbs” were observed most frequently in expanding cells (Saito *et al.* 2002).

The size of stigma epidermal cells and the presence of their large central vacuoles make them more comparable to pavement epidermal cells than to guard epidermal cells of the leaf, stem, and style (Figures 11, 14, 15, 16, 18, & 21). However, the presence of chloroplasts in stigma epidermal cells makes them more similar to guard cells than to pavement cells, as guard cells are the only leaf epidermal cell type to contain chloroplasts. It is interesting to note another similarity between guard cells and stigma epidermal cells: once mature, these cells are highly differentiated and specialized to perform their respective functions. Stigma epidermal cells have often been called "unicellular non-glandular trichomes" (Martin & Glover 2007), another highly specialized cell type of the plant epidermis. Like guard cells, stigma epidermal cells likely need continual recycling of proteins in order to be competent to respond to a multitude of signals, whereas pavement cells, once formed, may play more of a structural role.

Comparisons aside, it is clear that stigma epidermal cells are a truly fascinating and unique cell type of flowering plants. Stigma epidermal cells of the Brassicaceae could be considered even more unique and specialized than those of plant families with other SI systems, as these "dry" stigma epidermal cells are arguably the most efficient at discriminating between genetically-related and genetically-unrelated pollen in self-incompatible plants. This process occurs directly at the site of contact between pollen and stigma epidermal cells, and just one stigma epidermal cell has the capacity to simultaneously reject and accept incompatible and compatible pollen, respectively.

REFERENCES

Anderson RGW. 1998. The caveolae membrane system. *Annual Review of Biochemistry* **67**, 199-225.

Boggs NA, Dwyer KG, Nasrallah ME, Nasrallah JB. 2009*b*. In vivo detection of residues required for ligand-selective activation of the S-locus receptor in *Arabidopsis*. *Current Biology* **19**, 786-791.

Boggs NA, Dwyer KG, Shah P, McCulloch AA, Bechsgaard J, Schierup MH, Nasrallah ME, Nasrallah JB. 2009*c*. Expression of distinct self-incompatibility specificities in *Arabidopsis thaliana. Genetics* **182**, 1313-1321.

Boggs NA, Nasrallah JB, Nasrallah ME. 2009*a*. Independent *S*-locus Mutations Caused Self-Fertility in *Arabidopsis thaliana*. *PLoS Genetics* **5**, e1000426.

Bolte S, Talbot C, Boutte Y, Catrice O, Read ND, Satiat-Jeunemaître B. 2004. FM-dyes as experimental probes for dissecting vesicle trafficking in living plant cells. *Journal of Microscopy* **214**, 159-173.

Cabrillac D, Delorme V, Garin J, Ruffio-Châble V, Giranton J-L, Dumas C, Gaude T, Cock JM. 1999. The S_{15} Self-Incompatibility Haplotype in *Brassica oleracea* Includes Three *S* Gene Family Members Expressed in Stigmas. *The Plant Cell* **11**, 971-986.

Chapman S, Oparka KJ, Roberts AG. 2005. New tools for *in vivo* fluorescence tagging. *Current Opinion in Plant Biology* **8**, 565-573.

Clough S, Bent AF. 1998. Floral dip: a simplified method for *Agrobacterium*-mediated transformation of *Arabidopsis thaliana*. *The Plant Journal* **16**, 735-743.

Cutler SR, Ehrhardt DW, Griffitts JS, Somerville CR. 2000. Random GFP::cDNA fusions enable visualization of subcellular structures in cells of *Arabidopsis* at a high frequency. *Proceedings of the National Academy of Sciences of the United States of America* **97**, 3718-3723.

Doyle JJ, Doyle JL. 1990. Isolation of Plant DNA from Fresh Tissue. *Focus* **12**, 13-15.

Dwyer KG, Kandasamy MK, Mahosky DI, Acciai J, Kudish BI, Miller JE, Nasrallah ME, Nasrallah JB. 1994. A Superfamily of *S* Locus-Related Sequences in Arabidopsis: Diverse Structures and Expression Patterns. *The Plant Cell* **6**, 1829-1843.

Ferrándiz C, Pelaz S, Yanofsky MF. 1999. Control of Carpel and Fruit Development in Arabidopsis. *Annual Review of Biochemistry* **68**, 321-354.

Fobis-Loisy I, Chambrier P, Gaude T. 2007. Genetic transformation of *Arabidopsis lyrata*: specific expression of the green fluorescent protein (GFP) in pistil tissues. *Plant Cell Reports* **26**, 745-753.

Geldner N, Hyman DL, Wang X, Schumacher K, Chory J. 2007. Endosomal signaling of plant steroid receptor kinase BRI1. *Genes & Development* **21**, 1598-1602.

Giranton J-L, Ariza MJ, Dumas C, Cock JM, Gaude T. 1995. The *S* locus receptor kinase gene encodes a soluble glycoprotein corresponding to the SRK extracellular domain in *Brassica oleracea*. *The Plant Journal* **8**, 827-834.

Grebe M. 2005. Growth by Auxin: When a Weed Needs Acid. *Science* **310**, 60-61.

Griesbeck O, Baird GS, Campbell RE, Zacharias DA, Tsien RY. 2001. Reducing the Environmental Sensitivity of Yellow Fluorescent Protein. 2001. *The Journal of Biological Chemistry* **276**, 29188-29194.

Grossmann G, Opekarova M, Novakova L, Stolz J, Tanner W. 2006. Lipid Raft-Based Membrane Compartmentation of a Plant Transport Protein Expressed in *Saccharomyces cerevisiae*. *Eukaryotic Cell* **5**, 945-953.

Gu Q, Ferrándiz C, Yanofsky MF, Martienssen R. 1998. The *FRUITFULL* MADS-box gene mediates cell differentiation during *Arabidopsis* fruit development. *Development* **125**, 1509-1517.

Haseloff J, Amos B. 1995. GFP in plants. *Trends in Genetics* **11**, 328-329.

Heikal AA, Hess ST, Baird GS, Tsien RY, Webb WW. 2000. Molecular spectroscopy and dynamics of intrinsically fluorescent proteins: Coral red (dsRed) and yellow (Citrine). *Proceedings of the National Academy of Sciences of the United States of America* **97**, 11996-12001.

Hisada A, Yoshida T, Kubota S, Nishizawa NK, Furuya M. 2001. Technical Advance: An Automated Device for Cryofixation of Specimens of Electron Microscopy using Liquid Helium. *Plant & Cell Physiology* **9**, 885-893.

Ishikawa Y, Cho G, Yuan Z, Inoue N, Nakae Y. 2006. Aquaporin-5 water channel in lipid rafts of rat parotid glands. *Biochimica et Biophysica Acta* **1758**, 1053-1060.

Ivanov R, Gaude T. 2009. Endocytosis and Endosomal Regulation of the *S*-Receptor Kinase during the Self-Incompatibility Response in *Brassica oleracea*. *The Plant Cell* **21**, 2107-2117.

Iwano M, Shiba H, Matoba K, Miwa T, Funato M, Entani T, Nakayama P, Shimosato H, Takaoka A, Isogai A, Takayama S. 2007. Actin Dynamics in Papilla Cells of *Brassica rapa* during Self- and Cross-Pollination. *Plant Physiology* **144**, 72-81.

Kandasamy MK, Nasrallah JB, Nasrallah ME. 1994. Pollen-pistil interactions and developmental regulation of pollen tube growth in *Arabidopsis*. *Development* **120**, 3405-3418.

Kusaba M, Dwyer K, Hendershot J, Vrebalov J, Nasrallah JB, Nasrallah ME. 2001. Self-Incompatibility in the Genus *Arabidopsis*: Characterization of the *S* Locus in the Outcrossing *A. lyrata* and Its Autogamous Relative *A. thaliana*. *The Plant Cell* **13**, 627-643.

Letham DLD, Blissard GW, Nasrallah JB. 1999. Production and characterization of the *Brassica oleracea* self-incompatibility locus glycoprotein and receptor kinase in a baculovirus infected insect cell culture system. *Sexual Plant Reproduction* **12**, 179-187.

Li X, Wang X, Yang Y, Li R, He Q, Fang X, Luu D-T, Maurel C, Lin J. 2011. Single-Molecule Analysis of PIP2;1 Dynamics and Partitioning Reveals Multiple Modes of *Arabidopsis* Plasma Membrane Aquaporin Regulation. *The Plant Cell* **23**, 3780-3797.

Lin CJ, Tam RC. 2001. Transcriptional Regulation of CD28 Expression by CD28GR, a Novel Promoter Element Located in Exon 1 of the CD28 Gene. *The Journal of Immunology* **166**, 6134-6143.

Martin C, Glover BJ. 2007. Functional aspects of cell patterning in aerial epidermis. *Current Opinion in Plant Biology* **10**, 70-82.

Martinez-Trujillo M, Limones-Briones V, Cabrera-Ponce JL, Herrera-Estrella L. 2004. Improving Transformation Efficiency of *Arabidopsis thaliana* by Modifying the Floral Dip Method. *Plant Molecular Biology Reporter* **22**, 63-70.

Nasrallah JB, Yu S-M, Nasrallah ME. 1988. Self-incompatibility genes of *Brassica oleracea*: Expression, isolation, and structure. *Proceedings of the National Academy of Sciences of the United States of America* **85**, 5551-5555.

Nasrallah ME, Liu P, Nasrallah JB. 2002. Generation of self-incompatible *Arabidopsis thaliana* by transfer of two *S* locus genes from *A. lyrata*. *Science* **297**, 247-249.

Nasrallah ME, Liu P, Sherman-Broyles S, Boggs N, Nasrallah JB. 2004. Natural variation in expression of self-incompatibility in *Arabidopsis thaliana*: Implications for the evolution of selfing. *Proceedings of the National Academy of Sciences of the United States of America* **101**, 16070-16074.

Nelson BK, Cai X, Nebenführ A. 2007. A multicolored set of *in vivo* organelle markers for co-localization studies in Arabidopsis and other plants. *The Plant Journal* **51**, 1126-1136.

Nimchuk ZL, Tarr PT, Ohno C, Qu X, Meyerowitz EM. 2011. Plant Stem Cell Signaling Involves Ligand-Dependent Trafficking of the CLAVATA1 Receptor Kinase. *Current Biology* **21**, 345-352.

Oparka KJ. 1994. Plasmolysis: new insights into an old process. *New Phytologist* **126**, 571-591.
Prigoda NL, Nassuth A, Mable BK. 2005. Phenotypic and Genotypic Expression of Self-incompatibility Haplotypes in *Arabidopsis lyrata* Suggests Unique Origin of Alleles in Different Dominance Classes. *Molecular Biology and Evolution* **22**, 1609-1620.

Raffaele S, Bayer E, Lafarge D, Cluzet S, Retana SG, Boubekeur T, Leborgne-Castel N, Carde J-P, Lherminier J, Noirot E, Satiat-Jeunemaître B, Laroche-Traineau J, Moreau P, Ott T, Maule AJ, Reymond P, Simon-Plas F, Farmer EE, Bessoule J-J, Mongrand S. 2009. *The Plant Cell* **21**, 1541-1555.

Robatzek S, Chinchilla D, Boller T. 2006. Ligand-induced endocytosis of the pattern recognition receptor FLS2 in *Arabidopsis*. *Genes & Development* **20**, 537-542.

Russinova E, Borst J-W, Kwaaitaal M, Caño-Delgado A, Yin Y, Chory J, de Vries SC. 2004. Heterodimerization and Endocytosis of Arabidopsis Brassinosteroid Receptors BRI1 and AtSERK3 (BAK1). *The Plant Cell* **16**, 3216-3229.

Saito C, Ueda T, Abe H, Wada Y, Kuroiwa T, Hisada A, Furuya M, Nakano A. 2002. A complex and mobile structure forms a distinct subregion within the continuous vacuolar membrane in young cotyledons of *Arabidopsis*. *The Plant Journal* **29**, 245-255.

Samuel MA, Chong YT, Haasen KE, Aldea-Brydges MG, Stone SL, Goring DR. 2009. Cellular Pathways Regulating Responses to Compatible and Self-Incompatible Pollen in *Brassica* and *Arabidopsis* Stigmas Intersect at Exo70A1, a Putative Component of the Exocyst Complex. *The Plant Cell* **21**, 2655-2671.

Sardar HS, Yang J, Showalter AM. 2006. Molecular Interactions of Arabinogalactan Proteins with Cortical Microtubules and F-Actin in Bright Yellow-2 Tobacco Cultured Cells. *Plant Physiology* **142**, 1469-1479.

Scott RJ, Spielman M, Dickinson HG. 2004. Stamen Structure and Function. *The Plant Cell* **16** Supplement, S46-S60.

Shaner NC, Campbell RE, Steinbach PA, Giepmans BNG, Palmer AE, Tsien RY. 2004. Improved monomeric red, orange and yellow fluorescent proteins derived from *Discosoma* sp. red fluorescent protein. *Nature Biotechnology* **22**, 1567-1572.

Shimosato H, Yokota N, Shiba H, Iwano M, Entani T, Che F-S, Watanabe M, Isogai A, Takayama S. 2007. Characterization of the SP11/SCR High-Affinity Binding Site Involved in Self/Nonself Recognition in *Brassica* Self-Incompatibility. *The Plant Cell* **19**, 107-117.

Sieber P, Schorderet M, Ryser U, Buchala A, Kolattukudy P, Métraux J-P, Nawrath C. 2000. Transgenic Arabidopsis Plants Expressing a Fungal Cutinase Show Alterations in the Structure and Properties of the Cuticle and Postgenital Organ Fusions. *The Plant Cell* **12**, 721-737.

Stein JC, Dixit R, Nasrallah ME, Nasrallah JB. 1996. SRK, the Stigma-Specific S Locus Receptor Kinase of Brassica, Is Targeted to the Plasma Membrane in Transgenic Tobacco. *The Plant Cell* **8**, 429-445.

Stein JC, Howlett B, Boyes DC, Nasrallah ME, Nasrallah JB. 1991. Molecular cloning of a putative receptor protein kinase gene encoded at the self-incompatibility locus of *Brassica oleracea*. *Proceedings of the National Academy of Sciences of the United States of America* **88**, 8816-8820.

Strickler SR, Tantikanjana T, Nasrallah JB. *In preparation*. Regulation of the *S*-Locus Receptor Kinase and Self-Incompatibility in *Arabidopsis thaliana*.

Takayama S, Shimosato H, Shiba H, Funato M, Che F-S, Watanabe M, Iwano M, Isogai A. 2001. Direct ligand-receptor complex interaction controls *Brassica* self-incompatibility. *Nature* **413**, 534-538.

Tantikanjana T, Rizvi N, Nasrallah ME, Nasrallah JB. 2009. A Dual Role for the *S*-Locus Receptor Kinase in Self-Incompatibility and Pistil Development Revealed by an *Arabidopsis rdr6* Mutation. *The Plant Cell* **21**, 2642-2654.

Tung C-W, Dwyer KG, Nasrallah ME, Nasrallah JB. 2005. Genome-Wide Identification of Genes Expressed in Arabidopsis Pistils Specifically along the Path of Pollen Tube Growth. *Plant Physiology* **138**, 977-989.

Wilkinson JE, Twell D, Lindsey K. 1997. Activities of CaMV 35S and *nos* promoters in pollen: implications for field release of transgenic plants. *Journal of Experimental Botany* **48**, 265-275.

Wolters-Arts M, Lush WM, Mariani C. 1998. Lipids are required for directional pollen-tube growth. *Nature* **392**, 818-821.

Zheng X, Bollag WB. 2003. Aquaporin 3 Colocates with Phospholipase D_2 in Caveolin-Rich Membrane Microdomains and Is Downregulated Upon Keratinocyte Differentiation. *The Journal of Investigative Dermatology* **121**, 1487-1495.

CHAPTER 4

Conclusions and future directions in the investigative research on self-incompatibility in the Brassicaceae

Despite the use of several experimental approaches including targeted down-regulation, T-DNA insertional and point mutations, and yeast two-hybrid interaction studies described in this dissertation, testing of candidate genes/proteins in the transgenic self-incompatible *Arabidopsis thaliana* model system for potential signaling components downstream of the SRK-SCR interaction in the Brassicaceae SI system did not yield any obvious players. Candidates included several *AtPUB* genes, for their sequence similarity to a proposed positive regulator of SI, *Brassica ARC1*, and for their known involvement in pathogen resistance, which in several ways exhibits similarities to SI. Other candidates included additional pathogen resistance genes central to various defense pathways, and *AtS1*, a gene expressed highly and specifically in stigma epidermal cells.

The signaling events downstream of the SRK-SCR interaction in the Brassicaceae self-incompatibility (SI) system have yet to be determined conclusively. Perhaps ironically, this current status is due in part to progress made with the transgenic self-incompatible *A. thaliana* model system, which has been shown to be extremely useful in testing and challenging the previously-proposed mechanistic view of SI signaling in the Brassicaceae generated from studies with *Brassica*. Identification of the likely *A. thaliana* orthologs of *Brassica* genes that had been proposed to function in SI, followed by targeted knock-down using RNA interference as well as insertional or point null mutants is a relatively simple and tractable approach that can be employed in transgenic self-incompatible *A. thaliana* to test the involvement of these candidate

genes in SI. None of the putative *A. thaliana* orthologs tested to date have supported a role for these genes in SI. While it is possible that redundancy or cross-talk among various pathways is precluding the phenotypic identification of an SI signaling component, it is unlikely that this phenomenon would be operating in *A. thaliana* but not *Brassica*, since *Brassica* has the larger genome and is therefore more likely to exhibit redundancy. Nevertheless, use of transgenic self-incompatible *A. thaliana* has proved useful in identifying key regulators of SI in this system, including *RDR6* and *AtPUB8*, in identifying amino-acid residues that contribute to SI specificity in SRK and SCR, and in providing clues to the evolution of SI by revealing ecotypic variation in expression of the SI trait. Furthermore, as shown in this dissertation, the use of this transgenic self-incompatible model has demonstrated that eSRK is not required for SI, at least in the context of the *Sb* haplotype, a finding that resolves the long-standing question of whether eSRK is required for SI.

The transgenic self-incompatible *A. thaliana* model system has also been extremely useful in live-cell imaging studies of SRK localization and dynamics. Results in this dissertation demonstrate that cYFP-tagged SRKb is expressed and is functional in the stigma epidermal cells of transgenic self-incompatible *A. thaliana* and is therefore suitable for live-cell imaging studies using confocal microscopy. *A. thaliana* expressing cYFP-tagged SRKb will undoubtedly prove useful in future imaging of the dynamics of SRK and its interaction with other proteins. Additionally, this tagged SRK can be used for *in vitro* pull-down experiments and in cases where protein levels among different samples need to be compared by Western blot analysis, since the commercially-available α-GFP antibody recognizes the cYFP protein.

As expected, full-length SRKb was found to be localized to the plasma membrane in live stigma epidermal cells. However, live-cell confocal microscopy imaging with cYFP-tagged

SRKb revealed that full-length SRKb is also localized to as-yet-unidentified vesicle-like structures that likely represent endosomes. Additionally, tSRKb/eSRKb was visualized in the cortical ER and in as-yet-unidentified membranous structures in transvacuolar strands, which may represent non-cortical ER. Co-localization studies with markers for other organelle and various endosomal compartments are needed to help pinpoint the subcellular localization of SRKb in transvacuolar strands and in the observed vesicle-like structures. These results may provide more insight into how SRK may be trafficked in stigma epidermal cells and in response to binding to the SCR ligand.

Interestingly, SRKb subcellular localization does not appear to change significantly upon pollination, either with wild type pollen or with pollen expressing the SCRb ligand. However, potential subcellular redistribution upon ligand binding may not be clearly revealed unless purified SCRb ligand is applied at high enough concentrations over the entire surface of the stigma epidermis. Further experimentation is needed to address the question of how SRK is trafficked intracellularly in response to ligand binding and pollination.

SRKb signal was found in tissues other than the stigma epidermis, irrespective of which of the two promoters used in these studies were driving its expression. When driven by either the native *SRKb* promoter or the stigma-specific *AtS1* promoter, SRKb signal is localized preferentially to stigma epidermal cells, as expected, and minimally to all other epidermal cells of the flower. SRKb signal levels persist throughout floral bud development in style epidermal cells, but gradually rise and fall throughout floral bud development in stigma epidermal cells, the trend of which correlates directly with the competency of the stigma to both accept compatible pollen and reject incompatible pollen. The organelle marker proteins expressed with the *AtS1* promoter do not exhibit signal in non-stigma epidermal cells. In order to determine whether

SRKb signal in non-stigma epidermal cells is due to regulation by the *SRKb* gene itself or whether it is a result of an artifact of the presence of a regulatory element in the vector backbone from which the transgene containing the *SRKb* chimeric genes is derived, the *SRKb* chimeric genes could be cloned into a vector other than pCAMBIA 1300 for eventual transgene integration into the *A. thaliana* genome. If SRKb signal is detected in non-stigma epidermal cells, this result would support the hypothesis that the *SRKb* gene itself is influencing its tissue localization. Concurrently, one of the organelle markers, which utilized a different vector backbone and exhibited exclusive stigma epidermal cell localization, could be cloned into pCAMBIA 1300 for eventual transformation into *A. thaliana*. If the marker exhibits non-stigma epidermal cell localization, the observed SRKb signal was likely due to some regulatory sequence in the transgene derived from the pCAMBIA 1300 vector.

The live-cell imaging studies of SRKb in stigma epidermal cells, as described in this dissertation, also revealed characteristic architectural features of stigma epidermal cells. These include autofluorescence of the cell wall, chloroplasts that are smaller than those of leaf mesophyll cells, a central vacuole that does not consist of "bulbs," transvacuolar strands, and a high level of intracellular dynamism. Use of the imaging parameters determined to be optimal for visualizing fluorescent proteins in stigma epidermal cells and knowledge of the architectural features of these cells may prove useful in future experiments where studying intracellular dynamics of stigma epidermal cells is essential.